Carbon Fiber Reinforced Polymer Retrofits to Increase the Flexural Capacity of Deteriorated Steel Members

Samuel Sherry

Dissertation submitted to the faculty of the Virginia Polytechnic Institute and State University in partial fulfillment of the requirements for the degree of

Doctor of Philosophy

in

Civil Engineering

Matthew H. Hebdon, Chair

Matthew R. Eatherton

Maryam Shakiba

Bernard L. Kassner

July 29th, 2021

Blacksburg, Virginia

Keywords: CFRP, Strand Sheet, Steel, Corrosion, Retrofit, Bridges, Flexure

Carbon Fiber Reinforced Polymer Retrofits to Increase the Flexural Capacity of Deteriorated Steel Members

Samuel Sherry

Abstract

The load-carrying capacity of aging bridge members may at times be found insufficient due to deterioration and a historical trend towards increased truck axle loads beyond their design capacity. Structurally deficient bridges are problematic for bridge owners and users because they restrict traffic usage and require bridges to be posted (operate at less than their ideal capacity). Structural deficiency is the primary motivation for bridge owners to retrofit bridges to meet a specified operating demand. It may be required to replace or retrofit a portion or all of a deficient bridge. The replacement of an entire bridge or even a part of the bridge is generally less desirable than a retrofit solution because retrofits are generally a cheaper alternative to the entire replacement of a structure and usually do not require the bridge's closure. Standard strengthening solutions for corroded members include bolting or welding steel cover plates, replacing sections of the girder, or adding external prestressed tendons. However, these methods also have several challenges, including required lane closures, high installation costs, increased dead weight, and continuing corrosion issues.

One alternative to conventional retrofits is the use of carbon fiber-reinforced polymer (CFRP) laminates, which can be adhered to increase both strength and stiffness. CFRPs are a highly tailorable material with an extremely high strength-to-weight ratio, ease of installation and can potentially mitigate further corrosion concerns. Fiber Reinforced Polymers (FRPs) have already been widely accepted as a means of retrofitting reinforced concrete structures (AASHTO 2012, 2018a; ACI 2002, 2017; National Academies of Sciences, Engineering 2010, 2019) but have not yet been widely adopted in the steel industry due to the retrofit's material limitations (lower elastic modulus [less than 29,000 ksi], unanswered questions related to debonding, and no unified design or installation guides). However, newly developed materials and manufacturing processes have allowed for the economic development of stiffer CFRP materials suitable for steel structures, such as the high modulus (HM) CFRP strand sheet.

This research analytically and experimentally investigates how newly developed HM strand sheets perform in small scale tensile testing, and large scale flexural testing (laboratory and in situ testing). During the laboratory testing these HM strand sheets were compared against normal modulus (NM) CFRP plates to draw conclusions on these different retrofitting materials (strength, stiffness, bond behavior, and applicability of the retrofit). Another central point in examing these different retrofit materials is how CFRPs perform when attached to structural steel with significant corrosion damage. Corrosion damage typically results in a variable surface profile, which may affect a CFRP retrofit's bond behavior. While limited laboratory testing has been conducted on CFRP attached to steel structures with simulated deterioration, the surface profile does not represent realistic conditions. The effects of a variable surface profile on the NM plate material and HM strand sheet were investigated using small scale tensile testing, and large scale flexural testing. All the variable surface profiles tested for bond strength were fabricated

based on “representative” simulated corrosion samples or on specimens with significant corrosion.

Once all the variables pertaining to the new materials and the effect of a variable surface profile on CFRP retrofits had been examined in a laboratory setting, these retrofitting techniques were implemented on deteriorated in-service steel bridge structures. This research was the first to retrofit deteriorated in-service bridge structures with HM CFRP strand sheets in the United States. This in situ testing was used to compare the laboratory test data of an individually retrofitted girder to the behavior of a single girder that had been retrofitted in a bridge structure. This information was used to verify results on the behaviors of strengthening, stiffening, effects on live load distributions, and modeling assumptions of retrofitted bridge structures.

The results from the laboratory testing and in situ testing of CFRP retrofits on corroded steel structures were synthesized to provide information on performance and design guidance for future retrofits. This dissertation provides additional information on CFRP retrofits applied to variable surface profiles and provides data on new CFRP materials (HM strand sheets). With this information, Departments of Transportation (DOT) can be confident as to where and when different types of CFRPs are a suitable retrofit material for corroded or uncorroded steel structures.

Carbon Fiber Reinforced Polymer Retrofits to Increase the Flexural Capacity of Deteriorated Steel Members

Samuel Sherry

General Audience Abstract

The capacity of aging bridges may at times be found insufficient due to deterioration and a trend towards increased loading. Structurally deficient bridges are problematic for bridge owners and users because they restrict traffic usage and require bridges to operate at less than their intended capacity. Inadequate capacity are the primary motivation for bridge owners to repair (retrofit) bridges to meet specified traffic demands. Repairs usually do not require the bridge's closure to traffic. Standard repairs for corroded steel members include bolting or welding steel cover plates, replacing sections of the girder, or adding external prestressed tendons. However, these methods also have several challenges, including required bridge closures, high installation costs, increased weight, and continuing corrosion issues.

One alternative to conventional repairs is the use of carbon fiber-reinforced polymer (CFRP) laminates, which can be adhered to the deteriorated members to increase strength and stiffness. CFRPs are an extremely versatile material with high strength, high stiffness, ease of installation and can potentially mitigate concerns about further corrosion. Fiber Reinforced Polymers (FRPs) have already been widely accepted as a means of retrofitting reinforced concrete structures(AASHTO 2012, 2018a; ACI 2002, 2017; National Academies of Sciences, Engineering 2010, 2019) but have not yet been widely adopted in the steel industry due to the lack of literature and economical implementation of the CFRPs on steel. However, over the past 20 years, research has been completed on the application of CFRPs on steel, and newly developed materials were created for the economic implementation of CFRP materials suitable for steel structures. In particular, this material is a high modulus (HM) CFRP strand sheet, which has a higher stiffness than a conventional CFRP.

This research investigated how newly developed HM strand sheets perform in small-scale laboratory testing and large-scale laboratory testing. Where material strengths, bondability, and the efficacy of different repairs were examined against conventional means on steel structures with and without corrosion deterioration.

Once all the variables pertaining to the new materials and the effects corrosion had on CFRP retrofits had been examined in a laboratory setting, these retrofitting techniques were implemented on a deteriorated in-service steel bridge structure (field study) that required repair. This research was the first to repair deteriorated in-use bridge structures with HM CFRP strand sheets in the United States. This information was used to verify results on the material's behavior.

The laboratory testing and field testing of CFRP retrofits on corroded steel structures were summarized to provide information on performance and design guidance for future retrofits. This

dissertation provides additional information on CFRP repairs applied to corroded steel and provides data on new CFRP materials (HM strand sheets). With this information, Departments of Transportation (DOT) can be confident as to where and when different types of CFRPs are a suitable retrofit material for corroded or uncorroded steel structures.

To my parents, William Sherry and Judy Ray-Sherry, I cannot express my love and admiration for you enough. You are the best parents a son could ask for. I would never have made it to where I am today if it was not for your love and support. Like you like to remind me: “if it was easy, everyone would do it”.

Acknowledgments

I would like to express my gratitude and admiration to my advisor, Dr. Matthew Hebdon (or dad as we called him behind his back), for giving me the best academic guidance and solid life advice a young academic could ask for. The opportunity you provided me and your ability to set me up for success will not be forgotten. I am incredibly grateful for your mentorship, not only in the field of structural engineering but also in general life advice. I am extremely lucky to have had you as my advisor and even luckier to count you as a friend. There are few advisors that would gladly grab a belt sander and start installing strain gauges just to give you a hand, and I am glad to say you are one of them. Thanks for being the best, and I hope we can continue to collaborate and stay in touch after we both leave Tech. Lastly, don't worry; all this work will make its way to publication.

I would also like to thank Dr. Bernard Kassner for serving on my graduate committee and his mentorship from the industry's perspective. Without your help, these CFRP retrofits would have never happened, so thanks! I can, without a doubt, say you have made me a better writer, and I greatly appreciate all the insight you provided on all of my Ph.D. work. I also appreciate Dr. Matthew Eatherton, and Dr. Maryam Shakiba for serving on my graduate committee and providing valuable feedback and suggestions throughout my time at Virginia Tech. Interacting with you as your student and TA had provided me with an immense wealth of knowledge for which I am extremely grateful.

I would like to recognize the Virginia Transportation Research Council (VTRC) for funding the research project and making my doctoral studies possible at Virginia Tech. I would also like to acknowledge the Virginia Department of Transportation's Stanton District for their donation of

materials, manpower, and the corroded steel beams which were retrofitted for the first part of my research. Also, the Virginia Department of Transportation's Culpeper District for their help in working with me and planning the CFRP retrofit out in the field on the Simmons Gap Road Bridge.

I would also like to thank lab technicians, especially Dr. David Mokarem, Brett Farmer, Garrett Blankenship, and Dennis Huffman, for their help throughout the project. It was great having you around to assist me with technical questions and teach me things to help add more tools to my tool belt. A special thanks to my friends at Tech: Japsimran Singh, Ryan Stevens, Raul Avellaneda, Ali Alfailakawi, and Seth Lindley. A shout out to my good friend Dr. Cameron Murray for his constant guidance, mentorship, and friendship over the course of our academic careers. Hang ten my man! This project would not have been possible without everyone's constant help and support at every step of the way. Also, a shout out to all my internet pen pals for all the Friday game nights that got me through my Masters and Ph.D. countless hours played, and maybe one day we will be good. Lastly, a very special thank you to my girlfriend, Lilian Shen whose constant love and support was integral in my success. I love you.

TABLE OF CONTENTS

LIST OF FIGURES

LIST OF TABLES

CHAPTER 1: Introduction

1.1 Motivation and Overview

The load carrying capacity of steel bridge members can be found insufficient as a result of both a history of deterioration and a historical trend towards increased truck axle loads. These insufficient bridges are problematic for bridge owners and users because they restrict traffic usage and are required to operate at less than their maximum capacity. Aging steel bridge members can exhibit signs of varying levels of cross-section reduction as a result of corrosion, which can reduce their load-carrying capacity in critical locations of a member, such as at the point of maximum moment or point of maximum shear. In addition, the introduction of closely-spaced, multi-axle single-unit trucks in the last decade has changed the load demand on bridges, which in many cases is larger than the initially designed load-carrying capacity of older structures (Mertz and Kulicki 2006). Section loss and an increase in live load both contribute to an increase in stresses and deflections. The Federal Highway Administration (FHWA) sets limits for live load stresses and deflections that, if exceeded, can lead to a bridge being categorized as "structurally deficient" (2012). These structurally deficient bridges are sometimes "load posted", limiting the allowable legal truck weight to cross the bridge. The restriction of traffic creates hardships for bridge users who rely on traffic routes to efficiently move goods and services. These hardships are generally in terms of both lost time and money, due to the requirement of seeking an alternate route due the load postings.

Disruption of traffic and maintaining a sound bridge inventory are the motivations for bridge owners to retain bridges operating at their full potential (not load posted). In order to do so, it may be required to replace or retrofit a portion of or all of a load posted bridge. Where the

replacement of an entire bridge or even a part of the bridge is generally less desirable then compared to a retrofit solution. Retrofits are generally a cheaper alternative to the entire replacement of a structure and usually do not require the closure of the bridge in the retrofitting process. While there are cases where bridge replacement cannot be avoided (extreme deterioration, or a bridge well beyond its service life), retrofitting generally provides an intermediate solution to strengthen a deficient structure. Standard strengthening solutions for corroded members include adding steel cover plates, replacing sections of the girder, or adding external post-tensioned tendons. However, these methods also have several challenges, including: required lane closures, high costs, increased dead weight, and continual corrosion issues.

One alternative to conventional retrofits is the use of carbon fiber-reinforced polymer (CFRP) laminates, which can be adhered to the regions of desired strength and stiffness increase. CFRPs are a highly tailorable material with an extremely high strength-to-weight ratio (e.g. a Sika Type S 1012 CarboDur CFRP plate has a strength to weight ratio of 35.7 times that of an A572 Gr. 50 steel), easy to install, and can potentially mitigate concerns about further corrosion. CFRP has already been widely accepted as a means of retrofitting reinforced concretes structures (AASHTO 2012, 2018a; ACI 2002, 2017; National Academies of Sciences, Engineering 2010, 2019). Historically, these materials have an elastic modulus lesser than or equal to that of steel. The lower FRP moduli require an unfeasible number of FRP layers to be applied to a steel structure to account for the reduced stiffness. The materials and labor associated with this large number of FRP plies generally do not result in a cost-effective retrofit design for steel structures. These high costs and labor requirements are the main reasons FRP retrofits have not yet been widely adopted in the steel industry. However, newly developed materials and manufacturing

processes have allowed for the economical development of stiffer CFRP materials suitable for civil infrastructure, with elastic moduli greater than 29,000 ksi, like that of ultra high modulus (UHM), high modulus (HM), and strand sheet CFRP materials.

While there has been some basic research conducted on the topic of steel, which has been retrofitted with FRPs, there are still some gaps in the available data. An extensive overview of this research will be discussed in Chapter 2. This review will show that there is little to no research on the topic of CFRP materials being used on steel structures with realistic corrosion deterioration. This absence of literature highlights the limitations of what kind of corrosion or surface roughness CFRP is known to be applicable. While there has been laboratory work conducted on CFRPs attached to steel structures with simulated corrosion deterioration, those samples are not necessarily a good representation of realistic conditions. Furthermore, there have been no in-service structures (with significant corrosion deterioration) in the United States that have had CFRP retrofits applied to them. The effects CFRP retrofits have on load distribution of a deteriorated bridge is a topic where little to no research has been conducted. Finally, the implementation of HM CFRP strand sheets is a novel concept in the United States. The use of this new material, its installation, and performance need to be examined to determine its full capabilities. This examination required small and large scale testing. This dissertation aims to help fill in some of these gaps and provide some data on new CFRP materials. With this information, Departments of Transportation (DOT) can be confident as to where and when CFRPs are a suitable retrofit material for flexural retrofits on corroded or uncorroded steel structures.

1.2 Dissertation Organization

This dissertation is organized in a manuscript format, where traditional chapters are replaced by manuscripts. Each manuscript has, or will shortly be submitted to a peer-reviewed journal or international conference. Each of the manuscripts in this dissertation appears in their most refined format, either as the submitted version or based on improvements made during the peer-review process. Two journal papers and one conference paper are presented, of which a majority of the research and primary authorship was completed by the author of this dissertation.

Chapter 1 provides an introduction, motivation, and overview of the research to this dissertation. Chapter 2 provides a literature review comprised of relevant topics about steel retrofitted with CFRPs. A historical look at the initial design and strengthening behavior of steel retrofitted with CFRP will be examined. This historical review will be followed by a review of more contemporary research that investigated how different variables, (e.g., CFRP type, required bond length, fatigue life, and environmental exposure) can affect the overall behavior of a CFRP retrofit. The literature review was conducted for applications relating to flexural retrofits. Analytical prediction models were reviewed for both flexural NM and HM retrofit types. Lastly, an examination of the bond strength was carried out. This examination entailed looking at bond behavior subject to many different variables, (e.g., moisture, steel surface roughness, CFRP type, surface preparation, and chlorides).

Chapter 3 presents the conference paper titled "The Influence of Steel Surface Roughness and CFRP Material Types on Effective Bond Length". This paper was co-authored by the project's Principal Investigator, Dr. Matthew Hebdon, and is currently in preparation for submission to the 2021 International Bridge Conference.

Chapter 4 presents the journal article titled " Flexural Strengthening Retrofits of Corroded Steel Members Using CFRP—Large Scale Results and Implementation and Best Practices". This paper was co-authored by the project's Principal Investigator, Dr. Matthew Hebdon, and Dr. Bernard Kassner, and will be submitted to the ASCE Journal of Bridge Engineering.

Chapter 5 presents the journal article titled, "Load Test to Evalulate a Flexural Repair of a Deteriorated Bridge with Carbon Fiber Reinforced Polymer Strand Sheets." This paper was co-authored by the project's Principal Investigator, Dr. Matthew Hebdon, and will be submitted to the Elsevier Engineering Structures Journal.

Chapter 6 provides recommendations, conclusions, potential areas for future work relating to the research project and Ph.D. contributions.

1.3 Attributions

The research reported in this dissertation was supported and funded by the Virginia Transportation Research Council (VTRC). These research project titles and grant numbers are as follows:

- Flexural Strengthening of Heavily Corroded Steel Members Using CFRP (Grant No. VTRC 112768).
- Load Test to Evaluate a Flexural Repair of a Deteriorated Bridge with Carbon Fiber Reinforce Polymer (Grant No. VTRC 116471).

The Virginia Department of Transportation generously donated all the required CFRP materials and steel used in the testing of the Flexural Strengthening of Heavily Corroded Steel Members

Using CFRP project of this report. This donation was greatly appreciated and crucial to the testing of this research.

1.4 Research Purpose and Scope

The fundamental purpose of this research was to evaluate the materials, configurations, and effectiveness of flexural CFRP retrofits applied to deteriorated steel flexural members. This was be done experimentally, where these test results would be compared against conventional analytical models. There were two main variables of interest relating to this investigation: how newly developed-high modulus (HM) strand sheets affected retrofit behavior, and how different levels of steel corrosion (surface roughness) affect ultimate bond strength. The scope of work in this research can be categorized into four, sometimes overlapping and reoccurring, components: small scale laboratory testing, large scale laboratory testing, field testing, and analytical modeling. The scope of work for each of these components are as follows:

Small Scale Laboratory Testing (Double Strap Joint Testing (DSJ))

This research looked at bond behavior of two different CFRP materials (high modulus strand sheets and normal modulus plate material). While investigating these different CFRP types for bond behavior, varying corrosion levels were also included in the testing matrix to see how these would affect bond behavior.

Large Scale Laboratory Testing

Large-scale structural laboratory testing (on flexural CFRP retrofits) were carried out on corroded and uncorroded steel girders which were removed from service by the Virginia Department of Transportation (VDOT). This testing was performed to examine the

accuracy of the analytical prediction models, as well as how different CFRP types, placements, and orientations affected the overall strength and performance of the different retrofits. The large scale laboratory testing was conducted on actual or "re-created" steel bridge beams which were representative of in-service bridge beams. The "re-created" beams were corroded steel bridge beams that were removed from service; further deterioration was added to them to "re-create" exact parameters of specific deteriorated bridge beams in the field. VDOT had an interest in retrofitting these specific deteriorated bridge beams. The specific deteriorated beams, which were "re-created", were carefully analyzed for span length, beam size, and deterioration location to replicate their behavior.

Large Scale Field Testing

Following the "re-created" laboratory testing, the most favorable flexural retrofit was installed on a specific deteriorated bridge beam on an in-service VDOT bridge. Live load testing was performed before and after the implementation of the flexural retrofits to observe changes in the retrofitted girder and the bridge structure as a whole.

Analytical Modeling

Analytical modeling was crucial to the other three components of this research. These models provided researchers with baseline calculations on expected performance. These models were then verified, expanded upon, or changed to meet the results from testing. These differences in predictions were a result from the implementation of novel materials or untested material behavior.

In summary, the purpose of the project was to evaluate, document, and determine the limit states of select CFRP retrofits and its bond behavior. The final results of this research were broken up into three papers pertaining to specific research topics. These papers and this dissertation can help inform future bridge owners in determining how to design and apply CFRP retrofits on deteriorated steel structures.

1.5 Research Layout and Objectives

While this dissertation is organized into three distinct manuscripts, the research can be categorized into four, sometimes overlapping and reoccurring, components: small scale laboratory testing, large scale laboratory testing, field testing, and analytical modeling. The small scale laboratory testing is discussed in the manuscript contained in Chapter 3. Various large-scale laboratory tests were completed with different objectives, and are discussed in Chapters 4, & 5. The in situ bridge members that were retrofitted and live load tested are discussed in Chapter 5. The modeling encompassed configurations applicable to each of the different tests (small-scale, large-scale, and in situ), and the results are applicable to Chapters 3, 4, & 5. The objectives for each of these contributions are as follows:

<u>Small Scale Laboratory Testing (Double Strap Joint Testing (DSJ)) [Chapter 3]</u>

- Determine the effective bond length for two CFRP materials (regular modulus plate & HM strand sheet) attached to steel plates. These two CFRP materials were then used throughout the large-scale tests in this study.
- Determine the effective stiffness increase of the two CFRP retrofit materials when applied to steel loaded in tension.

- Determine the effects that "representative" simulated corrosion had on a CFRP's bond strength.

Large Scale Laboratory Testing

- Determine how newly developed HM strand sheet materials behave compared to a conventional normal modulus plate material used to retrofit the tension flange of flexural steel beams with corrosion section loss. Specifically, determine how CFRP placement (location on the beams) affects overall behavior and strength. [Chapter 4 & 5]
    - 'Determine if the corrosion/surface roughness of corroded steel sections had an influence on the CFRP's bond strength and behavior. Specifically, determine what kind of corrosion and roughness the experimental retrofits were subject to, and how those conditions influenced bond strength. [Chapter 4, & 5]

Large Scale Field Testing

- Determine how a flexural CFRP retrofit on an in situ deteriorated steel bridge beam will influence the overall structural behavior of the entire bridge(strength, stiffness, and load distribution). This retrofit was based on the most favorable performing flexural retrofit from this research. Live load testing was conducted on this bridge to obtain pre- and post-retrofit behavior. The HM strand sheet retrofit used in this retrofit was also the first of its kind in the United States. The HM strand sheet retrofit can be monitored long term to track its performance and ability to resist environmental exposure.[Chapter 5]

Analytical Modeling

- Determine how well effective length analytical models predict bond lengths and strengths on small scale testing. This modeling is of particular interest for the HM strand sheet. Propose changes to existing prediction models to account for the use of HM CFRP strand sheets. [Chapter 3]

- Determine how conventional *elastic* analytical models predict strength and stiffness for large scale testing completed with different retrofit materials and locations. Propose augmentation to the analytical models to account for the use of CFRP strand sheets. [Chapters 4, & 5]

- Determine how conventional *inelastic* analytical models predict strength and stiffness for large scale testing completed with different retrofit materials and locations. Propose augmentation to the analytical models to account for the use of CFRP strand sheets. [Chapters 4, & 5]

CHAPTER 2: Literature Review

2.1 Introduction to FRP materials

FRPs are a composite material comprised of a polymer matrix that has been reinforced with fibers. These fibers can be a variety of materials (carbon, aramid, glass, or basalt), depending on the FRP's desired behavior. The polymer matrix in the FRP is generally referred to as "resin" and usually comprises around 30 to 40% of the FRP by volume (Hyer 2009). The amount and types of resin and fiber material can be catered to specific requirements to achieve specific material behavior of the FRP.

When discussing a FRP retrofit, there is the item being strengthened/retrofitted and the FRP retrofit materials itself. In the case of this research, steel is the material that is being retrofitted and the FRP retrofit material is a CFRP strengthening system, which is comprised of two parts; the CFRP and the adhesive material used to "attach" the CFRP to the steel being retrofitted. An example of some CFRPs and adhesive material are shown in Figure 1 I. and II. respectively.

I. **II.**

Figure 1. I. Different Types of CFRPs (A. = Prepreg Plate Material, B = Prepreg Strand Sheet, C = Unimpregnated Fiber Sheet), II. Adhesive Material (2 part epoxy)

2.1.1 Manufacturing Process/Types

Just as FRPs can be comprised of a multitude of materials, they can also be manufactured/processed in many different ways. The end result produces some very different products. Figure 1 I. shows three different unidirectional single layer CFRP types (A.-C.). Unidirectional means that the fiber orientation is just running in one direction. However,

depending on what is required, there could be different fiber orientations specified or even multiple layers of differently oriented fibers.

Figure 1 I. A. is a plate type material, which has been impregnated with resin, meaning the fibers and the resin have been combined to create the CFRP matrix. This type of manufacturing process is referred to as pre-impregnated or "prepreg" (Hyer 2009). Figure 1 I. B. is a strand sheet type of material, which is made up of prepreg strands that have been bound together by a plastic string. This material looks and feels very much like a bamboo mat, which is commonly used to roll sushi. Figure 1 I. C. is a fiber sheet, which is made up of unimpregnated fibers that have been stitched together by a string. This material will be impregnated with a resin before the material can be applied to a surface.

There are different advantages to the three different unidirectional CFRP types (A.-C.) shown in Figure 1 I. Generally speaking, prepreg material uses less resin and has better quality control compared to a material that is impregnated in the field. However, a plate material like the one shown in Figure 1 I A can generally only be used on a flat surface, unlike the fiber sheet shown in Figure 1 I. C. The fiber sheet shown in Figure 1 I. C. can be used to wrap around any contours. The other benefit of a fiber sheet is it generally comes on a wider roll than that of a flat plate type material; this means it can be cut to specific dimensions. This is generally not the case for flat plate type material which comes in stock dimensional sizes; while they can be cut to size it is much more difficult. Lastly, the strand sheet shown in Figure 1 I B. tries to combine the best of both of these CFRP types. Where there is a high degree of tailorability in conjunction with that of the high-quality control of the prepreg manufacturing process.

Every CFRP type (A.-C.) shown in Figure 1 I will have to be applied to the material being retrofitted with an adhesive. The application process will be completed for the fiber sheet during

the impregnation process; however, for the prepreg sheet, epoxy will be required for the adhesion process. These procedures vary slightly from the impregnation process, were the FRP is being adhered to the material being retrofitted. The flat plate material will sit on top of the adhesive material, while the strand sheet will be pushed into the adhesive material (similar to the impregnation process). All of these different materials and types of CFRPs makes for a very broad range of CFRPs to select from, where the most important consideration factor is the material being retrofitted.

2.1.2 Material Differences of CFRPs

Section 2.1.1 *Manufacturing Process/Types*, highlights the fact that there are many different CFRP products available for retrofitting steel structures. While they come in many different dimensions and manufactured processes, they also come with different material properties. As a rule of thumb, the pronounced strength or stiffness value in these FRPs are generally how these materials are defined, e.g., high strength or high stiffness CFRP. However, this is not a set rule and the manufacturer will define the FRPs material as they see fit. Table A.1 in ACI 440.2-17 defines different FRP types by elastic modulus and ultimate strengths; however, the values listed in this table are only concerned with the strength or stiffness of the fibers inside the FRP system (excluding the resin) (ACI 2017). While this information can be useful, the general consensus of this and many other researchers is that the strength or stiffness of the entire FRP composite is of more interest (Cruz and Barros 2004; Fawzia 2007; Kazem et al. 2016; Peiris 2011; Photiou et al. 2006; Schnerch and Rizkalla 2008a; Wu et al. 2010; Zhao 2013). Unfortunately, there is no universally accepted system to classify different types of CFRP materials. What is considered to be a normal modulus CFRP material to one researcher might be a high modulus CFRP material to another researcher. To highlight these differences and have a source of many "defined" CFRP

types, Figure 2 presents a scatter plot of ultimate strains and peak stresses of different CFRP materials aggregated from many different literature sources (Cruz and Barros 2004; Fawzia 2007; Kazem et al. 2016; Peiris 2011; Photiou et al. 2006; Schnerch and Rizkalla 2008a; Wu et al. 2010; Zhao 2013). The labels in Figure 2 are how the researchers categorized their CFRPs.

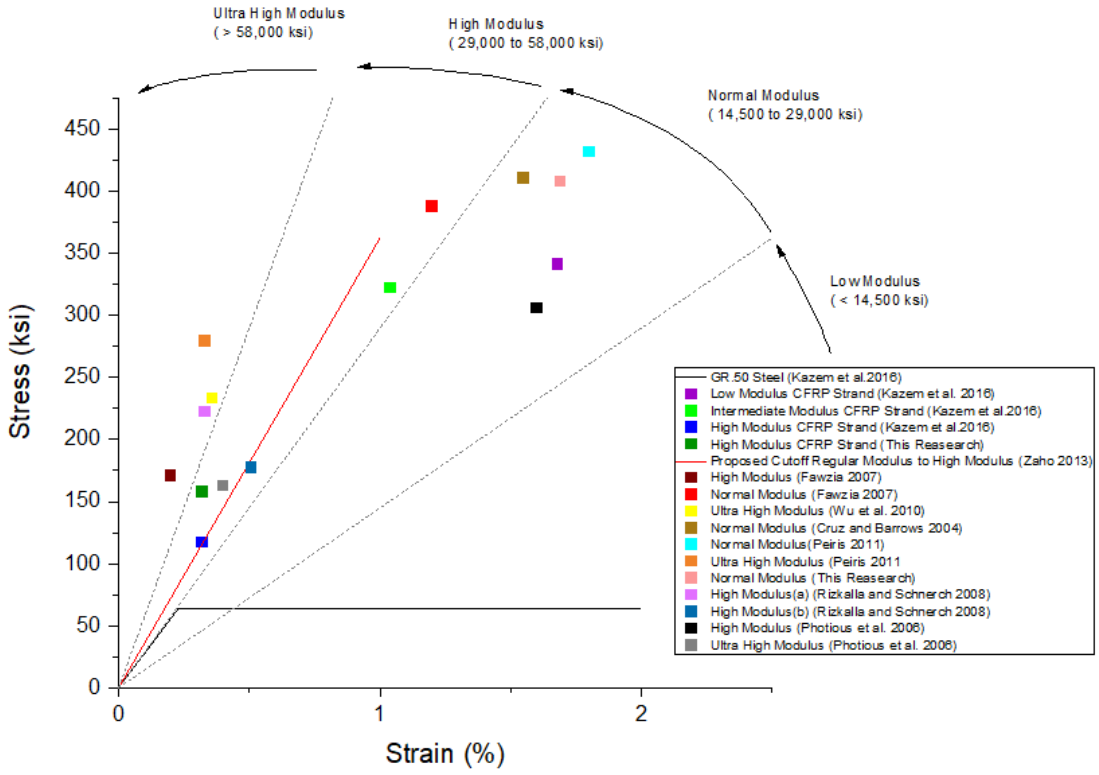

Figure 2. Stress-Strain Scatter Plot of Different Types of CFRPs

As Figure 2 shows, there is quite a bit of variability in the nomenclature that different researchers adopted. To simplify the variability, this dissertation will adopt the nomenclature Peiris devised for different moduli CFRPs in his dissertation (2011). This nomenclature divides the CFRP types into low, normal, high, and ultra high modulus. The cutoffs for these different classifications can be seen in Figure 2.

2.1.3 FRP Failure Modes

The potential failure modes of FRP to steel composites subject to loading (illustrated in Figure 3) include the following (Zhao and Zhang 2007):

a) Adhesion failure between steel and primer

b) Adhesion failure between a secondary adhesive and FRP primary adhesive

c) Adhesion failure between FRP and FRP primary adhesive

d) FRP delamination

e) FRP rupture

f) Adhesion failure between priming adhesive and insulating material

g) Cohesion failures

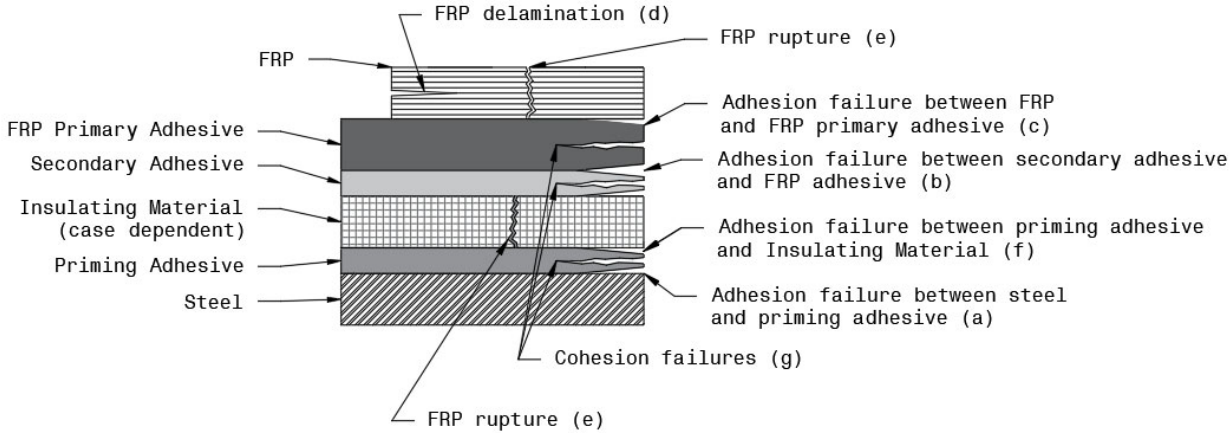

Figure 3. Failure Modes of FRP Composites

The failures presented in Figure 3 show two main types of material failures: CFRP failures and adhesive failures. Where for the adhesive failure there are two sub types of adhesive failures: cohesion and adhesive failures. Adhesion failures are less desirable because they indicate the

steel's surface was inadequately prepared for the adhesive. This improper preparation could be a lack of cleanliness, insufficient roughness or an overly rough surface. Contrasting this is the adhesion failure, which indicates adequate surface preparations. Adhesion failures generally denotes that the adhesive material reached its ultimate material properties. The next most desirable failure type is the FRP delamination, a failure within the FRP layer, which means that every layer below the delamination was sufficient at transferring the load into the FRP. Delamination is still not the ideal failure type and is usually caused by some internal flaw between FRP layers. Lastly, the most desirable failure type is FRP rupture, which means that the FRP material reached its ultimate strain and, therefore, the FRP material's ultimate potential. To reiterate, the least desirable failures to the most desirable are as follows: adhesion failure, cohesion failure, delamination, and rupture.

2.2 Small Scale Testing

A cost-effective way to examine many different parameters (bond strength, CFRP type, bond length, adhesive thickness, different loading conditions, and exposure conditions) in a CFRP-to-steel composite is through small scale testing. There are many different small scale specimen

types, but a common one is the double strap joint (DSJ) (shown in

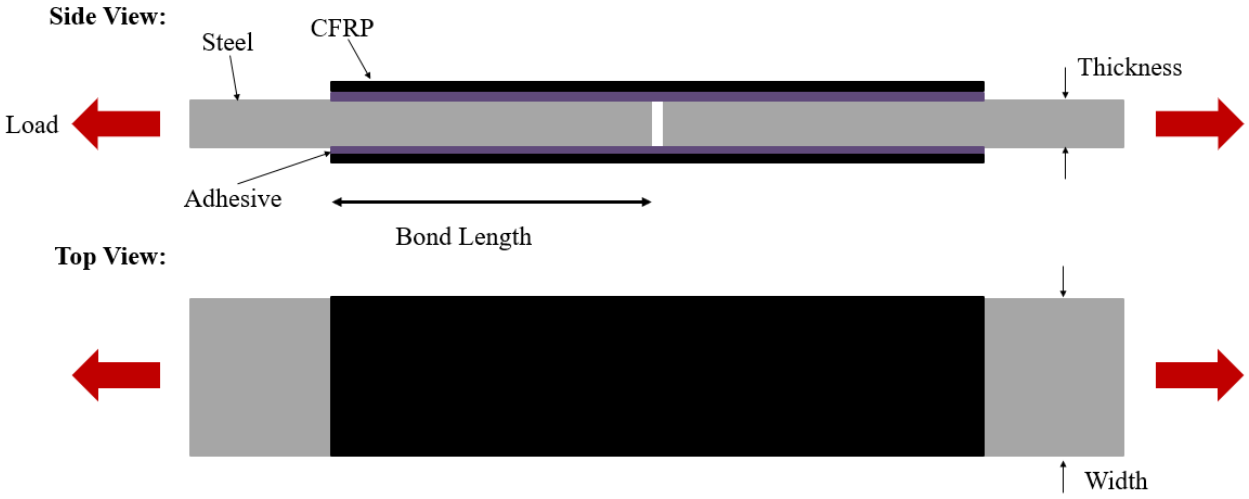

Figure **4**). An extensive list of these different specimen types can be found in a review paper by Zhao and Zhang (2007). The basic anatomy of a DSJ consists of two steel plates that are connected via adhesives and CFRP strips.

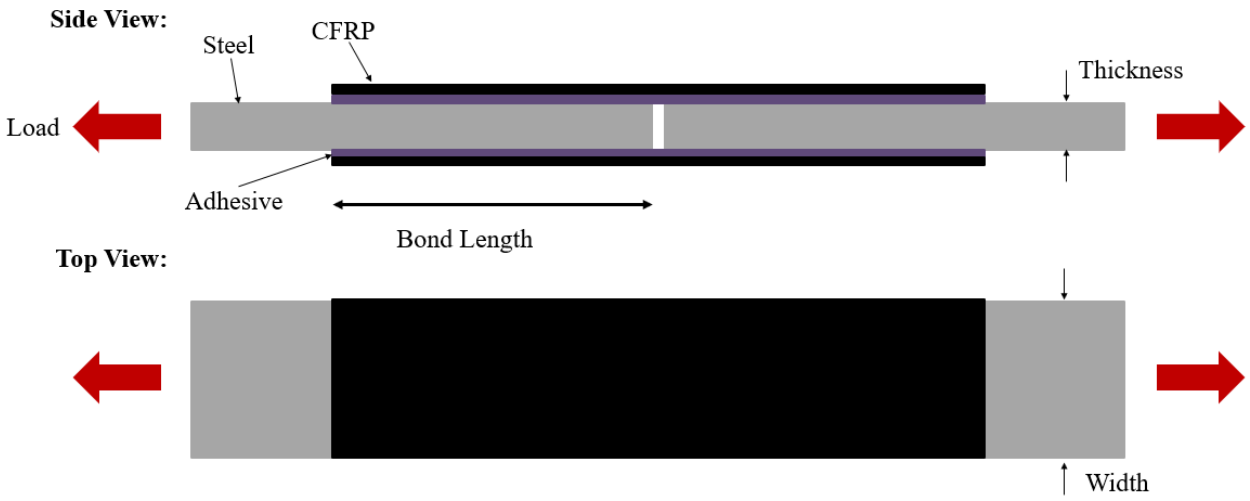

Figure 4. The Layout of a Double Strap Joint Specimen

2.2.1 Bond Strength

Bond strength is of the utmost importance when designing a FRP to steel bonded joint, as it can dictate the ultimate load of the joint. There are two conventional means of calculating bond strength: a strength-based and a fracture mechanics-based approach. Buyukozturk et al. completes a thorough review of these methods and the different prediction models that researchers have taken to calculate bond strengths (2004). The strength-based approach assumes ultimate bond strength occurs when the adhesive in the joints reaches a maximum strain or stress (Adams and Peppiatt 1974; Hart-Smith 1973; Volkersen 1938). The fracture mechanics-based approach assumes ultimate bond strength is related to interfacial fracture energy(Fawzia et al. 2010b; Fernando 2010; Xia and Teng 2005; Yuan et al. 2001). The strength-based and fracture mechanics-based approached each have their unique simplifying assumptions, which are important to note when examining different strength prediction models. An examination of an

adhesively bonded joint and the stresses that accompany the joint's loading need to be highlighted to discuss these different models and their variables of interest. Figure 5 shows a double strap joint that is being loaded in tension and plots of non dimensionalized stresses (normal [peeling] and shear) which occur as a result of this loading (Kinloch 1987).

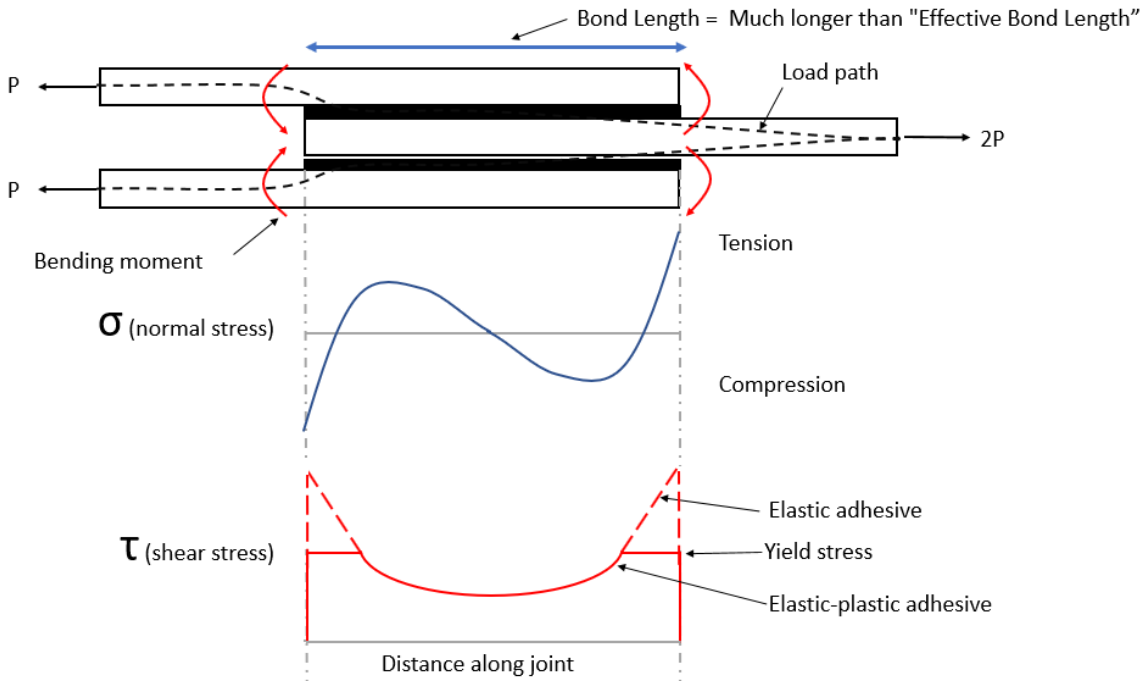

Figure 5. A Double Strap Joint Loaded in Tension and Plots of its Normal and Shear Stresses

Figure 5 shows that the DSJ has a bond length, which is much longer than the "effective bond length." The term effective bond length (Le) was coined by Chen and Teng (2001) and describes a bond length that develops the adhesive's full strength or rupture strength of the FRP. Any additional bond length added to the system after reaching the effective bond length will not increase the joint's ultimate strength (2P).

The stress plots in Figure 5 show that this specimen is subject to shear and normal stresses, which at first glance could have been missed due to the assumption that a symmetrically loaded

specimen would not have bending. However, internal bending moments cause normal stresses due to the misalignment of the internal neutral axis (due to the load progression through the adhered materials) (Nozaka et al. 2005a). The load path in Figure 5 shows the eccentricity of the loading and highlights the internal bending behavior. The normal stress plot's behavior should be noted because there are high-stress risers near the joint's ends, and they are of opposite signage (one in compression with the other in tension). The plot of shear stresses is more straightforward, except that there is different behavior observed for an elastic adhesive (solid red line) and an elastic-plastic adhesive (dotted red line). Both the normal and the shear stress have their maximums located near the joint's termination.

Historically, researchers used a strength-based approach to calculate the failure load associated with an adhesively bonded joint (Adams and Peppiatt 1974; Goland and Reissner 1944; Hart-Smith 1973; Volkersen 1938). The failure criteria for these strength-based approaches were maximum shear stress (Volkersen 1938), maximum shear and normal stresses (Goland and Reissner 1944), maximum principal stress (Adams and Peppiatt 1974), and max shear strain criteria (Hart-Smith 1973). Depending on the model, shear and normal stresses are taken into consideration of the failure criteria. Older prediction models are accurate when the CFRP's joint fails abruptly at the initiation of a first crack or the ultimate strength of the adhesive material is reached. In original derivations of this material (Goland and Reissner 1944; Volkersen 1938), highlight the assumptions that go into the derivation of the failure criteria for these joints. More recent researchers have built upon and updated those assumptions (Ojalvo and Eidinoff 1978; Sayman 2012; Tsai et al. 1998). Where these newer models work well but get increasingly more complex as more variables are considered, Yuan et al. suggested using nonlinear fracture mechanics to calculate the bond strength of these FRP bonded joints (2001). Many other

researchers went on to propose different models that consider different variables or are comprised of entirely empirical equations (Chen and Teng 2001; Xia and Teng 2005; Yuan et al. 2001, 2004). One of the most popular models for CFRP adheared to steel was created by Xia and Teng, which looked at bond-slip curves to calculate a joint's ultimate strength (2005).

2.2.2 Bond-Slip Models

Bond-slip models are used to predict the effective bond length and ultimate shear strength (also known as interfacial shear strength) of an FRP-to-steel bonded joint. This type of model specifically examines a shear-type failure (Mode II in fracture mechanics). The bond-slip model formation requires the tensile or shear testing of some adhesive joint (usually a single or double lap joint), which has been heavily strain gauged along its length (shown in Figure 6 I.). The strain gauges on the DSJ are used to measure "slip" or debond along the length of the DSJ. A DSJ has a constantly applied displacement until the specimen's failure (debond or rupture). A DSJ with a debond failure has a load-deformation plot that is bilinear in nature, a constant loading up to a peak load, and then there is continued deformation with little to no increase in load until failure. In the continued deformation stage of the loading, two behaviors occur: the adhesive's softening, and debonding. These occur in the following order: the adhesive softens, and then eventually it debonds. The debonding of the material is similar to crack propagation. The softening and debonding progressively move along the length of the material until it reaches a critical length. Once this critical length is reached, the entire system fails. Strain gauges can be used to monitor the peak stress, softening of the adhesive, and debonding of a DSJ over many finite locations. The softening and debond behavior is represented by a bond-slip curve, where shear stress is plotted against displacement or "slip" along a known length. Figure 6 II. and III. represent a bond-slip curve with a linear adhesive and a nonlinear adhesive, respectively (Xia

and Teng 2005; Yu et al. 2012). With these bond-slip models' formation, important information can be determined which is used to calculate the ultimate load and effective bond length of a CFRP joint.

I. Testing Configuration for a Bond-slip Model

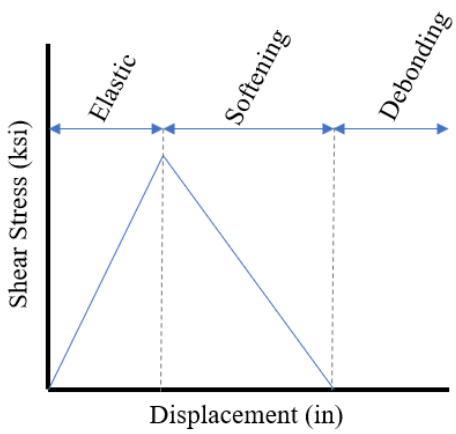

II. Bond-slip curve for CFRP and steel with a linear adhesive

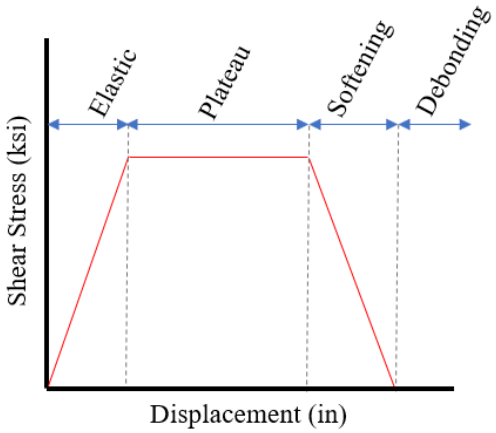

III.Bond-slip curve for CFRP and steel with a nonlinear adhesive

Figure 6. I. Bond-slip Test Setup, II. & III. Bond Slip Curves

Some of the first bond-slip modeling research, pertaining to the work in this dissertation, focused on CFRP/steel bonded to concrete (Chen and Teng 2001; Pham and Al-Mahaidi 2005; Yuan et al. 2001). This work paved the way for researchers looking at CFRPs bonded to steel. Xia and Teng were some of the first researchers to look at the bond-slip modeling of CFRP on steel (2005). Xia and Teng proposed equations for the effective bond lengths and ultimate strengths

for different CFRP and adhesives; this model was based on a linear adhesive like the one shown in Figure 6 II . The most significant contribution of this work pertained to the use of the interfacial fracture energy, G_f, to predict failure in a joint. The interfacial fracture energy is equal to the area under the curve shown in Figure 6 II. or III. This approach based the joint's failure on the tensile strength and the strain capacity of the adhesive.

Fawzia et al. (2010a) built upon Xia and Teng's (2005) bond-slip model, to include the prediction of multiple layers of CFRP bonded to steel. Wu et al. (2012b) further added to these models to include predictions for CFRP adhesives with nonlinear material properties, like the bond-slip curve shown in Figure 6 III. Where the implementation of a trapezoidal bond-slip curve was adopted for nonlinear adhesives. Wang et al. (2016) verified the model proposed by Wu et al. (2012b) and examined how adhesive thickness affects the bond models. This research also proved that a digital image correlation (DIC) system could detect and highlight the bond-slip behavior better than that of conventional strain gauges.

2.2.3 CFRP Modulus Types Effects On Bond

An area of great interest to the CFRP community is the effects of different moduli CFRPs on bond length. Specifically, researchers care about the “effective bond length”; this is the length of CFRP at which any further increases to the bond length will not increase the ultimate load of the system. The effective length can be thought of as the minimum amount of CFRP required to achieve the CFRP composite's full potential. Effective bond lengths will vary by CFRP type and adhesive. Researchers have found some very interesting trends from the side-by-side comparisons of different CFRP types attached to steel with the same adhesives (Al-Mosawe et al. 2015; Fawzia et al. 2005, 2006). The higher the elastic modulus of the CFRP, the smaller the required effective length. Ultra high modulus and high modulus CFRPs tend to rupture once they

exceed the effective length, while normal and low modulus CFRPs fail due to adhesive debonding. This behavior is a function of the material's strength and ultimate strain (in general, as moduli increases, strength decreases). Fawzia et al. (2005) noted that both high modulus and normal modulus CFRPs had similar strain profiles and distributions. While higher modulus CFRPs can achieve their ultimate strengths, these strengths can be down to around half that of a normal modulus CFRP. Of course, the trade-off is that higher modulus results in higher stiffness.

2.2.4 CFRP Adhesives Effects On Bond

Xia and Teng's (2005) work examined the bond strength of three different adhesive materials of varying thicknesses on the same CFRPs which were attached to steel. Their work concluded that thinner adhesives (less than 0.0787 in) achieved higher bond strengths (compared to the thick adhesives) and failed due to cohesive failures. Thicker adhesives tended to fail due to the delamination of the CFRP. This work also highlighted that the more ductile an adhesive was, the longer the time to failure and the higher the obtainable loads. As adhesives material properties become more ductile, the failure type transitions from an adhesive failure to a cohesive failure (Jiao and Zhao 2004; Wu et al. 2012a; Xia and Teng 2005).

2.2.5 Surface Preparation

Steel in any condition (fresh from the mill or severely corroded) needs some surface preparation before a coating is applied, whether it be paint or an adhesive. This preparation will create cavities on the steel surface that allow for the better bonding of adhesives and remove any contaminants (dirt, grime, rust, and mill scale). CFRP manufacturers (Nippon and Sika) specify a “white metal finish” on steel surfaces to which CFRP will be attached (Milliken Infrastructure 2018; Sika 2014a). The reason for this stringent requirement is because a white metal finish

(generally achenved through media blasting or sanding) is extremely efficient at preparing the surface and removing unsound material to which the CFRP is to be bonded. It is also vital that the adhesives be applied to this white metal finish before the newly exposed steel surface has time to oxidize (which creates a weak layer on the surface of the steel) (Kim et al. 2011). Researchers have varying opinions regarding how many hours between cleaning and application is ideal for best bond performance. Kim et al. (2011) only allowed a maximum of 3 hours to pass between cleaning and CFRP application, while Teng et al. (2011) allowed for a maximum of 24 hours. Twenty-four hours is typically the maximum time between cleaning and applying CFRP, and in general, the shorter the timeframe, the better.

A white metal finish can be achieved by sanding, grinding, needle gunning, or grit blasting. The use of grit blasting is generally the recommended procedure because it cleans a steel surface exceptionally well and is usually the fastest cleaning method. Fernando et al. (2013) examined different ways (solvent cleaned, ground, and varying sizes of alumina grit blasting) of prepping steel for bonding. The smaller size blasting material provided the highest strengths on small scale bonding tests. Their work also suggested that there is a point of diminishing returns as far as increasing roughness to increase bond strength. Kim et al. (2011) looked at the bond strength of steel cleaned with: solvent cleaned, needle gunned, sanded, and ground. The needle gunned, sanded, and ground specimens all achieved strengths within a few kN of each other. Meanwhile, the solvent cleaned specimens achieved strength that was only about 75% of the other cleaning types. Overall, Schnerch et al. (2007) does a good job laying out best practices and cleaning procedures in their work .

Recently researchers have been experimenting with acid etching to create a roughened surface profile and enhance the mechanical bonds between an adhesive and steel. Kleffel and Drummer

(2017) examined three different etching products and tested the roughened surface for bond performance. In comparison to the control joint, which held a trivial load, these etched specimens were able to withstand measurable loads, where the best performing etched sample carried five times the load of the least performing joint. Da Silva et al. (2010) examined chromatic etching on bonded joints, concurrently used with mechanical roughening. The etched and roughened specimens outperformed either individual process. This etching process can be used in combination with the current methods to increase bond strength and remove the oxidation layers on a steel's surface.

2.2.6 Corrosion/Surface Roughness

Every material inherently has a roughness; whether it can be seen on the micro or macro scale depends on the material and any completed preparation. For instance, a piece of steel from the mill, a piece of steel which was just grit blasted, and a piece of steel that has been weathering for years are all going to have different roughness values on both a micro and macroscopic level. A question pertaining to this research is: how will these different levels of roughness affect bond strength? There has been more research focused on the micro-scale rather than the macroscale level of roughness due to the ease of testing, the following two paragraphs will discuss the microscale and then macroscale roughness related to small scale testing. For the purposes of this literature review, the cut-off from the micro to the macro scale is 0.4 mm or 400 μm.

The microscale level roughness is significant for surface preparations, which is of extreme importance when determining bond strength. Yao and Qu (2002) looked at how the depth of surface roughness (depths of 0.07 to 5.5 μm) can control interfacial or cohesive failures. Their work had similar conclusions to Fernando et al. (2013); once a specific roughness depth, R, is achieved, there is little increase in bond strength. Chotickai (2018) performed CFRP DSJ testing

to evaluate how different levels of steel corrosion affect bond strength. The steel's corrosion was "created" in an electrochemical bath where the average pitting depths ranged from 5 to 178 μm. The most corroded specimens had an additional 5% increase in strength compared to that of the control. Da Silva et al. (2010) examined how differently machined surface profiles (depths of 100 to 300 μm) and chemically etching affected joint bond strength. In almost every case, chemical etching increased the strength of a joint over that of an acetone cleaning. Chemical etching on an unmachined surface generally outperformed that of a machined surface cleaned with acetone. Machining only affected the brittle adhesive, which was tested in this study. Furthermore, the more patterned machined surfaces (grids & diamonds) achieved higher bond strengths than vertical or horizontal lines. Lastly, an increase in these pattern depths did not mean that there was an increase in bond strength. Kleffel and Drummer (2017) also examined different chemical etching means and which method produced the best bond strength. The depth of roughness here ranged from around 1 to 10 μm. The unetched specimen held a negligible load, while the etched specimens were able to carry loads. Another finding of this work was undercutting, which is created during the etching process and adds considerable strength to a bonded joint. Undercutting can be thought of as an ink bottle shape, near the surface there is a small opening and then further down the neck of the bottle there is a bulbus opening under the surface. Conventional means of measuring roughness cannot capture these undercuts, and thus these roughness values do not show a good correlation to bond strength. Kim et al. (2010) examined how mechanically patterned grooves' spacing, and width affected the bond strength. As the groove's width was increased and the spacing between the grooves was held constant, the joint's bond strength increased.

There has been less research conducted on macro-scale bond strength, which is what this research is more concerned about. Haghpanah et al. (2014) conducted small scale bond strength testing on “saw tooth” joints specimens joined with an adhesive (tooth size 10 mm wide, 5mm deep. While these “saw tooth” specimens failed at similar loads, the teeths’ configurations had a big effect on the specimens' ductility. Wang et al. (2017) researched corroded steel members that were cleaned and then had their surface profiles examined with a DIC system, where the goal of the research was to look at the remaining thicknesses of the steel and develop equations to predict tensile strengths. In developing these equations, many useful surface roughness parameters and procedures were developed to analyze the steels surface profiles. Li et al. (2019) looked at corroded steel plates used in CFRP DSJs and how different corrosion levels affect overall strength. Using a non-contact 3D profiler, they were able to look at many different parameters to describe surface profiles. While there was significant information about the surface, it was hard to correlate one to bond strength. Fractal dimensions gave the best correlation between bond strength and roughness. DSJs exposed to more corrosion damage (section loss) had around a 6% strength increase compared to control specimens. Corrosion damage surface roughness ranged from 0 to 1.5 mm in depth. The corrosion damage also required longer effective lengths of the specimens. As it turns out, adhesive thickness made more of an impact on strength than surface roughness; in some cases, there was a 20% increase over the control specimens depending on adhesive thickness. Up until 1.5 mm, the bond strength of the DSJs went up, and bond strength decreased after 1.5 mm. Xu et al. (2020) looked at single lap shear joints made with CFRP and varying degrees of corroded steel. Like the work by Li et al. (2019), Xu et al. found that as corrosion damage increased, bond strength also increased; however, Xu et al. (2020) found that as corrosion levels increased, the required effective length

decreased. The steel mass loss ratio resulting from corrosion, ξ, gave good insight into how corrosion affects bond strength. There was a significant increase in bond strength above a mass loss ratio of 15%; however, around 30% loss, the strength increase reached an asymptote.

2.2.7 CFRP Terminations & Detailing

Near the termination of a laminate being adhered to a substrate via an adhesive, there is a region of high interfacial shear and normal (peeling) stresses, as shown in Figure 5. If improperly accounted for, these high stresses can cause the premature failure of the laminate system. A conventional square joint and a diagram of simplified stresses in a square joint can be seen in Figure 7 I and II, respectively.

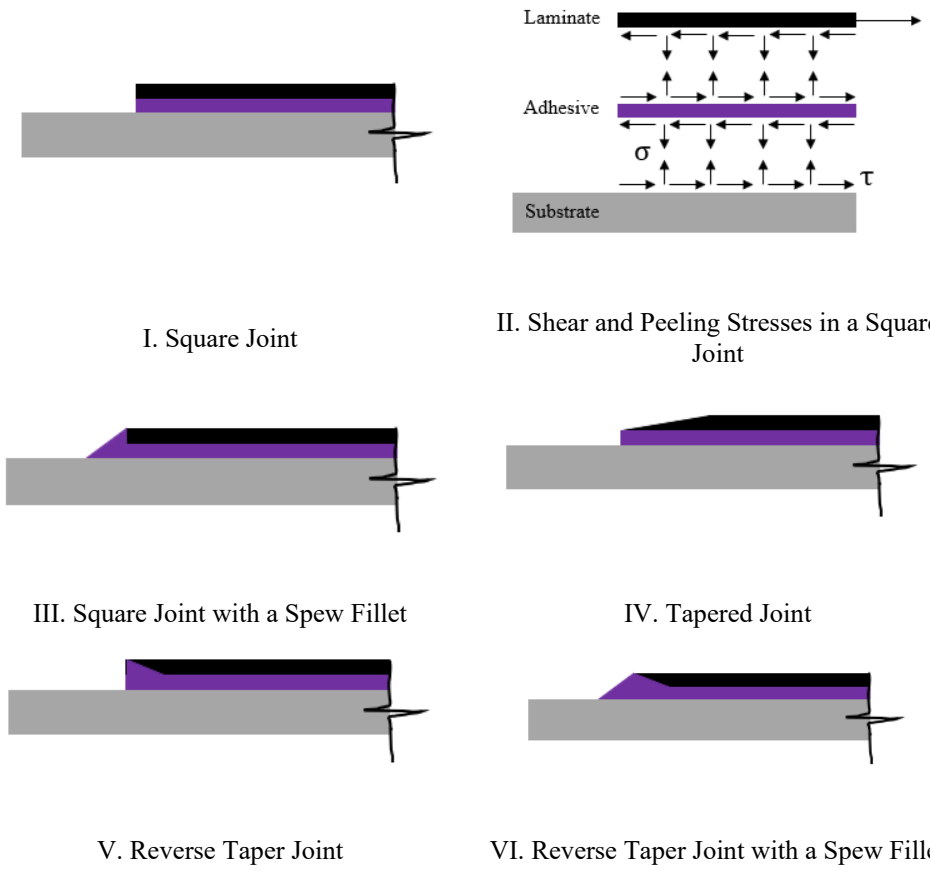

I. Square Joint

II. Shear and Peeling Stresses in a Square Joint

III. Square Joint with a Spew Fillet

IV. Tapered Joint

V. Reverse Taper Joint

VI. Reverse Taper Joint with a Spew Fillet

Figure 7. Different Joint Configurations

Hart-Smith (1973) and Adams and Peppiatt (1974) found that implementing a spew fillet, like the one in Figure 7 III, significantly reduced the peeling stresses at the laminate termination. Adams and Peppiatt specifically looked at implementing a 45 deg spew fillet, which varied in leg size. When the spew fillet was as thick as the laminate, it reduced shear stresses near the end region by over 30%. Belingardi et al. (2002) built upon this work and determined that as the spew fillet's angle became acute, the peeling and shear stresses also decreased. Rizkalla et al. (2008) examined how square joints, reverse tapered joints with spew fillets (shown in Figure 7 VI), rounded reversed taper joints, and mechanical fasteners influenced the bond strength of a joint. All of these end details at least doubled the ultimate loading over the square joint system, where the clamping system tripled that of the square joint. Haghani et al. (2010) compared the strengths of a tapered joint (Figure 7 IV) and a reverse taper joint (Figure 7V). This work's findings indicated that the reverse taper joint was the superior performing joint due to its ability to lower peeling stresses and lower/move the shear stresses' peak location further into the joint.

2.2.8 Environmental Effects

The effects of environmental exposure on a FRP retrofit is a topic of great interest because it informs users how the FRP retrofit is likely to perform over the course of its life in specified conditions. Many environmental variables may affect an FRP retrofit, such as: oxidation, degradation of bond due to time, the influence freeze-thaw has on bonding, performance in extreme temperatures, the effects of chlorides have on bond strength, water ingress' effect on bond, and UV degradation (Zhao 2013). While this research is not focused on a CFRP retrofit's durability, it is essential to verify when and where a CFRP is an appropriate retrofitting material. Researchers have tested all of the environment variables listed above, where these tests were mostly conducted in accelerated laboratory conditions. Accelerated laboratory testing of CFRP

to steel joints allows researchers to subject specimens to precisely controlled variables and report the observed behavior.

Batuwitage et al. (2017) examined the effects of multiple CFRP and glass FRP layers on the impedance of strength degradation when DSJs are subject to an electrochemical salt bath. This process was to help simulate in situ corrosion and exposure to chlorides. As the number of FRP layers increased, there was less strength loss on the DSJs exposed to the accelerated testing. CFRP served as a superior barrier over glass FRPs, because the CFRP starts at a higher initial strength while also providing barrier to the elements. Kim (2017) also tested CFRP DSJs exposed to an electrochemical salt bath, where at 72 hrs of exposure and an 18% loss of steel surface area, the strength of this joint was reduced by 77.7%. However, there was no degradation to the CFRP itself, only the bond to the steel, which is an indication that galvanic corrosion of the CFRP was not an issue. This is a sign that using an insulation material between a CFRP and steel is likely not required. Dawood and Rizkalla (2010) also looked at glass fibers and silane coupling agents as environmental barriers in CFRP DSJs, where the specimens were exposed to wet-dry cycles in salt baths for over six months. DSJs with a silane coupling agent observed minimal strength degradation after six months of exposure compared to the control specimens, while specimens with glass fiber sheets saw a 50% strength loss or more. Nguyen et al. (2012) examined CFRP DSJ's joint strengths, subject to a constant relative humidity of 90% and either a constant temp of 50C or cyclic temperature changes 20C to 50C. Both joint strengths tested were reduced by around 10% after 1000 hours of exposure, but the results showed that the constant vs. fluctuating temperatures had very similar performances. Pang et al. (2019) looked at how 200 freeze thaw cycles affect the bond strength of CFRP single lap joint specimens and individual joint materials' strength. CFRP plates had negligible strengths loss, while adhesive materials lost

around 25% of their tensile strength. The single-lap joint specimens lost approximately 30% of their strength after 200 freeze-thaw cycles. Heshmati et al. (2017) found that CFRP DSJs only received a strength reduction of 11% after being submerged in distilled water for eight months, while DSJs in saltwater observed a 47% loss in strength. Nguyen et al. (2012a) examined the effects of temperature on the joint strength of CFRP DSJs. If adhesive materials are exposed to temperatures at or above that of the adhesive glass transition limit, a DSJ could fail at loads a fraction of the specimens' normal ultimate. All of this research highlights the importance of knowing the intended application of a specific material in a known environment.

2.3 Flexural Retrofits

2.3.1 General

The initial research on structural steel bridge beams with flexural CFRP retrofits looked at big picture topics such as: how well conventional mechanics predicts strengths, what CFRP design/detail parameters work the best, and what kind of behavior can be expected from a retrofit (Mertz and Gillespie 1996). After this proof of concept was shown to be capable of reducing stresses, deflections, and moments on flexural steel members, there was a significant increase in the research around flexural CFRP retrofits. Researchers tested flexural CFRP retrofits on steel in both the laboratory and in situ to examine different variables of interest and observe the CFRP retrofits' behavior. Some important variables (pertaining to this research) researched in a laboratory setting in the last 25 years will be discussed in 2.3.4 Large Scale Laboratory Testing of Specific Parameters. The implementation of CFRP retrofits on actual bridge girders and the behavior these retrofits exhibited will be discussed in 2.3.5 In situ Testing & Field Work. While these are topics are of the most interest relating to this dissertation, it is important to discuss the

potential failure limit states of a flexural CFRP retrofit (2.3.2 Failure Modes) and how these flexural CFRP retrofits are typically designed (2.3.3 Prediction Models). It is worth noting that all the flexural retrofits discussed in this section are considered large scale flexural test specimens, span lengths greater than 5 ft.

2.3.2 Failure Modes

When considering a flexural CFRP retrofit, the different failure modes associated with the flexural CFRP strengthening systems need to be examined. The ideal design can maximize the retrofit's strength and stiffness by mitigating a failure. Even when a CFRP retrofit is operating below the CFRP's limit states, it is important to know what type of failure can be expected if the system is overloaded. Furthermore, if the system is overloaded, a designer can detail the CFRP system so that a specific failure type is achieved. Figure 8 shows a shear and moment diagram of a simply-supported steel girder that had been retrofitted with CFRP on its bottom flange and was subjected to a midspan point load. Figure 8 also shows the typical locations where different types of CFRP retrofit failures can potentially occur:

- Intermediate debond of the CFRP from steel **(**region I**)**
- Debond near CFRP's termination **(**region II**)**
- Rupture of the CFRP **(**region III**)**

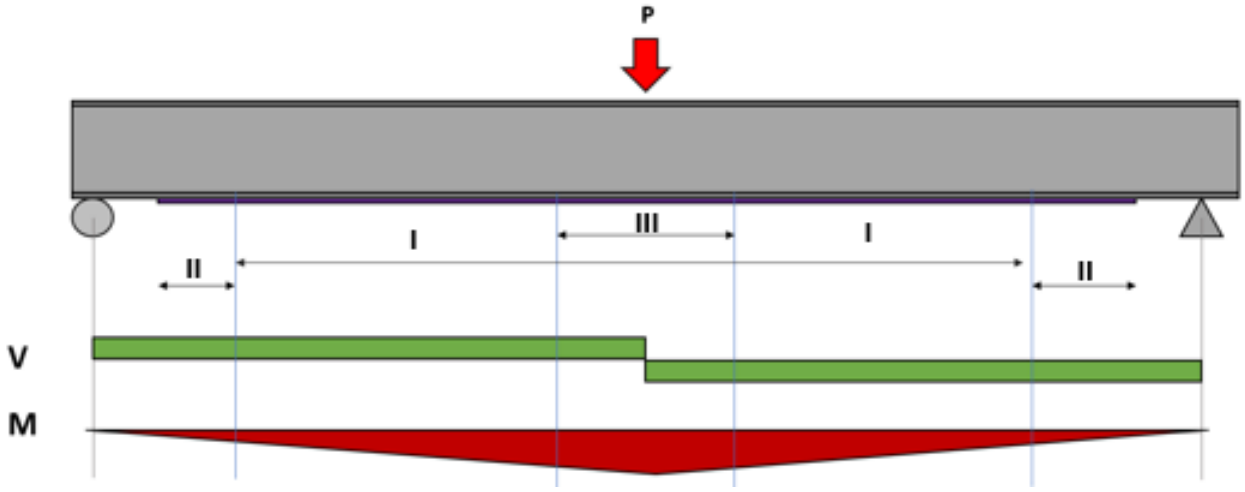

Figure 8. Shear and Moment Diagrams and General Location of Different CFRP Failure Types (Failure mode zones: I. = debonding, intermediate region; II. = debonding, near CFRP terminus, III. = CFRP rupture)

2.3.2.1 Intermediate Debond

Intermediate debond is a failure mode where a FRP bonded to a steel surface initiates some sort of debonding along a flexural member's length. This region is generally located somewhere inside the region I shown in Figure 8. This failure initiation is not located in the end region but typically in areas of high moment. This failure generally initiates at some flaw or damaged region (e.g., voids/cracks in the adhesive or CFRP, notches or cracks in the steel, or localize yield of the steel) (Kim and Brunell 2011a; Kim and Kent 2012; Sallam et al. 2006). The work completed by Kim and Brunell (2011) specifically examined notched steel beams that were retrofitted with CFRP; where the depth of the notches on these steel beams greatly influenced the intermediate debond rate (the rate at which CFRP becomes debonded (unengaged) from a surface) . As the depth of the notch increased, so did the debond rate. Sallam et al. (2006) noted that the intermediate debond occurred at similar strain values for multiple beams, which indicated that there was a critical strain value that causes debond. This initial flaw of the debonded region usually propagates as more load is applied and can eventually cause the entire

CFRP retrofit to debond. This failure progression can be progressive or rapid, depending on the debond region's length/flaw and applied loading. The literature review revealed little research on the topic of intermediate debonding occurring on steel structures retrofitted with CFRP (where some initial flaw was not purposefully created). However, the topic of intermediate debond on reinforced concrete structures retrofitted with CFRP is well documented (Bilotta et al. 2013; Fu et al. 2017; Lu et al. 2007; Teng et al. 2003). The debonding process described above still holds, but the failure initiation is caused by large flexural cracks that open up during the loading of reinforced concrete beams. These crack openings serve as the initiation flaws for debonding of the FRP and adhesives.

2.3.2.2 End Debond

End debond on large scale flexural members have the same stress profiles(normal and shear) as discussed in section 2.2.1 Bond Strength, and employs the same types of fixes to mitigate premature failures as discussed in 2.2.7 CFRP Terminations & Detailing. The major difference between the small single/double lap joint specimens and large flexural members is the difference in applied loading (tensile vs. flexural, respectively) and specimen type. For the most part, the small scale testing is only loaded in tension, while the flexural tests include shear, bending moments, and axial loading for the end debonding calculations. Just like in section 2.2.2 Bond-Slip Models, there are two conventional approaches for determining failure criteria (strength-based and fracture mechanics-based) and a newer method that uses a combination of energy-based and strength-based approaches known as mixed cohesive zone (CZ) modeling.

Roberts (1989) completed some of the first work in the field of civil engineering on the calculation of normal and shear stresses for plates being attatched to reinforced concrete beams in flexure. This derivation can be applied to general forms of loading on beams to calculate the

interfacial shear stress. The derivations of these types of equations to calculate normal and peeling stresses on FRP are a general form that can be used on steel or concrete beams. This research provided the basis for the development of many different analytical solutions for specified and generalized loadings to calculate normal and shearing stresses in a plate bonded to a beam (Colombi and Poggi 2006; Deng et al. 2004; Frostig and Rabinovich 2000; Lau et al. 2001a; Malek et al. 1998; Quantrill et al. 1996; Shen et al. 2001; Smith and Teng 2001; Stratford and Cadei 2006; Taljsten 1997; Varastehpour and Hamelin 1997). More recently, Bocciarelli (2009) expanded upon peeling and shearing stresses to consider the non-linear behavior of steel beams.

Complementing these analytical prediction models, finite element models (FEM) were also created to examine the accuracy of results when studying different geometric parameters subjected to any specified loading (Colombi and Poggi 2006; Teng et al. 2002; Zhang and Teng 2010). The efforts by Buyukozturk et al. (2004) and Zhang and Teng (2010) do a good job at reviewing and discussing some of the shortcomings of these different approaches to calculate normal and shearing stresses.

The most straightforward approach to calculate the failure load of a beam's end region uses the concept of principal stresses near the end region's termination (Adams and Peppiatt 1974; Malek et al. 1998; Schnerch 2005). The recommended design procedures for an analysis of this type can be found in (Schnerch et al. 2007). Normal and peeling stresses for a specific CFRP and adhesive should be verifed through small scale testing. These tested values and the principal stresses determined from testing can be compared against one of the many different strength based prediction models (Colombi and Poggi 2006; Deng et al. 2004; Frostig and Rabinovich 2000; Lau et al. 2001a; Malek et al. 1998; Quantrill et al. 1996; Shen et al. 2001; Smith and Teng 2001;

Stratford and Cadei 2006; Taljsten 1997; Varastehpour and Hamelin 1997) to calculate an ultimate load. Alternatively, these procedures can be applied to FEMs.

When considering using a fracture mechanics-based approach, Buyukozturk et al. (2004) did a good job of reviewing the history and different methods available to carry out an analysis of this type. The initial research utilized linear elastic fracture mechanics (LEFM) with an assumed crack length to estimate an elastic energy release rate (Au and Büyüköztürk 2006; Carpinteri et al. 2009; Hamoush and Ahmad 1990; Hearing 2000; Lau et al. 2001b; De Lorenzis et al. 2010; Rabinovich and Frostig 2000; Rabinovitch 2004; Yang et al. 2006). This release rate was then compared to the fracture energy of adhesive materials being examined. Generally, the overarching goal of this work was to calculate some maximum loading scenario a flexural CFRP retrofit could withstand. Some of this work specifically applied to reinforced concrete beams (Au and Büyüköztürk 2006; Hamoush and Ahmad 1990; Hearing 2000; Lau et al. 2001b; Rabinovich and Frostig 2000; Rabinovitch 2004; Yang et al. 2006), while others considered beams of other types (Carpinteri et al. 2009). Schnerch (2005) has pointed out that these fracture-based approaches have had mixed results in predicting failure loads for FRP strengthened beams, but have worked well to predict fatigue life in steel structures .

Zhao (2013) also pointed out that using interfacial shear stresses alone is likely to underestimate the end debond loading, which is the case for some of these prediction models.

As a means to bridge the gap between a strength-based approach and a fracture-based approach, some researchers have adopted the use of cohesive zone (CZ) models. A CZ model is developed in the same manner as a bond-slip model, where stresses are nonlinearly related to displacements. The area under a stress vs. displacement plot is used to calculate fracture energy, which in turn is used to calculate an ultimate load on a retrofit. Where a CZ model is different

from LEFM is that CZ allows for crack nucleation/growth (debonding) in the stress analysis procedure, and there is not a singularity at the crack tip but rather a damage zone, which is a region near the front of the crack (Anderson 2017; De Lorenzis et al. 2013). CZ models can consider individual types of loading (fracture mechanics loading modes I, II or III) or a combination of different fracture modes, which are referred to as mixed-mode CZ models. A description of mixed-mode CZ models and some examples of these can be found in the work by Högberg (2006). A mixed-mode CZ model's benefit includes both normal and shear failure criteria, which tend to produce more realistic results. Examples of small scale CZ models can be seen in 2.2.2 Bond-Slip Models; however, Yuan et al. (2004) provide a good example of CZ mode II modeling and De Lorenzis and Zavarise (2008) give an excellent view of CZ mixed-mode modeling (). A few analytical studies have examined the failure criteria for large scale flexural reinforced concrete structures strengthened with CFRP, which employed the use of CZ models (De Lorenzis et al. 2013; De Lorenzis and Zavarise 2009; Rabinovitch 2008). Fernando used mixed-mode CZ laws in a FEM to recreate test data from steel beams reinforced with CFRP, where failure initiated from the end region (2010). These prediction models were able to show the end region damage and debond initiation points.

While a strength-based approach and a fracture mechanics-based approach have been discussed to determine the failure criteria for typical end region geometries, it is critical to note the importance of detailing the end region and its effect on the bond strength and behavior of a joint. As discussed in 2.2.7 CFRP Terminations & Detailing, end region geometries can have a significant effect on a joint's strength. The difference in joint strengths behavior is best highlighted by Rizkalla et al. (2008), where specific non-typical end region details doubled the ultimate loading compared to a square joint system. The difficulty in using these non-typical

joints is that analytical prediction models do not exist, become complex, or are too burdensome to evaluate for numerous configurations. However, there are some non-typical joint details that have analytical solutions (e.g., reverse taper) (Schnerch 2005) or FEMs that could be used to calculate shear and normal stresses of the joint's configuration. There is solace in the fact that conventional analytical models (Smith and Teng 2001) give estimations that can only be positively influenced (i.e., reduction in stresses) by a non-typical joint, assuming that joint has been vetted through testing.

2.3.2.3 Rupture

Rupture of a CFRP in flexure is the most straightforward failure mode. As long as end debond and intermediate debond can be avoided, the CFRP's ultimate strain controls the design of the flexural retrofit. These types of failures tend to occur on HM and UHM CFRPs, which generally have lower rupture strains and strengths (Zhao and Zhang 2007). HM and UHM rupture can be observed in multiple researcher's flexural beam tests (Al-Saidy 2001; Lenwari et al. 2005; Peiris 2011; Photiou et al. 2006; Rizkalla and Dawood 2006; Schnerch 2005).

2.3.3 Prediction Models

From an academic standpoint, there are two analytical approaches when designing CFRP retrofits— elastic and inelastic. The elastic and inelastic methods are driven by the material properties that a structure exhibits during its loading. The elastic method uses conventional mechanics on a composite system and assumes the entire retrofitting system remains elastic. This is the design approach used from a bridge owner's perspective because bridge owners are generally not allowed to exceed some percentage of a girder's yield capacity (AASHTO 2018b). A transformed area method, where the CFRP's area is modified by a ratio of the CFRP's elastic modulus to the steel's elastic modulus, has been shown to provide good design results (Hidekuma

et al. 2011; Miller et al. 2001; Nagai et al. 2012). With this information, deflections, stresses, and strains can be calculated for a retrofitted structure as long as the structure remains elastic. Chajes et al. (2005) was able to predict strains on an in-service bridge retrofitted with CFRP within a 9% error.

The inelastic model uses strain compatibility and force equilibrium to calculate a moment strength at a specified strain. While typically bridge beams operate below their yield point, knowing how much residual capacity is left in a newly retrofitted system and at what loading a failure of the retrofit can be expected is still important. This inelastic method is accurate and can account for the steel's plasticity in the retrofitting system (Al-Saidy 2001; Lenwari et al. 2005; Mertz and Gillespie 1996; Peiris 2011; Schnerch et al. 2007).

2.3.4 Large Scale Laboratory Testing of Specific Parameters

2.3.4.1 Bond Length

The bond length on a flexural CFRP retrofit is one of the most important variables which will dictate the ultimate loading and failure mode on a structure. As the end region of a CFRP retrofit is located further away from high moments, the structure's overall capacity goes up, due to the decreasing stresses (normal and flexural) at the location of the CFRP's termination. Increased strength due to increased bond length is best highlighted by Deng and Lee's (2007) work, where steel beams were retrofitted with CFRP of varying lengths and subject to flexural loads. A flexural CFRP retrofit that spanned 90% of the length of a beam compared to a retrofit that spanned 27 % of the length of a beam increased loading by 30% and decreased stresses near the end region by 80%. The increased CFRP length also changed this beam's failure mode from end debond to top flange's local buckling. Other researchers have also verified that longer bond

lengths have led to higher ultimate loads and, if adequately long, can mitigate end debond failure modes (Narmashiri et al. 2012; Yu et al. 2011).

2.3.4.2 CFRP Types

A CFRP's tensile strength and modulus of elasticity is the second most important variable that will dictate the ultimate loading and failure mode on a flexural CFRP-retrofitted structure. In examing Figure 2, a relationship between strength and stiffness of a CFRP can be observed. As a CFRP gets stronger (usually coupled with higher elongation at failure), the CFRP tends to have a lower modulus, and thus, be less stiff. This relationship becomes important when looking at large scale flexural research. CFRPs with low modulus (LM) and normal modulus (NM) material properties tend to fail due to end debonding (Deng and Lee 2007a; Narmashiri et al. 2012; Tavakkolizadeh and Saadatmanesh 2003b; Yu et al. 2011). However, Deng and Lee (2007) did show that debonding failure modes on a NM CFRP can be avoided if the CFRP's bond length is long enough. Tavakkolizadeh and Saadatmanesh (2003) noticed that the effects of a NM CFRP did not significantly impact the elastic stiffening of the retrofitted steel beams. This work also showed that as more plies of CFRP were applied to the retrofitted structure, the increase in strength per applied CFRP ply became less efficient.

In contrast to end debonding of lower modulus CFRPs, HM and UHM CFRPs typically tend to fail in CFRP rupture due to the lower rupture strains of these types of CFRPs, coupled with the reduced normal stress at the ends of the CFRPs (Peiris 2011; Schnerch 2005; Zhao and Zhang 2007). These lower normal stresses are attributed to the use of thinner CFRP plates in HM and UHM retrofits (Peiris and Harik 2018).

2.3.4.3 Strand Sheet

The use of CFRP strand sheets is an emerging application that has slowly been gaining traction over the past five years. Kobayashi et al. (2015) has shown some potential applications (flexural, axial, and shear retrofits) of CFRP strand sheets and their use in the field. To date, all of the in situ CFRP strand sheet's applications have been located in Japan. Hidekuma et al. (2011) made a direct comparison of different types of CFRPs (pre-cured strand sheets, plate material, and uncured sheet material), subject to tensile and flexural loading . The CFRP plates could only achieve tensile strengths associated with 30 to 60 percent of steel yield before the plate materials debonded. The pre-cured strand sheet and uncured sheet material achieved strengths beyond the yielding of steel for both the pure tensile and flexural testing. This work highlighted the importance of impregnation and how bond transfer makes a significant difference in material behavior.

In terms of large scale flexural testing, Nagai et al. (2012) looked at steel beams retrofitted with 10 plies of CFRP strand sheets to investigate how CFRP splices affect bond behavior and what dictates material debond for CFRP strand sheets. The spliced flexural retrofits performed better because these splices allowed for longer bond lengths (no material length constraints) that could locate the CFRP terminations into regions of lower stress. This work also proposed that debond for this HM CFRP was a strength-based failure. Nagai et al. (2012) proposed that debond of this CFRP to steel would occur when the stress of the steel near the CFRPs termination exceded 280 MPa (40.6 ksi). This work also suggested that the debond between CFRP layers is correlated to the steel's stress, which corresponded to CFRP debonding around 310 MPa (45 ksi). A final interesting note about this work is that even if outer layers debonded, the inner plies of CFRP did not debond, and in some cases, were able to achieve CFRP rupture.

Finally, the most recent work on large-scale flexural CFRP strand sheet retrofits on steel beams was completed by Tabrizi et al. (2015). This work examined how normal and high modulus CFRP strand sheets influenced the flexural behavior of steel beams. As expected, the HM CFRP had a much more pronounced increase on the elastic strengthening of the steel beams compared to the NM CFRP; however, shear lag was observed for the HM CFRP. This shear lag indicated that this material was not utilized to its full potential; however, the HM CFRPs were able to increase yield stiffness over the control by over 35% and the post-yield stiffness increased over 200%. There was no indication of shear lag occurring for the NM CFRP. All the tested beams here had the CFRP extend to the beams' supports, and none of the beams failed due to debonding.

2.3.4.4 Fatigue

Fatigue life is extremely important in steel structures or any material prone to cracking that is subject to repetitive loading. Steel bridges have been prone to have significant cracks as a result of fatigue loading (Fisher et al. 1979). As a result, different methods to reduce these stresses on these crack-prone regions have been researched (Fisher et al. 1979, 1980). The Specification for Structural Steel Buildings gives details and design parameters for structural steel subject to cyclic stresses; however, this specification does not extend to externally adhesively-bonded CFRP to steel (AISC 2016). While there are no fatigue specifications on adhesively-bonded CFRP to steel, there has been a fair amount of research on CFRP's fatigue life/performance. CFRP-to-steel-related flexural fatigue research can be broken into two subsets: beams with notches/flaws and beams without flaws. Research examining structures with flaws is a specialized case where the retrofits are subject to extreme loadings to study the viability of CFRP as a means to retrofit fatigue cracked beams (Hmidan et al. 2011; Liu et al. 2009; Nozaka et al.

2005b; Tavakkolizadeh and Saadatmanesh 2003a; Wu et al. 2012b). The beams without flaws can be thought of as general retrofitted beams, where the purpose of testing is to evaluate how fatigue will affect the longevity of the structure (Dawood et al. 2007; Deng and Lee 2007b; Moy 2002; Tabrizi et al. 2015).

When examining notched steel beams, which were retrofitted with CFRP, Tavakkolizadeh and Saadatmanesh (2003a) were able to extend the fatigue life of notched beams by 2.6 to 3.4 times when a retrofitted was applied. These flexural CFRP retrofits also decreased the crack growth rate on the beams. Liu et al. (2009) also observed extended fatigue life on retrofitted flawed steel specimens. The NM retrofits saw an average fatigue life increase of 2.2 times the control, while HM CFRP retrofits observed a fatigue life increase of 4.7 times that of the control. Wu et al. (2012b) looked at different crack bridging media (CFRP, basalt fiber, and steel plates) to complete flexural fatigue retrofits. The fatigue life of a notched steel beam retrofitted with CFRP was around 3 to 5 times that of the control beam, whereas the fatigue life of the steel beam retrofitted with a welded steel plate was only 1.74 times that of the control beam. Lastly, Nozaka et al. (2005b) developed an equation to calculate the effective bond length of CFRP needed to repair a crack in bridge girders. This work was verified through laboratory testing and provides good information on strain distribution in these types of retrofits.

This paragraph pertains to research where no notches or cracks were present during the fatigue testing of CFRP retrofits. Mertz et al. (2002) tested two corroded American standards I I-shaped (24 X 80) steel bridge girders, from their previous research (Mertz and Gillespie 1996), which examined the fatigue life of the CFRP retrofits. The corrosion damage on these beams had no detrimental effects on the CFRP's strength/stiffness even after 10 million stress cycles, simulating 4.6 years of average daily truck traffic. Deng and Lee (2007b) looked at

undamaged/unnotched steel beams retrofitted with flexural CFRP. These beams were loaded cyclically with a percentage of their static failure load until the CFRP retrofit failure was observed. When the debonding failure occurred in the retrofit, the debonding cracking initiated more due to the opening (mode I) than that of shearing (mode II) loading. Based on S-N curves generated from the data, the researchers recommended an unlimited fatigue life limit of 30% of the ultimate load. It should also be noted that this work did not examine bond length as part of the study, so the results here are dependent on these exact parameters. Dawood et al. (2007) examined undamaged composite concrete-steel beams, which were retrofitted with CFRP that extended to the supports and loaded cyclically. All the retrofitted beams achieved 3 million cycles at 60% of the beams yield before the beams were loaded statically until failure. The failure mode was concrete crushing. The big difference between the CFRP-repaired beams and the control was that the deflection in the control beam was much greater than that of the CFRP beams. The CFRP-strengthened beams likely delayed the concrete deck's fatigue creep behavior, giving a better overall performance. Tabrizi et al. (2015) completed very similar work to (Dawood et al. 2007), except that the CFRP used was HM CFRP strand sheets. The specimens were fatigued for 2 million cycles at loadings associated with 80 percent of yield. Little to no effects on the CFRP retrofits due to fatigue were observed. Lastly, while not specifically examining fatigue life, Moy (2002) looked at how cyclic loading affected CFRP's adhesive ability to cure when subject to different stress ranges. Moy found that the bond will fail to develop if deformation in the adhesives are too large and that cyclic loading reduced the bond strength. Limits on the amount of stress that would disrupt bond behavior were not suggested based on the limited amount of data; however, this is a topic of high interest to consider when applying retrofits on beams in situ.

2.3.4.5 Corroded Specimens

CFRP manufacturers, Milliken and Sika, suggest that themaximum out-of-plane deviations for metallic surfaces on which a CFRP retrofit will be adhered to should be any visible deviations and 0.04 in, respectively (Milliken Infrastructure 2017; Sika 2014b). However, in the cases of corrosion, Having a surface fitting these rigorous tolerances is unfeasible if not impossible. The limited research that has applied CFRP retrofits on full-scale flexural testing with excessively roughened/corroded profile has little documentation on what that corrosion actually looks like. The I-beams in the previously mentioned Mertz and Gillespie study (1996) were reported as having nonuniform and pitted surfaces with evenly distributed corrosion along the tension flange. The DelDOT inspection report estimated 40% section loss and the experimental stiffness loss for the girders was around 30%. These retrofitted girders were able to achieve strengths above that of the original uncorroded girders, and the CFRP strengthening system remained intact as the girders failed due to lateral-torsional buckling. Mertz et al. (2002) tested the fatigue life of CFRP retrofits on two more corroded American standard I-shaped (24x80) steel bridge girders . This corrosion damage had no detrimental effects on the CFRP's strength or stiffness even after 10 million stress cycles, which simulated 4.6 years of average daily truck traffic. Chajes et al. (2005) were able to reduce strains using CFRP on a structurally deficient steel through-girder bridge; however, the extent of the corrosion damage was not documented.

2.3.4.6 Simulated Corroded Specimens

Due to the difficulty of finding corroded steel members of the same size and relative amounts of corrosion damage, researchers have opted to create “simulated” corrosion damage on steel beams (Al-Saidy et al. 2004; Kim and Brunell 2011a; Liu et al. 2001). This corrosion is not conventional because it does not have a variable roughness along the length of a girder but has a

section of steel removed from an area to represent localized section loss. Generally, these are steel beams that were obtained directly from a steel mill or manufacturer. This type of research focused on the retrofit behavior rather than that of the effects a corroded surface profile has on strength.

Liu et al. (2001) removed 4 in sections of the tension flange of steel beams (at midspan) to see how different CFRP retrofit configurations would influence bond length, flexural strength, and the beam's general behavior. The lesser performing retrofit was able to increase elastic strength by around 8%, where all the retrofits failed due to CFRP debonding near the notch. The authors suggested that glass fiber wraps should be tested as a debond mitigation strategy in the future to prevent early debonding. Al-Saidy et al. (2004) also tested flexural CFRP retrofits, where up to 75% of the tension flange's width near the midspan of the beam was removed. These retrofitted structures were able to regain strengths above 6 to 26% of the original girders' capacity. No debonding of the CFRP plates were observed during testing. The controlling failure modes for these failed beams were concrete crushing and CFRP rupture. Finally, Kim and Brunell (2011b) statically tested steel beams that had notches of varying sizes, which were repaired with CFRP. These retrofits increased the damaged beams' strengths by 22%, and debonding propagated from the crack opening. An interesting point about this research was that debonding failures were independent of the cracks' size and depth.

2.3.5 In situ Testing & Field Work

There have been many effective research studies conducted on the flexural strengthening/retrofitting of in situ bridges comprised of steel beams with CFRP (Chajes et al. 2005; Mertz et al. 2002; Miller et al. 2001; Moy 2002; Moy et al. 2000; Peiris 2011; Phares et al. 2003; Wipf et al. 2005). The vast majority of these bridges were proof of concept and had little

to no structural damage that required a CFRP retrofit. However, these studies do provide data points that CFRP retrofits are capable of reducing stresses, strains, and deflections on a steel bridge structure.

Moy et al. (2000) retrofitted cast iron cruciform railway struts with CFRP to increase their design life. These retrofits increased strength by 10 to 39% and increased the struts' design life by an estimate of 40 years. Another benefit of this process was the non-invasive nature of the retrofits; no closings were required for the install. Miller et al. (2001) strengthened a steel-concrete composite bridge beam in Delaware to serve as a case study on strengthening and application procedures. The CFRP retrofits reduced strains by 10% and increased stiffness by 11% during the live load testing. Chajes et al. (2005) completed CFRP retrofits on the floor beams of a steel through-girder bridge to see how these retrofits would affect the bridge's overall behavior. The CFRP retrofits reduced stresses in the retrofitted beams by 5% and increased the distribution factors in the retrofitted beams. Peiris (2011) applied UHM CFRP retrofits on a load posted integral abutment steel bridge to see what kind of strength could be added to the bridge . Part of the retrofit procedures included converting the non-composite concrete decking into a composite steel-concrete system and then applying the retrofit. The shear stud retrofit decreased deflections by 27%, while the UHM retrofits decreased deflections by 5%. This work also created a FEA model that was utilized to calculate the bridge's current rating factor and allowed for the changing of CFRP-related variables to see their influence on the bridge’s rating factor.

CHAPTER 3: Small Scale Laboratory Testing – Bond Strength Investigation

Chapter 3 consists of the manuscript: "The Influence of Surface Roughness and CFRP Material Types on Effective Bond Properties." This paper is currently in preparation for submission to the 2021 International Bridge Conference.

The Influence of Steel Surface Roughness and CFRP Material Types on Bond Properties

SAMUEL SHERRY, & MATTHEW HEBDON,

Virginia Tech, Blacksburg, VA

3.1 Abstract:

This paper provides an evaluation of the difference in bond behavior between a normal modulus carbon fiber reinforced polymer (CFRP) plate material and a high modulus CFRP strand sheet. Their bond behavior relative to simulated corrosion (surface roughness) was also analyzed. Comparable amounts of normal modulus and high modulus CFRP were applied to double strap joint (DSJ) specimens and tested in tension until failure. The high modulus strand sheet material achieved higher loads, shorter effective bond lengths, and more uniform strain distributions along the bond length of the DSJ compared to the normal modulus plate material. This paper additionally focuses on evaluating how simulated pitting corrosion affected the two CFRP bond strengths. A 2.2% mass section loss had negligible effect on the ability of either CFRP to achieve their ultimate bond strengths. The only impact the simulated corrosion had was on the CFRP system with a more ductile adhesive, which increased the displacement at failure by 12.5% compared to the control specimens with no section loss.

3.2 Introduction

The use of carbon fiber reinforced polymer (CFRP) materials on steel structures in civil engineering has been investigated for the past 25 years (Chajes et al. 2005; Mertz and Gillespie 1996; Moy et al. 2000; Phares et al. 2003; Wipf et al. 2005). The high strength-to-weight ratio of the materials, low installation costs, resistance to fatigue, corrosion resistance, ease of installation, and ability to retrofit a structure with minimal impact on users or traffic are all major benefits for CFRP implementation. This highly tailorable material can be applied in both shear and flexural applications. Nippon Steel developed a high modulus (HM) CFRP strand sheet, which is novel because it combines the high stiffness of a HM CFRP with that of the versatility of a sheet-like material (Milliken Infrastructure 2017). The HM strand sheet was developed by Sika and was tested against a normal modulus (NM) plate material to compare the relative bond performance. This research's primary objective was to examine bond performance and determine how well the bond prediction models work for the newly developed HM CFRP strand sheet. In addition, steel specimens with variable corrosion section loss levels were tested to determine the influence of a non-uniform surface roughness on bond strength.

3.2.1 CFRP Material Properties

Various CFRP materials are available (plates, rods, sheets), but one of the primary differentiating characteristics is how the fibers in the CFRP are saturated within an adhesive and cured. Different CFRP materials can be seen in Figure 9. When producing CFRPs, the saturation and curing process can either be completed at the manufacturer's facilities or in the field. These two curing methods/locations are referred to as pre-preg (pre-impregnated at a manufacturer's facilities) and field-preg (field impregnated in situ). A pre-preg plate and a field-preg sheet

CFRP is shown in Figure 9, items A. and C., respectively. Pre-preg is an industry term, but field-preg is a nomenclature adopted for this paper. The pre-preg process allows for a controlled fabrication process which typically results in higher levels of quality and consistency in the product. While not as precise, the field-preg process can be customized to almost any desired shape as well as accommodate in situ conditions. In 2017, Nippon Steel developed CFRP strand sheets that combine pre-preg quality and field-preg customization (Milliken Infrastructure 2017). The CFRP material consists of pre-preg strands (or rods) that are bound together by a plastic string to form a sheet-like material, shown in Figure 9 B. This CFRP material is highly tailorable in one direction, transversely to the direction of the strands. In contrast to HM strand sheets, a conventional CFRP plate like the one shown in Figure 9 A, Sika Carbodur CFRP, generally comes in specified manufactured widths. Two downsides of a plate material are that it is more difficult to cut to a specified width and cannot conform to any shape other than a relatively flat surface. Another major difference between a plate material and a strand sheet is its location relative to adhesives. A plate material generally sits on top of an adhesive, while a sheet material is embedded into the adhesive. The location of the CFRP relative to the adhesive can have a significant effect on bond behavior. While there are many distinct differences in CFRP types, generally, the retrofit application dictates which material will be used.

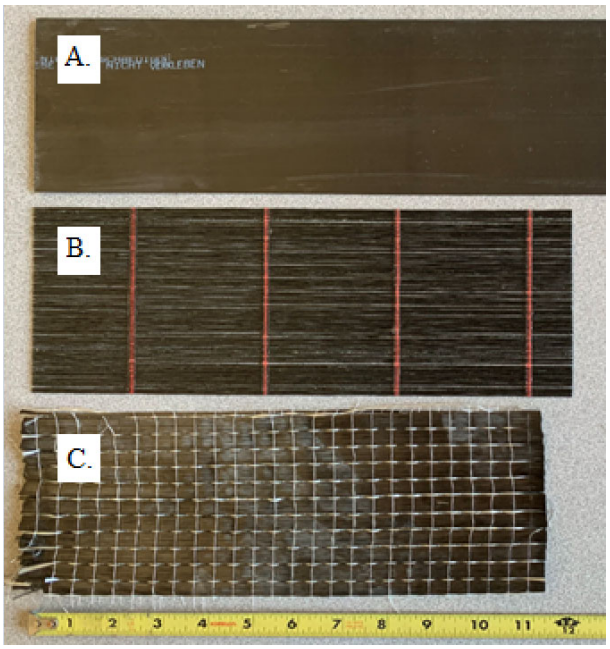

Figure 9. Different Types of CFRPs (A. = Prepreg Plate Material, B = Prepreg Strand Sheet, C. = Unimpregnated Fiber Sheet)

There are large variations in the elastic modulus of different CFRP materials (where this research only considers the gross area of the material). Researchers and manufacturers (Fawzia 2007; Kazem et al. 2016; Milliken Infrastructure 2017; Peiris 2011; Schnerch and Rizkalla 2008; Sika 2011) use different elastic modulus ranges to delineate where HM naming convention starts and NM ends. This paper has adopted Peiris' (2011) nomenclature created for CFRPs with different elastic moduli. This nomenclature divides the CFRP types into low, normal, high, and ultra-high moduli. The associated naming convention with the elastic modulus ranges are shown in Table 1.

Table 1. CFRP Naming Convention

Naming Convention	Elastic Modulus Range (ksi)
Ultra-High Modulus (UHM)	Greater than 58,000
High Modulus (HM)	29,000 to 58,000
Normal Modulus (NM)	14,500 to 29,000
Low Modulus (LM)	0 to 14,500

3.2.2 Theoretical Failure Modes

In order to understand whether a CFRP reinforced structure is failing prematurely, it is crucial to understand the subtlety in the different failure modes that can occur in a CFRP retrofit. Understanding the failure modes can tell a lot about the structure and how/why it failed. The potential failure modes of fiber-reinforced polymers (FRPs) to steel composites subject to loading (shown in Figure 10) include the following (Zhao and Zhang 2007):

a) Adhesion failure between steel and primer

b) Adhesion failure between the secondary adhesive and FRP primary adhesive

c) Adhesion failure between FRP and FRP primary adhesive

d) FRP delamination

e) FRP rupture

f) Adhesion failure between priming adhesive and insulating material

g) Cohesion failures

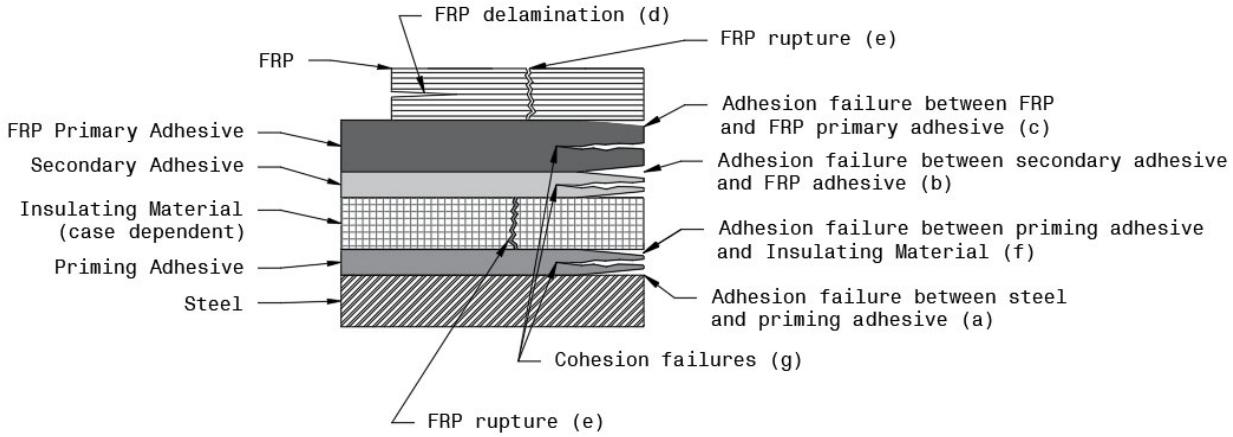

Figure 10. Failure Modes of FRP Composites

3.2.3 Effects of Moduli on Bond Performance

The higher the elastic modulus of a CFRP, the smaller the required effective bond length of a CFRP laminate bonded to steel (Al-Mosawe et al. 2015; Fawzia et al. 2005, 2006). The effective bond length is the shortest length of a CFRP joint that will develop the highest obtainable load in a CFRP system (Chen and Teng 2001). Ultra-high modulus and high modulus CFRPs tend to rupture once they exceed their effective bond length, while normal and low modulus CFRPs typically fail due to adhesive debonding (Al-Mosawe et al. 2015). While UHM and HM CFRPs can achieve their ultimate tensile strengths, these strengths are generaly half that of a normal modulus CFRP. In general, as CFRPs' stiffness increases, their tensile strength and failure strain tend to decrease. Figure 11 shows the difference between the strength, stiffness, and ultimate elongation behavior between a HM (Nippon), NM CFRP (Sika), and A36 Steel.

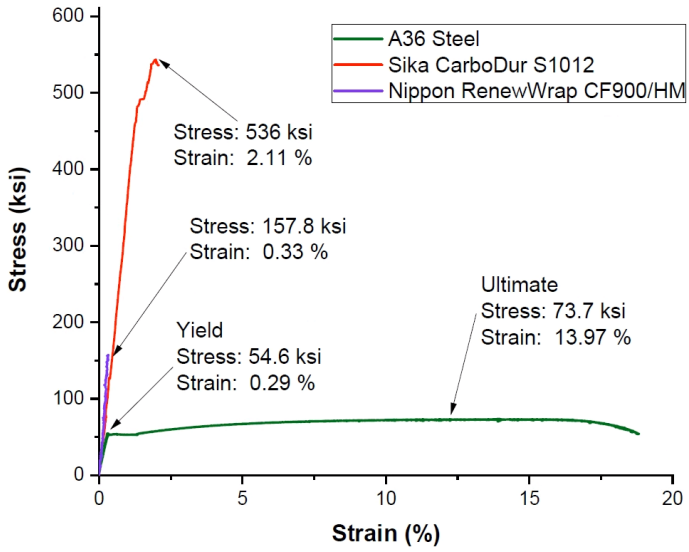

Figure 11. Stress-strain Plot of CFRP Materials Tested in this Research (Compared Against an A36 Steel)

3.2.4 Effects of Adhesives

The amount and type of an adhesive in a CFRP material can directly influence the overall strength and ductility of a joint's capacity. Xia and Teng (2005) examined the bond strength of three different adhesive materials of varying thicknesses on the same CFRP material attached to steel. The bond strength of the double strap joint (DSJ) specimens increased for adhesive thickness up to 0.0787 in, after which the bond strength began to decrease. As the material properties of an adhesive become increasingly ductile, the failure type of single lap and double lap joints transition from an adhesive failure to a cohesive failure (Jiao and Zhao 2004; Wu et al. 2012a; Xia and Teng 2005). Cohesive failure types are desirable because conventional calculations can solve for this failure load through bond modeling.

3.2.5 Effects of Surface Preparation/Roughness

Ideal bond strengths can be achieved as long as initial surface preparation is performed to clean the steel surface and remove dirt, grime, rust, and mill scale (Fernando et al. 2013; Kim et al. 2011; Schnerch et al. 2007). Almost all cleaning forms (needle gun, sanding, grit blasting, and grounding) assist in achieving adequate bond strengths; however, grit blasting has been found to be the best performing cleaning method.

Macroscale surface roughness (surface depth deviations greater than 0.00158 in) are also important to consider when examining the strength of a joint (Haghpanah et al. 2014; Li et al. 2019; Xu et al. 2020). Generally, as the corrosion/surface roughness of a joint becomes more pronounced, the bond strength of a joint increases. Xu et al. (2020) showed in their testing that mass loss below 10% had a small effect on increasing the strength of a joint; however, mass loss over 27.5% gained no additional strength. The increase in roughness also increased the ductility of a joint and decreased the required "effective bond length" of bonding.

3.2.6 Bond Strength

Bond strength is the most important metric when designing a FRP-to-steel bonded joint, as it dictates the ultimate load of a joint. There are two conventional methods of calculating bond strength: a strength-based and a fracture mechanics-based approach. Buyukozturk et al. (2004) reviews both of these methods and the different prediction models that researchers have used to calculate bond strengths. The strength-based approach assumes ultimate bond strength occurs when the adhesive in the joints reaches a maximum strain or stress (Adams and Peppiatt 1974; Hart-Smith 1973; Volkersen 1938). The fracture mechanics-based approach assumes ultimate bond strength is related to interfacial fracture energy (Fawzia et al. 2010; Fernando 2010; Xia

and Teng 2005; Yuan et al. 2001). The strength-based and fracture mechanics-based approaches both have unique simplifying assumptions that need to be noted when examining these bond strength prediction models.

Historically, researchers used a strength-based approach to calculate the failure load associated with an adhesively bonded joint (Goland and Reissner 1944; Volkersen 1938). The failure criteria for these strength-based approaches typically depend on a maximum stress. Newer models have built off this work to consider more variables and fix equilibrium violations (Hart-Smith 1973; Ojalvo and Eidinoff 1978; Sayman 2012; Tsai et al. 1998). These models work well but get increasingly more complex as more variables are considered.

Instead, others have proposed different models using fracture mechanics to calculate the bond strength of these FRP bonded joints, either considering many variables or comprising entirely of empirical equations (Chen and Teng 2001; Xia and Teng 2005; Yuan et al. 2001, 2004). The big difference between the strength-based and fracture mechanics-based approaches is the failure criterion stress/strain versus interfacial fracture energy. It should also be noted that the fracture mechanics-based approach only considers a shear-type failure (Mode II – shear loading). One of the more popular models for CFRP adhered to steel was created by Xia and Teng (2005), which looked at bond-slip curves to calculate the ultimate strength of a joint; this approach is also referred to as bond-slip modeling. Fawzia et al. (2010), Fernando (2010), and Wu et al. (2012b) all built upon the work completed by Xia and Teng (2005) to create new prediction models. These new prediction models include the use of non-linear adhesives, different modulus CFRPs, and multiple plies of CFRPs. These models can predict the ultimate strength and effective bond length when supplied with material properties.

3.3 Objectives

This research was primarily focused on the bond behavior of a new HM strand sheet. The HM strand sheet analysis was completed through the use of small-scale testing and was compared against the testing of a NM CFRP plate. The NM and HM material utilized conventional bond strength prediction models(strength and fracture mecahnics based) to determine how accurately they could predict these materials' ultimate tensile strengths. Lastly, the NM and HM CFRPs were tested on steel specimens with and without representative simulated pitting corrosion to see how surface roughness affected the bond behavior of these materials.

This research had four key objectives:

1. Determine the effective bond length of the two CFRP materials, NM plate and HM strand sheet, as well as how conventional bond strength models predict that effective bond length and ultimate bond strength .
2. Examine and analyze the bond properties and performance of Nippon Steel's new HM strand sheet compared to that of the NM plate material.
3. Determine how different parameters (CFRP type, adhesive type, bond length) affect bond behavior, strength, and stiffness of these different CFRP-steel bonded system.
4. Determine how much impact corroded surfaces have on bond strength or stiffness.

3.4 Specimen Design

This research employed small-scale testing using DSJs. The DSJs give information about bond behavior, effective bond length, and the ultimate load of the joint.

3.4.1 Specimen Layout

A plan and profile view of a typical doubles strap joint (DSJ) specimen is shown in Figure 12. The steel plates used to make these specimens were A36 Gr.36 with a width of 2 in and thickness of 0.5 in. The term "Le" in Figure 12 is the bond length of the DSJ and will be used in its naming convention. Various Le were tested to determine the effective bond length of the different CFRPs tested in this research. One end of the DSJ joint had a CFRP bond length that was 1.5 times longer than the other to intentionally force failure in the shorter bond length region, which had simulated corrosion and was instrumented with strain gauges.

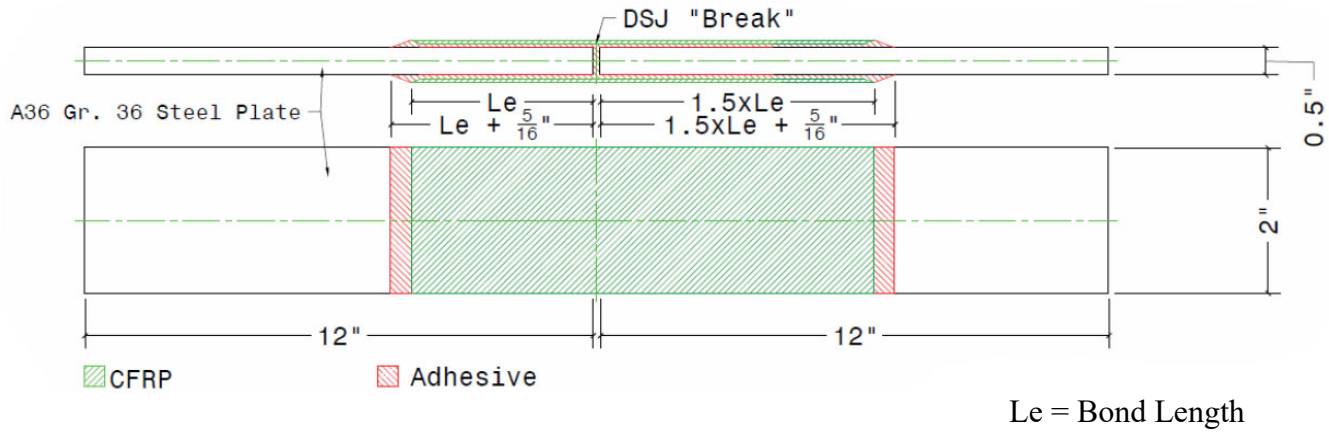

Figure 12. DSJ Typical

3.4.2 Simulated Corrosion

This study compared various bond lengths on grit-blasted control DSJs without corrosion to grit-blasted DSJs with corrosion that had simulated pitting and section loss achieved through a machining process. The comparison helped examine the effects of corrosion and section loss on the bond length and ultimate strength of CFRPs bonded to steel. In carrying out this experiment, a targeted corrosion profile was selected after a statistical analysis of five surface profile samples

taken from retired Virginia Department of Transportation (VDOT) steel beams. One of the five analyzed sample surfaces is shown in Figure 13. Digital images of the steel surfaces were scaled and digitized to quantify the pitting diameters and pitting frequency.

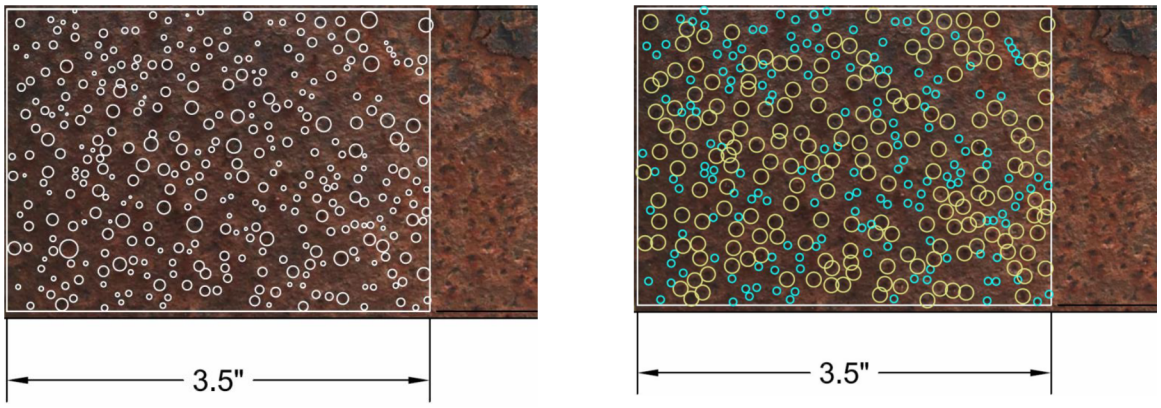

I. Superimposed Corrosion Pitting Diameters

II. Simplified Superimposed Corrosion Pitting Diameters

Figure 13. Corroded Steel Profiles Used to Create Simulated Corrosion for Testing

The researchers selected two representative simulated corrosion pitting diameters based on histogram data for all five samples and an iterative binning process: 0.125 in and 0.0625 in. The frequency of each of these pit diameters in an area of 8.75 in^2 was 206 and 194, respectively. The pitting was then redistributed from the most common pit diameters in Figure 13 I to either 0.125 in or 0.0625 in diameters, as seen in Figure 13 II. This profile was repeated and translated accordingly to meet the needs of the DSJ specimens.

Depth measurements of each of the pits were captured using calipers, where the pit depth was calculated by taking a non-pitted profile and subtracting it from the measured depth of corrosion pitting. The average pit depth was measured to be 0.016 in. Using this average depth and the

quantity and distribution of simulated pitting diameters, a 3D rendering of the surface profile was created and loaded into a computer numerically controlled (CNC) milling machine to fabricate the specimens. The simulated pitting distribution and depth resulted in an equivalent mass loss of 2.2 %. The DSJ specimen with simulated corrosion is shown in Figure 14.

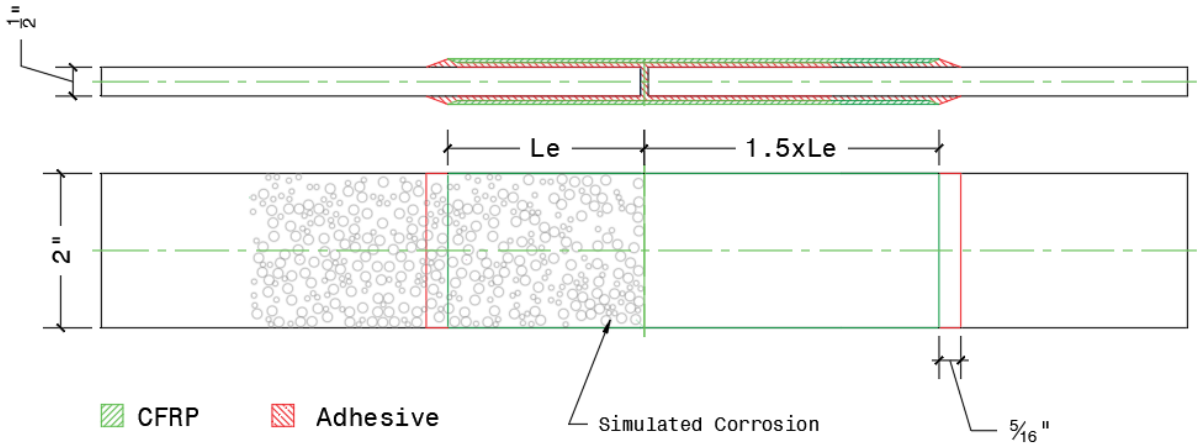

Figure 14. DSJ Specimen with Simulated Corrosion

3.4.3 Material Properties

In this research, two different CFRP strengthening systems were selected, denoted by Sika and Nippon, their respective manufacturers. The CFRP and adhesive components that make up these overall systems are listed in Table 2.

Table 2. Components that Comprise the Sika and Nippon Strengthening Systems

Component	**Strengthening Systems**	
	Sika	*Nippon*
Steel Priming Adhesive	SikaDur 330	Renew Wrap Strand Sheet Adhesive (FP-WE7)
Insulation Material	SikaWrap Hex 106G	NA
Primary Adhesive	Sikadur 30	Renew Wrap Strand Sheet Adhesive (FB-E7S)
CFRP	Sika CarboDur Type S 1012	Renew Wrap Strand Sheet CF900/HM

The significant differences between the Sika CarboDur Type S 1012 and Renew Wrap Strand Sheet CF900/HM CFRP materials was their strength/stiffness and type. The Sika CarboDur Type S 1012 had a modulus of elasticity similar to that of steel (26,930 ksi), while the stiffness of the Renew Wrap Strand Sheet CF900/HM was around 1.77 times higher (47,575 ksi). The material properties and product dimensions of these strengthening systems were obtained through laboratory testing and are found in Table 3. The Sika CarboDur Type S 1012 is a pre-preg CFRP plate; while the Renew Wrap Strand Sheet CF900/HM is a CFRP sheet made up of individual pre-preg strands that have been joined by adhesive strips running perpendicular to the longitudinal direction of the CFRP. The Sika CarboDur Type S 1012 and Renew Wrap Strand Sheet CF900/HM materials are shown in Figure 9 A. and B., respectively. As a result of this, the Sika CarboDur Type S 1012 lays on top of the joining adhesive, while the Renew Wrap Strand Sheet CF900/HM is embedded into the joining adhesive (the adhesive can seep through the gaps between the strands). The bond behavior of the Renew Wrap Strand Sheet CF900/HM is the area of most interest, and the Sika CarboDur Type S 1012 provides a good baseline for comparison against the "unconventional" Renew Wrap Strand Sheet CF900/HM CFRP.

Table 3 Material Properties of the Strengthening Systems

Property or Dimension	**Sika**		**Nippon**	
	CFRP	*Adhesive*	*CRFP**	*Adhesive*
Tensile Strength (ksi)	536	3.2	157.8	5.8
Modulus of Elasticity (ksi)	26,930	1,643	47,575	896
Elongation at Break (%)	2.11	0.23	0.33	1.18
Thickness (in)	0.047	--	0.057**	--
Width (in)	3.94	--	19.7	--
Length (ft)	100	--	10	--

* Material properties based on the diameter of a strand (13 strands per in of width)
**Diameter

3.4.4 Effective Bond Length Design

The effective bond lengths and ultimate load for each strengthening system were calculated using two prediction models (Hart-Smith 1973; Xia and Teng 2005). Unconventional/non-typically given material properties(shear strength, failure displacements, and poissons ratio) were calculated based on the literature (Fawzia et al. 2010; Fernando 2010; Hart-Smith 1973; Xia and Teng 2005). The results from the calculations are shown in Table 4. At the time of the design, the material properties were calculated without having critical information supplied by the manufacturer or found in the literature to calculate effective bond length. Estimations of the critical material properties provided the necessary insight into how prediction models would work. An effective bond length of 2.5 in was selected for both the Sika and Nippon specimens. This length was close to the median calculated bond length and provided a direct comparison between strengthening systems.

Table 4. Calculated Effective Bond Lengths and Ultimate Loads

Prediction Model Used	Literature used to Predict Material Properties	Sika		Nippon	
		Effective Bond Length (in)	Ultimate Load (kip)	Effective Bond Length (in)	Ultimate Load (kip)
S.H. Xia and J.G. Teng (2005)	S.H. Xia and J.G. Teng (2005)	2.73	18.05	3.3	27.7
S.H. Xia and J.G. Teng (2005)	Fawzia et. Al (2010)	2.43	19.76	2.8	29.2
S.H. Xia and J.G. Teng (2005)	Fernando (2010)	1.09	8.015	5.3	49.8
L.J. Hart-Smith (1973)	L.J. Hart-Smith (1973)	1.73	11.28	3.05	31.34
Average Values		2.00	14.28	3.61	34.5

3.5 Experimental Investigation

3.5.1 Test Matrix

In total, 40 DSJ specimens were tested, which included 20 specimens for each strengthening system (Nippon and Sika). Ten specimens had simulated corrosion, and another 10 were uncorroded (control specimens). The 10 control and 10 simulated corrosion specimens had five different bond lengths tested, ranging from 0.5 in to 4.5 in in 1-inch increments. The incremental changes in length were used to determine the effective length of the CFRP retrofitting systems. The complete DSJ testing matrix is shown in Table 5. The naming convention used to denote DSJ specimens indicates which strengthening system was used, bond length, specimen number, whether it was a control specimen or a simulated corrosion specimen, and if the specimen had an array of heavy or light strain gauges. These gauges were used to calculate bond slip paramiters of the joints. Figure 15 shows the naming convention for the DSJ specimens.

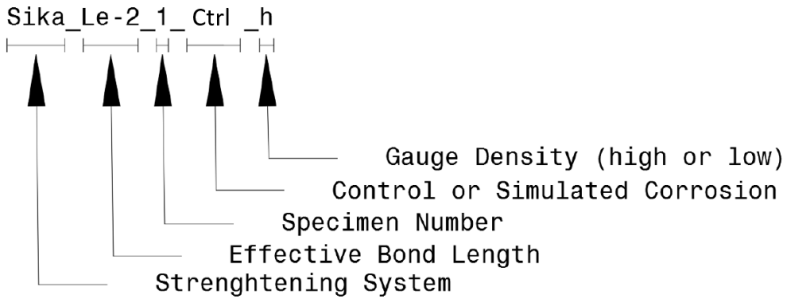

Figure 15. DSJ Naming Convention

3.5.2 Test Setup

All small-scale testing was completed on an MTS Landmark 370.50 universal testing machine with a 110 kip capacity and hydraulic wedge grips (shown in Figure 16). Load and crosshead displacement data was collected at a rate of 10 Hz. These tests were displacement-controlled, conducted at a rate of 0.005 in/min in tension. Termination of testing was controlled by the total debonding or rupture of the CFRP, indicated by a near-zero load.

Figure 16. MTS Landmark 370.50 Testing a Double Strap Joint

3.5.2.1 Instrumentation

Foil strain gauges were used on the DSJ specimens to measure bond slip. The gauges were placed on the longitudinal centerline of the CFRP and spaced evenly along its bond length. The gauges are named for their material and location along the bond line length. On the DSJ specimens, the first gauge is FRP_0 (located at the DSJ joint), and the last gauge is Steel_5, located at the end of the DSJ. Not all specimens have the same amount of strain gauges. Specimens with a high density (denoted as "h" at the end of their naming convention) have five CFRP gauges and one steel gauge. Specimens with a low density (denoted as "l" at the end of their naming convention) have two CFRP gauges (located at the ends of the CFRP (FRP_0 and FRP_4) and one steel gauge. The high density specimens were used to investigate bond slip behavior of the joint while the low density specimens were used to verify mechanical behviour of the joint. The strain gauge layout is shown in Figure 17.

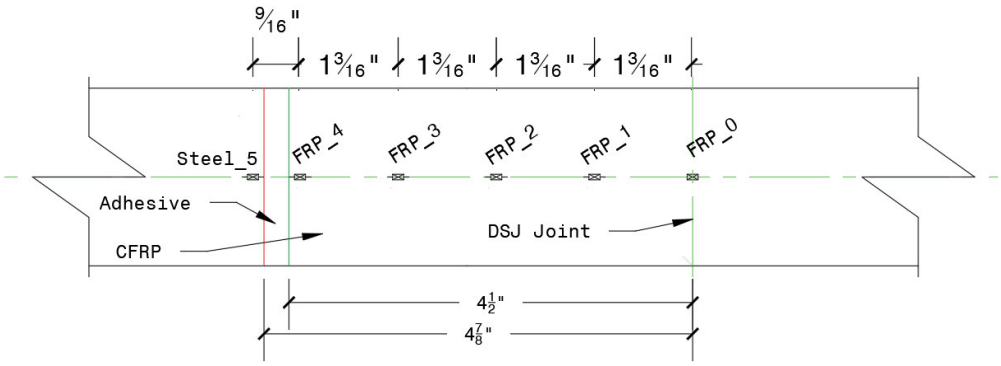

Figure 17. Example Locations of Strain Gauges (DSJ Le+2_1_Ctrl._h)

3.6 Results and Discussion

3.6.1 Experimental Failure Modes

Figure 18 shows the different types of failure modes that were observed during this testing.

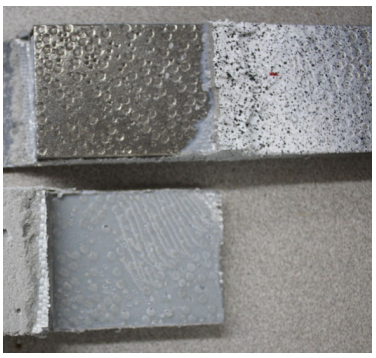

I. (a.) Adhesion failure between steel and priming adhesive

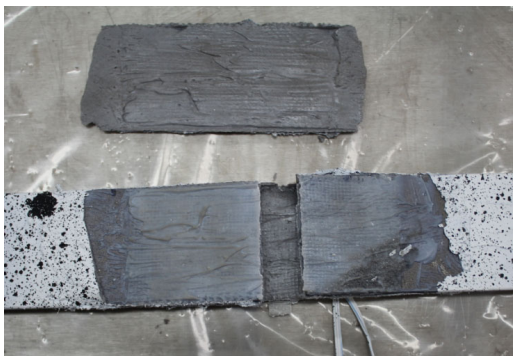

II. (b.) Cohesion failure between priming adhesive and FRP adhesive

III. (c.) Adhesion failure between FRP and FRP adhesive

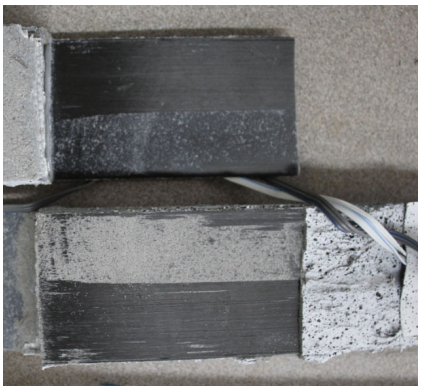

IV. (d.) FRP delamination

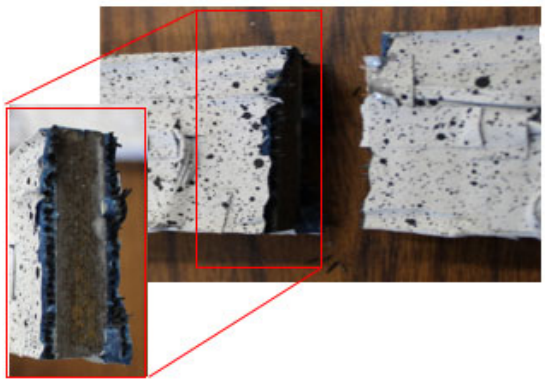

V. (e.) FRP rupture

Figure 18. Failure Modes of CFRP Specimens Observed Over the Course of Testing (Letters Correspond to Failure Types in Table 5)

3.6.2 Performance of Double Strap Joint Specimens

There was one Nippon specimen whose data was disregarded (data indicated as "--" in Table 5). The Nippon LE_1_Cor._h DSJ was loaded improperly, and its data provided no meaningful results. The peak loads, corresponding displacements, and failure modes for each of the DSJ specimens are shown in Table 5.

Table 5. DSJ Test Parameters and Results

Specimen Name	*Bond Length (in)*	**Sika**				**Nippon**			
		Load (kips)	*Displacement (in)*	*Failure Mode*		*Load (kips)*	*Displacement (in)*	*Failure Mode*	
				Side a	*Side b*			*a Side*	*b side*
LE+2_1_Ctrl._h	4.5	15.9	0.0218	c	c	22.6	0.0294	e	e
LE+2_2_Ctrl._l	4.5	14.9	0.0184	a	a	23.3	0.0268	e	e
LE+2_1_Cor._h	4.5	14.8	0.0212	a	c	21.7	0.0278	e	e
LE+2_2_Cor._l	4.5	12.9	0.0146	a	a	23.8	0.0315	e	e
LE+1_1_Ctrl._h	3.5	13.1	0.011	c	c	25.6	0.0349	e	e
LE+1_2_Ctrl._l	3.5	17.1	0.0144	c	c	24.9	0.0354	e	e
LE+1_1_Cor._h	3.5	17.2	0.012	c	d	26.8	0.039	e	e
LE+1_2_Cor._l	3.5	16.8	0.0164	c	c	26.1	0.0377	e	e
LE_1_Ctrl._h	2.5	17.8	0.023	a	c	22.5	0.0297	e	e
LE_2_Ctrl._l	2.5	16.1	0.0213	c	d	22.7	0.0296	e	e
LE_1_Cor._h	2.5	16	0.0211	a	c	--	--	e	e
LE_2_Cor._l	2.5	17.9	0.0252	d	c	22.1	0.0297	e	e
LE_1_1_Ctrl._h	1.5	10.1	0.0072	a	c	20.8	0.0315	e	e

LE-1_2_Ctrl._1	1.5	13.9	0.0101	a	a	22	0.0338	e	e
LE-1_1_Cor._h	1.5	6.3	0.0082	b	c	20.2	0.0319	e	a
LE-1_2_Cor._1	1.5	4.4	0.0051	a	b	20.6	0.0327	e	e
LE-2_1_Ctrl._h	0.5	6.2	0.008	a	c	8.6	0.0107	a	a
LE-2_2_Ctrl._1	0.5	6.5	0.0084	a	a	9.3	0.0132	a	a
LE-2_1_Cor._h	0.5	6.3	0.0083	a	c	7.8	0.0138	a	a
LE-2_2_Cor._1	0.5	4.4	0.0051	a	a	9.7	0.0131	a	a

3.6.3 Bond Behavior of the Double Strap Joints

Specimens Sika_LE+2_Cor_h and Nippon_LE+2_Cnt_h are individual instances from testing that are used to describe the behavior of the two CFRP types used in this research. The remainder of the specimens tested in this research had similar behavior. Figure 19 I and II shows the axial strain distribution at discrete points (strain gauge locations) along the length of the two double strap joints at varying percentages of loading. *Pu* is the ultimate load of the joint. The anatomy of these specimens is as follows: the joint location is the middle of the DSJ, and the far end of the specimen is refered to as the CFRP termination. Figure 19 I and II are the longest bond length specimens (Le + 2) that were tested for each strengthening system.

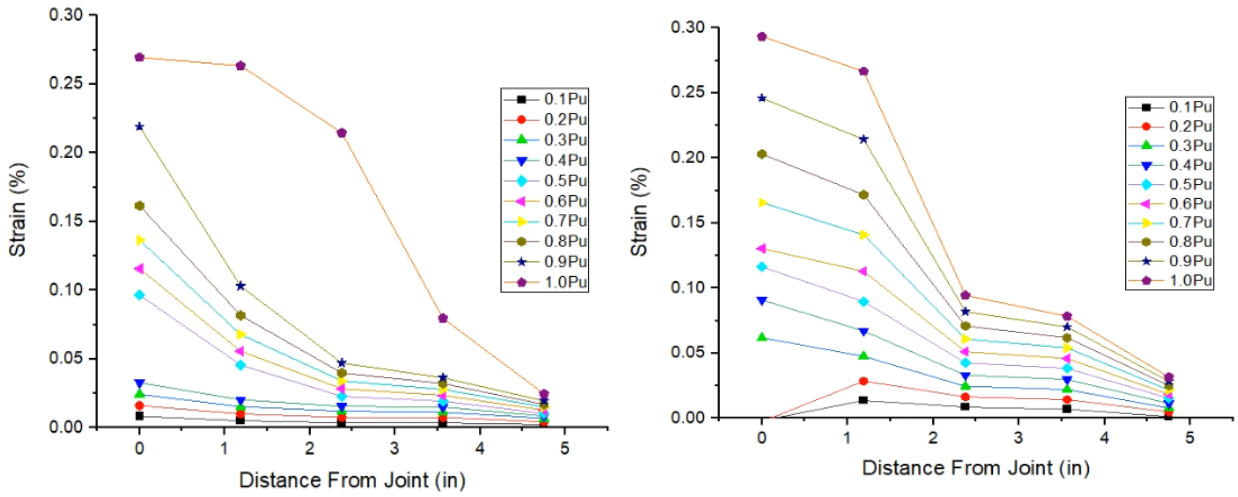

I. Sika_LE+2_Cor_h II. Nippon_LE+2_Ctrl_h

Figure 19. Axial Strain Distribution Diagrams for the Different Strengthening Systems Used

In comparing Figure 19 I and II, there are two distinct differences between these different strengthening systems. Firstly, the Nippon system appeared to have a shorter effective bond length (based on approximate strain gauge data). The effictive gauge length is determined by the drop off in strain values. Secondly, the Nippon strengthening system did a better job of more evenly (linearly) distributing the loading over the entire length of the DSJ; however, a majority of the loading still occurred in the effective length of the joint. There is one last thing to consider when looking at these graphs, which is the behavior right as 1.0Pu was reached. The Sika system had a progressive debonding failure, while the behavior of the Nippon system does not reflect this. This progressive failure is indicated by the transition of hight strains along the length of the specimen. The Nippon system did not show signs of softening or debonding near its failure load because this system failed due to CFRP rupture.

3.6.4 Sika Double Strap Joint Performance

As the bond length of the DSJ specimens increased, the failure displacement and ultimate strength of the joint also increased until the effective bond length was reached. The most common failure types of these joints were adhesion failure between the steel and priming adhesive, closely followed by an adhesion failure between the FRP and the FRP adhesive. DSJs of the same bond length that failed due to the adhesion failure between the steel and priming adhesive had lower strengths (ranging from 1.8 to 9.6% lower) than those of the specimens that had adhesion failures between the FRP and the FRP adhesive.

Figure 19 I shows that below loads of 0.9Pu, the strain distribution can be represented by a decaying exponential profile. A majority of the strain transfer occurs in the specimens within the first three inches, where the first three inches approximate the effective bond length of the strengthening system. However, this effective bond length determination was limited by the density of the strain gauges on the specimens. At a load of 1.0 Pu, the "approximate effective bond length" and exponential decay strain profile translated longitudinally further away from the joint. This translation is occurred because the shear strength of the adhesive material had been reached and the adhesive started to "slip." The failure of the adhesive and translation along the bond length continued until the entire system failed. Recall that this Sika specimen mostly failed due to debonding while a similar Nippon specimen failed due to CFRP rupture.

3.6.5 Nippon Double Strap Joint Performance

For the Nippon strengthening system, as the bond lengths of the DSJs increased, the failure displacement and ultimate strength of the joints also increased until the effective bond length was reached. When the bond length was less than the effective bond length of the DSJs, all the failure modes were adhesion failure between the steel and priming adhesive. When the bond length was greater than the effective bond length, all failure modes were CFRP rupture, and all of these specimens failed at similar loads.

Figure 19 II shows a parabolically decaying function over the entire course of its testing. The parabolic shape of the strain distributions indicates that the Nippon strengthening system did a better job at evenly spreading the load over the effective bond length of the joint. The information from Figure 19 II also suggests that the "approximate effective bond length" of the

specimen was less than two and a half inches. It is of note that this Nippon strengthening system failed due to CFRP rupture.

3.6.6 Interfacial Fracture Energy and Bond Slip of the Double Strap Joints

A significant value used to calculate the ultimate capacity and effective bond length (like those seen in Table 4) of a DSJ is the interfacial fracture energy, G_f. The interfacial fracture energy of a DSJ configuration corresponds to the area under a bond-slip curve. A bond-slip curve is created by measuring shear stress and slip between strain gauges along the length of a DSJ. Bond-slip curves for the different strengthening systems tested in this research are shown in Figure 20. A detailed explanation of how these curves are created can be found in (He and Xian 2017).

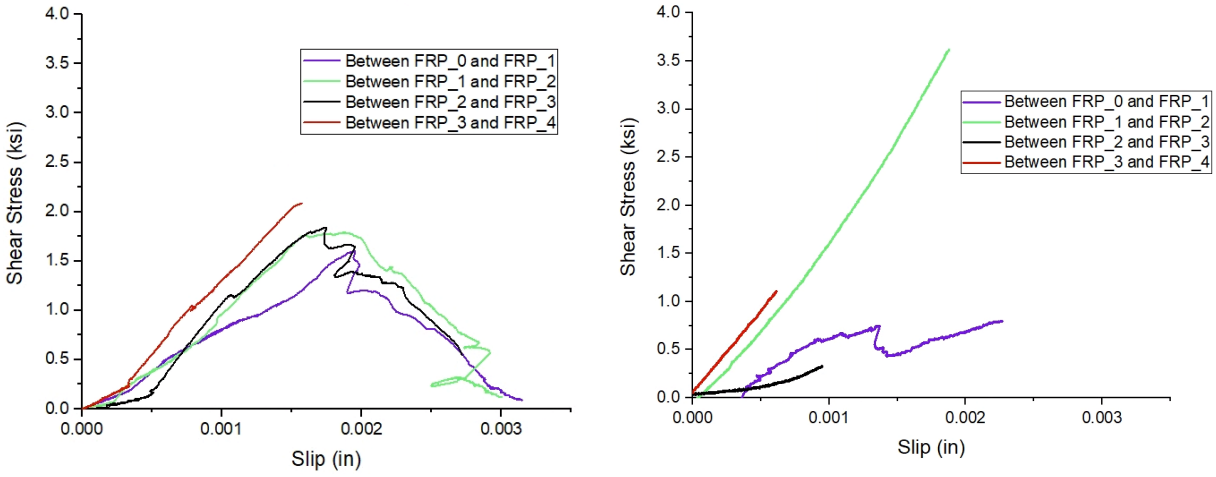

I. Bond-slip Curve for Sika_LE+2_Cor_h II. Bond-slip Curve for Nippon_LE+2_Ctrl_h

Figure 20. Bond-Slip Diagrams for the Different Strengthening Systems Used

The equation used to calculate the ultimate load of a DSJ specimen is shown as equation (1).; where b_p is the total width of the CFRP in the DSJ, E_p is the elastic modulus of the CFRP, and t_p is the CFRP thickness (Xia and Teng 2005). The only unknown variable is $G_{f,}$ which can be

obtained from the bond-slip curve shown in Figure 20 I, where G_f is equal to 0.003 kip/in. This G_f was calculated from the average of the 3 curves shown in Figure 20 I. Based on Equation (1), the predicted ultimate load for the Sika_LE+2_Cor_h specimen was 12.37 kips, which corresponds to a 16.4% error from the actual ultimate load of 14.8 kips . While this predicted strength is low compared to the test data, it is a reasonable value considering the strain behavior on the ungauged face of the length of interest on the DSJ is assumed to be the same as the gauged side. This prediction value was one of a very limited number of samples that could be made through the use of a G_f value, due to the limited number of viable tests that captured this behavior. Where useful tests did occur, oneside of the DSJ tended to fail first. Due to failures occurring on the opposite side of the strain gauges, the required data could not be collected to make the predicted strength calculations for all of the tested specimens.

$$P_u = (min) \quad b_p\sqrt{2E_p t_p\, G_f} \quad or \quad A_P\sigma_P \qquad (1)$$

When looking at the bond-slip curve for Nippon_LE+2_Ctrl_h (Figure 20 II), there is no adhesive slip before the CFRP fiber rupture. These bond-slip curves are missing pertinent information (the full area underneath the curve) to calculate G_f; however, this is the behavior (no adhesive slip or failure) when rupture controls the failure mode. Also note that the b_p from equation (1) for the strand sheet is of the true width of the CFRP applied (that is, strand diameter multiplied by strands per inch, which is then multiplied by nominal width of the strand sheet), not that of the nominal width of the CFRP applied. In this research, the nominal width applied on one side of the DSJ was 2 in, so the total nominal width applied is 4 in while the actual total width applied is 2.96 in.

Another equation of interest is the effective bond length(Le) (Xia and Teng 2005). The equation for L_E is shown in equation (2), where τ_f is the shear stress at the failure of an adhesive, and δ_f is the largest slip value on the bond-slip curve.

$$Le = \frac{\pi}{2\sqrt{\frac{\tau_f}{E_p t_p \delta_f}}} \qquad (2)$$

3.6.7 Ultimate Loading and Effective Bond Lengths of Double Strap Joints

Equations (1) and (2) highlight how the effective bond length and ultimate strength of a joint can be calculated analytically. These predicted values were compared with the results from the experimental testing. Figure 21 shows the average failure loads for the given bond lengths for all of the DSJ specimens and a linear piecewise function for each strengthening. This piecewise function was developed in two steps. The first step involved plotting an horizontal line through the average failure load of three points of the plateau data (L_E, L_E+1, and L_E+2. Once the plateau portion of the plot was created, the remaining data points were used to create a linear regression going through zero and intersecting the horizontal line. While there is some variation in ultimate loads for those specimens with bond lengths greater than the effective bond length, these variations in the loading can be attributed to fabrication tolerances such as varying adhesive thickness, different adhesive batches, and other subtle variations in quality control. Based on Figure 21, conservative effective bond lengths of the Sika and Nippon specimens are suggested to be 2.0 in and 1.75 in, respectively.

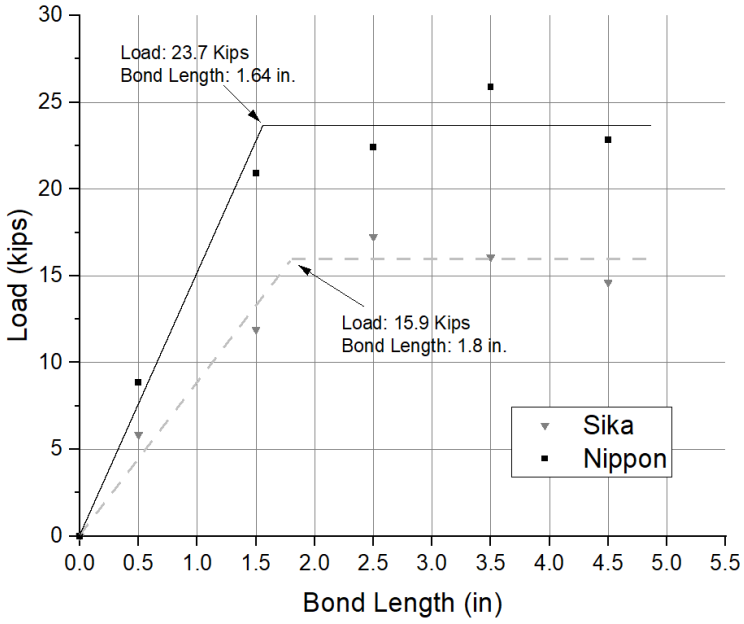

Figure 21. Averaged Loads vs. Bond Length of DSJ Specimens

The prediction results from four different models for the Sika strengthening system have mixed results. Although the values appear to be reasonable, testing for material properties provided the closest prediction estimations in terms of accuracy. Table 6 shows the ratio of the models' predicted ultimate strength over that of test data. The prediction models for the Sika strengthening system demonstrated estimations within 29% of actual, except for Fernando's prediction model (2010). The Nippon strengthening system results were not as consistent; in some cases, the predicted values were double or triple the experimental values. However, these prediction models only consider the state of adhesive failure, which did not occur during most of the testing on the Nippon specimens. Therefore, these predicted values are not applicable because they assume that the CFRP can be strained infinitely without failure. Thus, any calculation must account for the CFRP's rupture capacity in the strengthening system and

compare that to the debond models. The calculated ultimate load (rupture) of the CFRP in Nippon DSJ is 20.9 kips, which is within 11.8 % of the tested value.

Table 6. Ratio of Predicted to Experimental Effective bond lengths and Ultimate Loads for the DSJs

Prediction Model Used	Literature used to Predict Material Properties	Sika		Nippon	
		Calculated Effective Bond Length (Predicted/ Exp)	**Ult. Load** (Predicted/ Exp)	**Calculated Effective Bond Length** (Predicted/ Exp)	**Ult. Load** (Predicted/ Exp)
Xia and Teng (2005)	Xia and Teng (2005)	1.52	1.14	2.01	1.17
Xia and Teng (2005)	Fawzia et. al (2010)	1.35	1.24	1.71	1.23
Xia and Teng (2005)	Fernando (2010)	0.61	0.50	3.23	2.10
Xia and Teng (2005)	Material Properties via Bond-Slip Diagrams	1.18	0.78	NA	NA
L.J. Hart-Smith (1973)	L.J. Hart-Smith (1973)	0.96	0.71	1.86	1.32
Experimental Data		*1.8 in*	*15.9 kips*	*1.64 in*	*23.7 kips*

Focusing on the Sika DSJ specimens and excluding Fernando's (2010) predicted material properties, the Xia and Teng (2005) model used with the Fawzia et al. information yielded the poorest predictions for ultimate loads,with a percent error of 24%. On the other hand, the Xia and Teng (2005) model used with the Xia and Teng (2005) data resulted in experimental strengths that were within 14% of expected. Overall the strength prediction equations do an adequate job at estimating the ultimate load of a DSJ specimen. The predicted bond length equations provide a reasonable estimate (within 52% of actual) at estimating the bond length for the Sika strengthening systems. For all of the Sika tests, the L.J. Hart-Smith (1973) model performed the most favorably out of all the (unknown material properties) prediction models used for the Sika materials. The Fernando's (2010) material prediction equations do not yield good

results in terms of prediction of the materials actual behaviour and should not be used with these CFRP and adhesive types.

However, these material prediction models were all developed for specific adhesives and thicknesses, which have been adopted for similar but not exact conditions here. If accurate results are required, the exact DSJs should be tested to determine G_f and δ_f. These values are important in calculating ultimate loads and effective bond length for a specific set of adhesives and CFRP. The results of this testing show that with known material properties, the effective bond length and ultimate strength of the joint were calculated to be within 18% and 22% of the average test results, shown at the bottom of Table 6. Granted, these calculations are subject to some variability due to the small sample size and non-uniformly loaded DSJ specimens.

The Nippon strengthening systems predictions are reasonable in comparison to the adhesive failure prediction loads (assuming that this system is actualy close to an adhesive failure); however, the predicted effective bond lengths were drastically off, ranging from 171% to 323% times the actual length. This is a good indication that equation (2) is not a good predictor of bond length for the Nippon strengthening system, the reason likely being a combination of a number of factors, including the Nippon material's high elastic modulus, the strand sheet material has a different physical from than the CFRP plate used in the Xia and Teng model development, and the equation is a simplification of the equations originally developed by Yuan et al. (2004), including the assumptions that the CFRP has the same width as the substrate material and the elastic bond-slip is much smaller than the final slip value.

In comparing the Sika and Nippon strengthening systems, the Sika material sits on top of its adhesive (seen in Figure 22 I.), while the Nippon material is embedded into its adhesive (seen in

Figure 22 II.). The entire perimeter of the Nippon CFRP is embedded in adhesive, while the Sika CFRP only has a portion of its perimeter surrounded by adhesive. The length of CFRP covered by adhesive (L_c), for one side of a DSJ, at a cross-sectional cut is 2 in and 4.66 in for the Sika and Nippon specimens, respectively. While the bond transfer is not linearly related to CFRP contact surface, it provides additional benefits to bond transfer and shorter effective lengths.

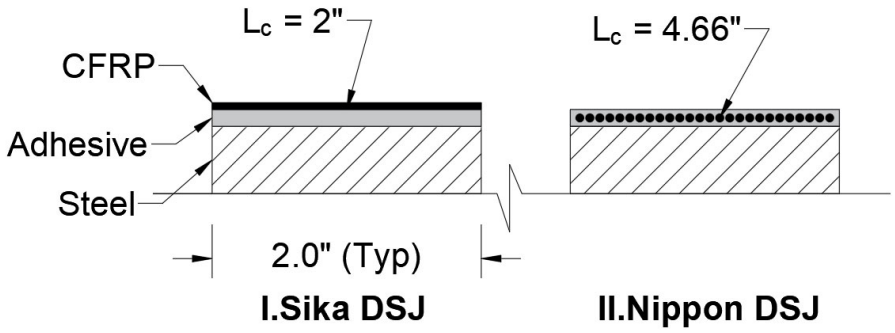

Figure 22. Cross-sectional Cut of DSJs with CFRP Exposure (L_c)

A further investigation of the bond length was carried out by looking at the Yuan et al. (2004) equation, which considers CFRP width in the calculation of the effective bond length. A comparison of the Yuan et al. (2004) and the Xia and Teng (2005) equations evaluated for a L_c of 2.85 in (half of the entire pirimiter of the CFRP) can be seen in Table 7. The Yuan et al. (2004) prediction was 50% closer to the experimental bond length compared to Xia and Teng (2005) prediction. Increasing the L_c to nearly 50% and 100% of the CFRP's embedded perimeter further increased the accuracy of the predicted effective bond length, shown in Table 7. While using the nominal width of the CFRP strand sheet returned more conservative bond length values, the inclusion of more perimeter of the CFRP strand sheets provided better accuracy in the prediction. Because it is not likely that 100% of the CFRP perimeter influences

the bond length of the DSJ, assuming that 50% of the CFRP's perimeter offers a reasonably accurate and conservative calculation of the effective bond length. Furthermore, it is also recommended that the Yuan et al. (2004) equation be used when working with CFRP strand sheets when predicting effective bond length.

Table 7. Ratios Predicted/Experimental Nippon Effective Bond Lengths for Different Prediction Models and CFRP Lc

Prediction Model Used	Literature used to Predict Material Properties	CFRP Lc "Width" (in)	Nippon
			Calculated Effective Bond Length (Predicted/ Exp)
Xia and Teng (2005)	Xia and Teng (2005)	2.85	2.0
Yuan et al. (2004)	Xia and Teng (2005)	2.85	1.5
Yuan et al. (2004)	Xia and Teng (2005)	4.51	1.3
Yuan et al. (2004)	Xia and Teng (2005)	9.14	1.1

3.6.8 Simulated Corrosion Effects

The ability of variable surface profile (simulated corrosion) to bond to a CFRP is of great interest due to the large number of in-service, deteriorated structures that have significant corrosion damage. Table 8 shows the percent change of both failure displacement and load due to simulated corrosion for both CFRP strengthening systems. A negative number denotes that the simulated corrosion performed less favorably than that of the control. In general, the specimens with section loss due to simulated corrosion had lower loads at its failure for both strengthening systems; however, these values were within 1.48 standard deviations from the average corrosion damage (within the outlier threshold). The simulated corroded Sika DSJ specimens also tended to have a lower displacement at failure, while the Nippon DSJ specimens had an increase in

failure displacements. It would appear this level of corrosion had little effect on the overall bond strength and bond performance.

Table 8. Percent Change of Load and Displacement Due to Simulated Corrosion

Specimen Name	Bond Length (in)	Sika		Nippon	
		Load (%)	Displacement (%)	Load (%)	Displacement (%)
LE+2	4.5	-10.14	-10.83	-0.66	5.51
LE+1	3.5	12.5	11.81	4.72	9.15
LE+0	2.5	-0.28	4.46	-2.32	0.02
LE-1	1.5	-3.35	-7.5	-4.61	-1.06
LE-2	0.5	-14.99	-18.46	-1.93	12.50

When looking at the failure modes of specimens with and without corrosion, there were no predominant failure modes for the Sika specimens. It was believed that the corrosion on the surfaces of the steel would serve as a bond enhancer using mechanical interlock. However, after examining the Sika and Nippon DSJ specimens that exhibited adhesion failures between the steel and priming adhesive, there was no residual adhesive in the pitting corrosion on the Sika specimens. Yet, there were signs that some mechanical interlock occurred in the Nippon DSJs. These Nippon DSJs, which showed interlock signs, had a 12.5% increase in failure displacement over the control specimens. Photos of Nippon and Sika adhesion failure surfaces are seen in Figure 23.

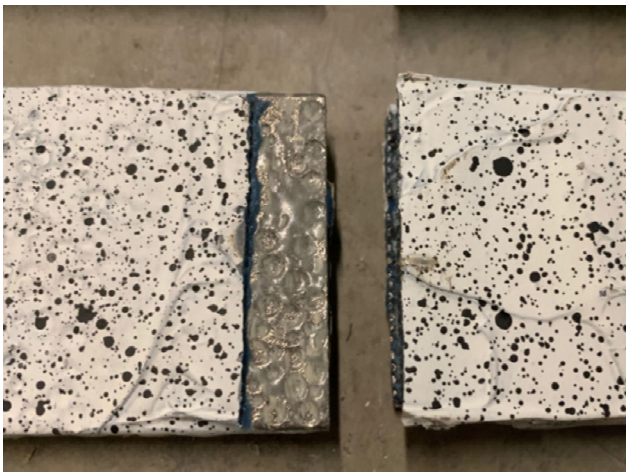

I. Nippon DSJ with Residual Adhesive in the Simulated Corrosion Pits

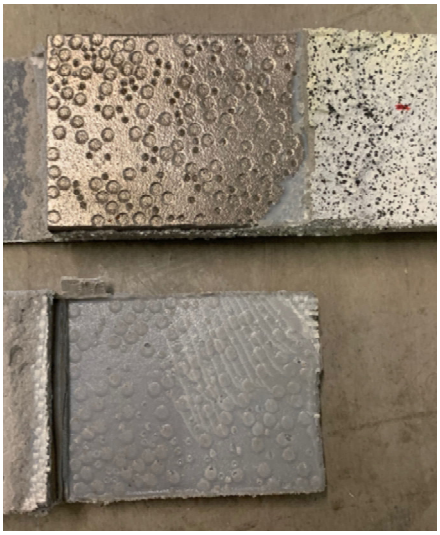

II. Sika DSJ with a "clean" Failure Surface

Figure 23. DSJs with and without Adhesive Interlock

3.7 Summary and Conclusions

The results of this study are as follows:

3.7.1 Prediction Equations and Bond Performance

- Prediction models (with the exclusion of Fernando (2010)) for conventional CFRP types, like the Sika CarboDur laminate, can be used to estimate the ultimate strength of CFRP-to-steel bonded systems to within 24% of tested values and estimated effective bond length predictions within 52% of tested values.
- The accuracy of the strength predictions for the Nippon specimens can not be commented on due to the CFRP rupture limit state. Further testing on non-conventional CFRP types (Nippon) is needed to analyze the accuracy of these prediction models.

- This research highlights the need to check the additional limit state of CFRP rupture when calculating the ultimate capacity of a joint. The calculated failure due to rupture of a Nippon DSJ was within 10% of the average rupture failure test data.
- The effective bond length prediction models provide overly conservative values (around double or triple) for non-conventional CFRP types, such as [HM] strand sheets, unless the Yuan et al. (2004) prediction model is used. When using Yuan et al. (2004), a L_c value greater than 50% up to the entire perimeter of the CFRP strand sheet's perimeter is recommended in the calculation of the effective bond length for more accurate results.
- The Nippon strand sheet distributes strains more uniformly along the effective bond length of the DSJ compared to the Sika Material.
- Out of all the prediction models, the L.J. Hart-Smith (1973) prediction model performed more favorably in estimating ultimate strength and effective bond length in comparison to the Xia and Teng (2005) model.However if G_f and δ_f are found experimentally, the Xia and Teng (2005) model can conservatively calculate the effective bond length and ultimate strength of the joint to be 18% and 22%, respectively of the actual values.

3.7.2 Simulated Corrosion

- The simulated corrosion has little effect on enhancing the ductility of the Sikadur30 adhesive. What little effects the corrosion did seem to effect was the 12.5% increase in the displacements of the Nippon DSJs prior to failure. The

large difference in these failure displacements demonstrates the increased ductility in the Nippon's adhesive.

- The 2.2% mass loss had moderate effects on the ultimate bond strength of these DSJs. Varying ranges of mass losses more significant than what was tested here need to be examined to further study the effects corrosion has on bond strength.
- Superficial corrosion pitting damage, like the one shown in Figure 13 I, when adequately cleaned, is not likely to cause problems in developing adequate bond strengths associated with CFRP retrofits' effective bond lengths.

3.8 Acknowledgements

The authors would like to acknowledge the Virginia Department of Transportation for the donation of the CFRP and materials used to create specimens tested in this research.

References

Al-Mosawe, A., Al-Mahaidi, R., and Zhao, X. L. (2015). "Effect of CFRP properties, on the bond characteristics between steel and CFRP laminate under quasi-static loading." Construction and Building Materials, Elsevier Ltd, 98, 489–501.

Chajes, M. J., Chacon, A. P., Swinehart, M. W., Richardson, D. R., and Wenczel, G. C. (2005). "Applications of Advanced Composites to Steel Bridges: A Case Study on the Ashland Bridge." 19716(March).

Fawzia, S., Al-Mahaidi, R., Zhao, X. L., and Rizkalla, S. (2006). "Strengthening of circular hollow steel tubular sections using high modulus CFRP sheets." Construction and Building Materials, 21(4), 839–845.

Fawzia, S., Zhao, X., and Al-mahaidi, R. (2010). "Bond – slip models for double strap joints strengthened by CFRP." 92, 2137–2145.

Fawzia, S., Zhao, X. L., Al-Mahaidi, R., and Rizkalla, S. (2005). "Bond characteristics between cfrp and steel plates in double strap joints." Advanced Steel Construction, 1(2), 17–27.

Fernando, D., Teng, J. G., Yu, T., and Zhao, X. L. (2013). "Preparation and Characterization of Steel Surfaces for Adhesive Bonding." Journal of Composites for Construction.

Fernando, N. D. (2010). "Bond behaviour and debonding failures in CFRP-strengthened steel members." PhD Thesis, Civil and Structural Department, PhD Thesis, 343.

Haghpanah, B., Chiu, S., and Vaziri, A. (2014). "Adhesively Bonded Lap Joints with Extreme Interface Geometry." International Journal of Adhesion and Adhesives, Elsevier, 48, 130–138.

Hart-Smith, L. J. (1973). Adhesive-Bonded Double-Lap Joints. Hampton, VA.

He, J., and Xian, G. (2017). "Bond-slip behavior of fiber reinforced polymer strips-steel interface." Construction and Building Materials, Elsevier Ltd, 155, 250–258.

Jiao, H., and Zhao, X. L. (2004). "CFRP strengthened butt-welded very high strength (VHS) circular steel tubes." Thin-Walled Structures, Elsevier Ltd, 42(7), 963–978.

Kim, S. J., Smith, S. T., and Young, B. (2011). "Effect of Surface Preparation on the Strength of FRP-to-Mild Steel and FRP-to-Stainless Steel Joints." Advances in FRP Composites in Civil Engineering - Proceedings of the 5th International Conference on FRP Composites in Civil Engineering, CICE 2010, 869–872.

Li, A., Xu, S., Wang, H., Zhang, H., and Wang, Y. (2019). "Bond behaviour between CFRP plates and corroded steel plates." Composite Structures, Elsevier, 220(March), 221–235.

Mertz, D. R., and Gillespie, J. W. J. (1996). NCHRP-IDEA Final Report: Rehabilitation of Steel Bridge Girders Through the Application of Advanced Composite Materials. Washington, DC.

Moy, S. S. J., Barnes, F., Moriarty, J., Dier, A. F., Kenchington, A., and Iverson, B. (2000). "Structural Upgrade and Life Extension of Cast Iron Struts Using Carbon Fibre Reinforced Composites." FRC 2000–Composites for the Millennium, (March), 3–10.

Phares, B. M., Wipf, T. J., Klaiber, F. W., Abu-Hawash, A., and Lee, Y.-S. (2003). "Strengthening of steel girder bridges using FRP." Proc., 2003 Mid-Continent Transportation Research Symp, (August 2003), 1–12.

Schnerch, D., Dawood, M., Rizkalla, S., and Sumner, E. (2007). "Proposed Design Guidelines for Strengthening of Steel Bridges with FRP Materials." Construction and Building Materials, 21(5), 1001–1010.

Wipf, T. J., Phares, B. M., Klaiber, F. W., Lee, Y. S., and Al-Saidy, A. H. (2005). Strengthening Steel Girder Bridges with Carbon Fiber – Reinforced Polymer Plates. Transportation Research.

Wu, C., Zhao, X., Duan, W. H., and Al-Mahaidi, R. (2012a). "Bond characteristics between ultra high modulus CFRP laminates and steel." Thin-Walled Structures, Elsevier, 51(January), 147–157.

Wu, G., Wang, H. T., Wu, Z. S., Liu, H. Y., and Ren, Y. (2012b). "Experimental Study on the Fatigue Behavior of Steel Beams Strengthened with Different Fiber-reinforced Composite Plates." Journal of Composites for Construction, 16(2), 127–137.

Xia, S. H., and Teng, J. G. (2005). "Behaviour of FRP-To-Steel Bonded Joints." Proceedings of the International Symposium on Bond Behaviour of FRP in Structures.

Xu, S., Li, H., Wang, Y., Wang, Y., and Wang, Y. (2020). "Influence of corrosion on the bond behavior in CFRP-steel single lap joints." Construction and Building Materials, Elsevier Ltd, 236, 117607.

Zhao, X. L., and Zhang, L. (2007). "State-of-the-art review on FRP strengthened steel structures." Engineering Structures, 29(8), 1808–1823.

CHAPTER 4: Large Scale Laboratory Testing and Modeling of Flexural CFRP Retrofits on Corroded Steel Girders

Chapter 4 consists of the manuscript: "Flexural Strengthening Retrofits of Corroded Steel Members Using CFRP—Large Scale Results and Implementation and Best Practices". This paper is to be submitted to ASCE's Journal of Bridge Engineering.

Flexural Strengthening Retrofits of Corroded Steel Members Using CFRP – Large Scale Results and Implementation Best Practices

Samuel T. Sherry, M.ASCE[1*], Matthew Hebdon[1], Ph.D., P.E., M.ASCE, Bernard L. Kassner[2], Ph.D., P.E.

[1]Thomas M. Murray Structural Engineering Laboratory, Charles E. Via, Jr. Department of Civil Engineering and Environmental Science, Virginia Tech, 255 Inventive Lane, Blacksburg, VA 24060

[2]Virginia Transportation Research Council, 530 Edgemont Rd, Charlottesville, VA 22903

[*]Corresponding Author. sher3004@vt.edu

4.1 Abstract

With steel bridge infrastructure deteriorating and being subject to ever-increasing demands, one easily-implementable technique to flexurally strengthen steel bridge beams is the use of carbon fiber reinforced polymers (CFRP). CFRP is ideal because of its high strength-to-weight ratio and ease of installation. This study investigated the application of flexural CFRP retrofits to steel surfaces having nonuniform profiles resulting from corrosion section loss. In doing so, researchers investigated the design process, strengthening effects of the CFRP system, and the impact of surface variation on bond behavior. Two CFRP strengthening systems and three retrofit configurations on large-scale specimens subjected to flexure were examined. One retrofit material is a newly-developed high modulus strand sheet, and the other a normal modulus plate material. Design procedures, best practices, and the efficacy of the CFRP strengthening systems

for flexural strengthening on steel are described herein. Pitting corrosion up to 0.125 in had little effect on CFRP retrofits in achieving their design strength. Strain compatibility with a force equilibrium design approach predicted the retrofit strength improvements within 11% of experimental values.

4.2 Introduction

Cross-sectional reduction resulting from corrosion can be a significant problem in aging steel bridge members. This section loss can reduce a bridge's load-carrying capacity, which coupled with an increase in modern traffic demands, contributes to greater stresses on aging infrastructure. The Federal Highway Administration (FHWA 2012) sets limits for live load stresses and deflections that, if exceeded, can lead to a bridge being categorized as "structurally deficient." As a means to combat these issues, conventional strengthening solutions for deteriorated flexural members include adding steel cover plates, replacing sections of the beam, or adding external prestressed tendons. However, these methods potentially have several shortcomings, including required lane closures, high costs, increased dead weight, and continued corrosion issues.

An emerging alternative to traditional retrofits is the implementation of carbon fiber-reinforced polymer (CFRP) laminates attached to the bottom flanges of steel beams. CFRP is a highly tailorable material with an extremely high strength-to-weight ratio, is easy to install, and can potentially mitigate further corrosion. To date, some research on bond strength and flexural strengthening increase between CFRP and newly-fabricated steel (having a smooth surface) have been conducted; however, there is a gap in the literature concerning the bond when excessive roughness and surface variations exist. Thus, there is a need for a better understanding of

CFRP's strengthening ability on deteriorated structures with severely corroded steel. In this paper, flexural CFRP retrofits on corroded steel are examined on large-scale test specimens subject to flexure.

4.2.1 General CFRP Retrofits

While CFRP has been shown to improve the flexural strength of steel bridge beams, the vast majority of such studies are limited to members with no structural damage (Chajes et al. 2005; Mertz et al. 2002; Miller et al. 2001; Moy 2002; Moy et al. 2000; Peiris 2011; Phares et al. 2003; Wipf et al. 2005). These studies do, however, demonstrate that CFRP retrofits improve both strength and stiffness of steel bridge members. Similarly, laboratory testing of CFRP retrofitted steel members have focused on members with uniform surface profiles to evaluate parameters including: modulus, development length, number of layers, anchorage, fatigue life, and flaws (Galal et al. 2009; Kim and Brunell 2011a; Liu et al. 2001; Nagai et al. 2012; Narmashiri et al. 2012; Peiris 2011; Rizkalla et al. 2008; Salama and Abd-El-Meguid 2010; Schnerch and Rizkalla 2008b; Shields et al. 2004; Yu et al. 2011). Schnerch et al. (2007) summarizes much of these conclusions and provides guidance on design, best practices, and substrate cleaning methods to achieve favorable performance on steel members with smooth surface profiles.

4.2.2 Prediction Models

From an academic standpoint, there are two widely accepted analytical approaches when designing CFRP retrofits— elastic and inelastic. The elastic method makes use of conventional mechanics on a composite system and assumes the entire retrofitting system remains elastic. This design approach would typically be used from an application design standpoint. This method, which requires finding the transformed section, using the CFRP area modified by its modular

ratio can be used to calculate deflection, stress, and strain (Hidekuma et al. 2011; Miller et al. 2001; Nagai et al. 2012). Using this method, Chajes et al. (2005) were able to predict strains on an in-service bridge that was retrofitted with CFRP within a 9% error.

The inelastic model uses strain compatibility and force equilibrium to calculate a moment capacity at a specified strain. While bridge beams typically are designed to remain below the yield point of a member, there is value in determining how much residual capacity remains in a retrofitted system and at what load the failure of the retrofit is expected. This inelastic method is accurate and can account for the plasticity of the steel in the retrofitted system (Al-Saidy 2001; Lenwari et al. 2005; Mertz and Gillespie 1996; Peiris 2011; Schnerch et al. 2007). The inelastic approach was used throughout the analysis in the research presented herein.

4.2.3 Surface Roughness

CFRP manufacturers provide guidance on maximum out-of-plane deviations for metallic surfaces on which a CFRP retrofit will be adhered to; Milliken Infrastructure (2017) suggests any visible deviations and and Sika (2014b) recommends 0.04 in. However, in the cases of corrosion, smoothing a surface to such rigorous tolerances is not feasible. The limited research that has investigated CFRP retrofits on roughened profiles has little documentation on the corrosion profile. Mertz and Gillespie (1996) applied and tested CFRP retrofits on American standard I-shaped (24x80) steel beams that had been removed from a bridge, due to corrosion concerns. The surface profiles were simply reported as “nonuniform and pitted with evenly distributed corrosion along the tension flange.” The Delaware Department of Transportation inspection report estimated 40% section loss, and the experimental stiffness loss for the beams was approximately 30%. These retrofitted beams achieved strengths above that of the original nominal strength, and the CFRP strengthening system remained intact as the beams failed due to

lateral-torsional buckling. Mertz et al. (2002) tested two additional corroded American standard I-shaped (24x80) steel bridge beams, examining the fatigue life of the CFRP retrofits. This corrosion damage had no detrimental effects on the CFRP's strength or stiffness even after 10 million stress cycles, which simulated 4.6 years of average daily truck traffic. Chajes et al. (2005) were able to reduce strains using CFRP on a structurally deficient steel through-beam bridge; however, the extent of the corrosion damage was not documented. Haghpanah et al. (2014) conducted small scale bond strength testing on epoxy-adhered, steel "saw tooth" joint specimens, with a tooth size that was 0.4 in wide and 0.2 in deep. While these specimens failed at similar loading, the tooth configurations had a large effect on the ductility of the specimens. Other small-scale studies also investigated bond strength related to surface roughness (Fernando et al. 2013; Kim et al. 2010; Kleffel and Drummer 2017; Da Silva et al. 2010; Yao and Qu 2002); however, their research examined bond behavior at the microscale level. The translation from microscale behavior to macroscale behavior needs further examination.

4.3 Objectives

The objectives of this research were as follows:

- Quantify the type/amount of corrosion to which CFRP retrofits were applied.
- Evaluate the effectiveness of CFRP as a retrofit solution on bridge beams that have substantial section loss and pitting corrosion.
- Determine which strengthening system and configurations performed most favorably.
- Compare calculated capacity to test data to determine the efficacy of analytical models.
- Develop best practices for installing CFRP on a corroded steel surface.

4.4 Test Methodology

4.4.1 Beam Specimens

CFRP retrofits were applied to W18x50 grade A36 steel beams, donated by the Virginia Department of Transportation (VDOT) and retired from service due to extensive corrosion section loss on both the top and bottom flanges. Seven beams were tested, one of which was unreinforced and the other six were retrofitted with CFRP. Prior to and after blast cleaning, all surfaces were inspected, using both a visual grading system and a quantitative surface profiling.

Visual grading of the surface and rust condition followed ISO 8501-1 (2007). These rust grades ranged from 'A' (little to no rust) to 'D' (millscale had rusted away and had general pitting). Representative rust grades for these beams can be seen in **Error! Reference source not found.** I. & II. The majority of the observed rusting on the surfaces to be retrofitted comprised of grades 'C' and 'D'. However, in some cases paint was still intact, indicating a rust grade 'A'.

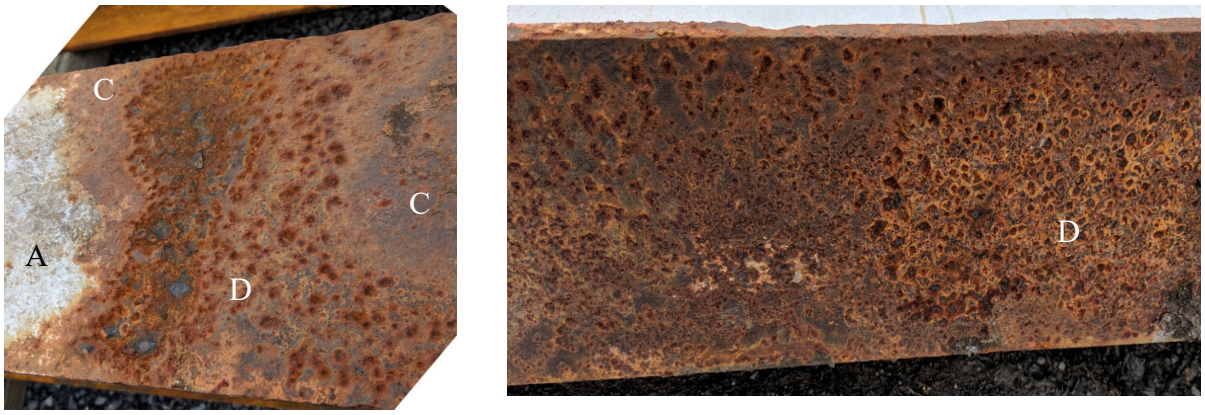

I. Light to Severe Grades of Rust II. Severe Grade of Rust

Figure 24. Surface Conditions of representative Steel Beam Specimens

Flange thickness measurements were taken from each of the specimens at 12 in. intervals along each beam's entire length. A total of four measurements were taken at each interval, including the top and bottom flanges on each side of the web. The average top and bottom flange thicknesses for each beam are shown in Table 9.

Table 9. Average Measured Flange Thickness for Each Test Specimen

Specimens		Average Flange Thickness		% Section Loss from Original	
		Top Flange (in)	Bottom Flange (in)	Top Flange	Bottom Flange
Original Section		0.57	0.57	NA	NA
Control		0.56	0.52	-1.8	-9.3
Sika	1-BBF	0.56	0.52	-1.8	-9.3
	2-BBF	0.52	0.52	-8.8	-8.4
	1-TBF	0.53	0.54	-7.0	-5.3
Nippon	1-BBF	0.51	0.52	-11.2	-9.3
	2-BBF	0.51	0.47	-11.1	-18.0
	1-TBF	0.52	0.52	-8.7	-8.7

The flanges of each retrofitted beam were blast cleaned to grade Sa 2 ½ or Sa 3 (ISO 2007). After the cleaning, 834 in^2 of total surface area from the flanges of each specimen were inspected with a digital image correlation (DIC) system. These profiles were then analyzed to quantify surface deviations from the original flange surface plane. Each profile consisted of over 850,000 nodes, or inspection points. Figure 25 shows an example surface deviation profile.

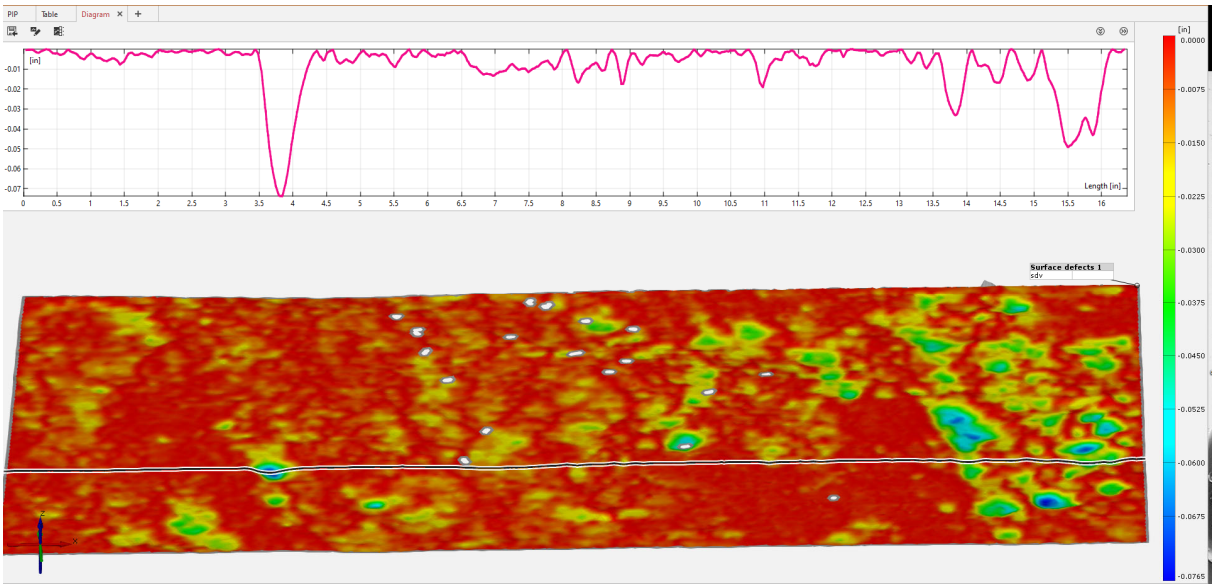

Figure 25. Example Surface Deviation Profile of Steel Beam Flanges

All of the surface deviation data was extracted and used to create a histogram to determine the distribution of section loss depth, as shown in Figure 26. A mean section loss of 0.008 in from the original plane was found, with a standard deviation of 0.0097 in. While the mean-centered data is a good characterization of the overall surface, the extreme deviations are of more interest due to the limitations of the CFRP retrofit bond. Surface deviations greater than 0.04 in (Sika's recommended limits and 3.3 standard deviations from the normal) made up 2% of all data. Larger deviations ranged up to 0.136 in, which is important because a pit with a depth of 0.125

in represents a 22% section loss of the flange at that location. This data demonstrates the amount of section loss present on the beam flanges, which were retrofitted.

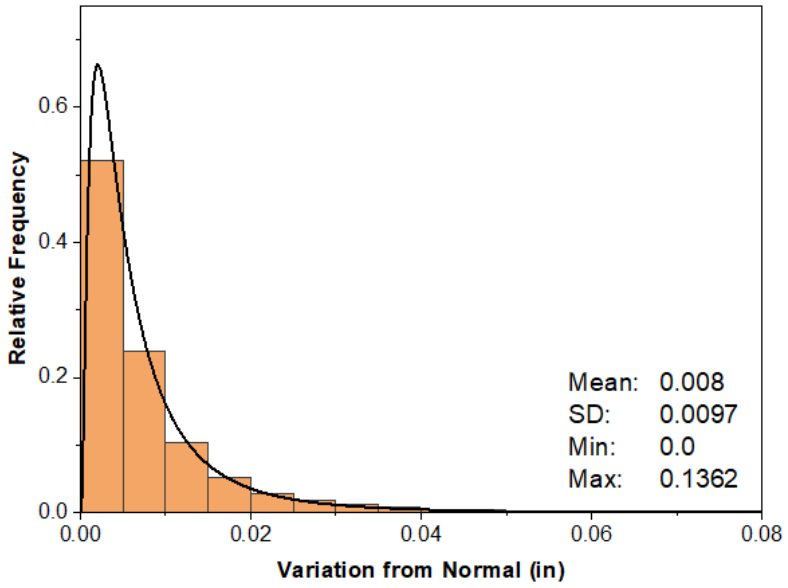

Figure 26. Histogram of Corroded Steel Surface Deviations

4.4.2 Retrofit Configurations

This research considered two different CFRP retrofitting systems on the beams, each of which was comprised of different product types and material properties. The CFRP retrofit systems are denoted by their manufacturers: Sika and Nippon. Three retrofit configurations were tested for each CFRP material. Ease of installation was a consideration when selecting retrofit configurations. Applying CFRP and adhesives overhead is possible; however, it is easier to apply CFRP when the material can be supported by the existing structure. Thus, the researchers considered the effectiveness of installing CFRP on the top face of the bottom flange.

These CFRP configurations, product dimensions, and naming convention can be seen in Figure 27 and are as follows:

- Unreinforced (Control beam)
- 1 ply of CFRP on the bottom of the bottom flange (1-BBF)
- 2 plies of CFRP on the bottom of the bottom flange (2-BBF)
- 1 ply of CFRP on each of the top sides of the bottom flange (1-TBF)

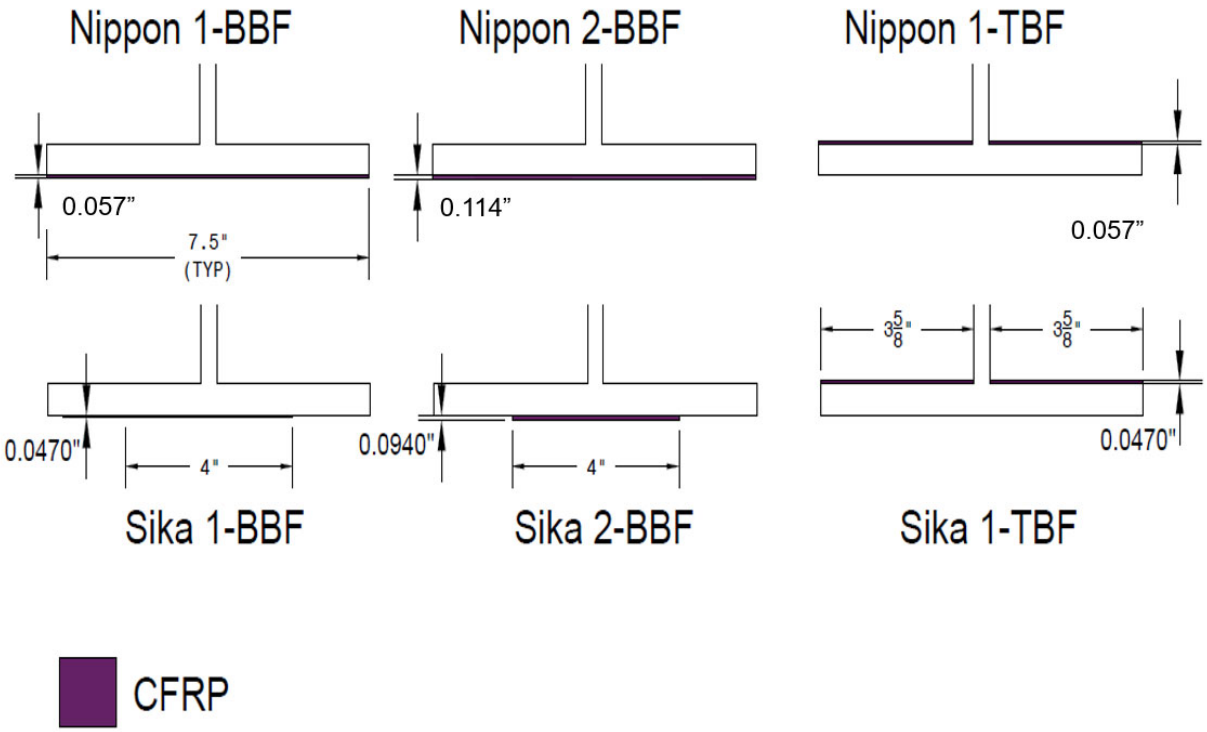

Figure 27. CFRP Configurations on Flexural Test Specimens

4.4.3 CFRP Materials

The Sika and Nippon CFRP strengthening systems vary in material properties, manufacturing, and application processes. The Sika CFRP is a normal modulus plate material, while the Nippon high modulus CFRP is made up of pultruded strands that are stitched together in a bamboo mat-like fashion. These different manufacturing processes drove the design and application of each

material, which is reflected in the width of the CFRP applied, as shown in Figure 27. Each material component that makes up these different systems and their technical names are listed in Table 10.

Table 10. CFRP Strengthening Systems Selected for Testing

Strengthening Components:	Strengthening System:	
	Sika	Nippon
CFRP	Sika CarboDur Type S 1012	Renew Wrap Strand Sheet CF900/HM
Adhesive	Sikadur 30	Renew Wrap Strand Sheet Adhesive (FB-E7S)
Insulation Material	SikaWrap Hex 106G	NA
Steel Primer	SikaDur 330	Renew Wrap Strand Sheet Adhesive (FP-WE7)

The researchers verified the mechanical properties of the CFRP and adhesive, as provided by the manufacturers. The steel material properties were taken from an average of 6 tensile specimens; three specimens from the web and three from the flange material. All tests were displacement-controlled and data was collected at a rate of 5 Hz. The average results from testing the mechanical properties of the adhesive, CFRP, and steel are shown in Table 11.

Table 11. Tested Material Properties

Property or Dimension	Sika		Nippon		Steel
	CFRP	Adhesive	CRFP*	Adhesive	
Tensile Strength (ksi)	536.0	3.2	157.8	5.8	Fy: 43.2 Fu:65.8
Modulus of Elasticity (ksi)	26,930	1,643	47,575	896	29,800
Elongation at Break (%)	2.11	0.23	0.33	1.18	18.7
Thickness (in)	0.047	--	0.057**	--	--
Width (in)	4	--	19.7	--	--

* Material properties based on the diameter of a strand (13 strands per in of width)
**Diameter

4.4.3.1 CFRP Installation

Both CFRP systems were installed per the manufacturer's recommendations (Milliken Infrastructure 2018; Sika 2014b). The general procedures for CFRP installation were as follows:

- Remove all corrosion, paint, and other contaminants from the area of the steel where the CFRP was to be applied by sand-blasting the surface to a “white metal” condition.
- Vacuum the sand-blasted surface to remove excess debris and then wipe down with acetone.
- Apply a priming adhesive to the cleaned surface.
- For the Sika material only, apply a glass fiber mat to the prepared surface to act as an insulator against galvanic corrosion between the CFRP and the steel.
- Apply the adhesive.
- Apply the CFRP by pushing it into the adhesive using a rubber roller, forcing the adhesive to squeeze out the side of the adhesive CFRP, and in the case of the Nippon material, in between individual rods.
- Clean the edges from excess adhesive.

- Allow the epoxy to cure in ambient temperatures (~70 deg F) for a minimum of 7 days.

4.4.4 Retrofit Design

When considering the use of a CFRP retrofit, the different failure modes associated with each strengthening system needs to be examined. Figure 28 shows a shear and moment diagram of a simply-supported steel beam with a CFRP retrofit on its bottom flange, subjected to a midspan point load. A steel beam subject to flexural stresses with flexural CFRP retrofits can fail in the following ways:

- Lateral torsional buckling of the steel beam
- Local compression buckling of the steel beam
- Intermediate debond of the CFRP from steel **(**region I in Figure 28**)**
- Debond near CFRP's termination **(**region II in Figure 28**)**
- Rupture of the CFRP **(**region III in Figure 28**)**

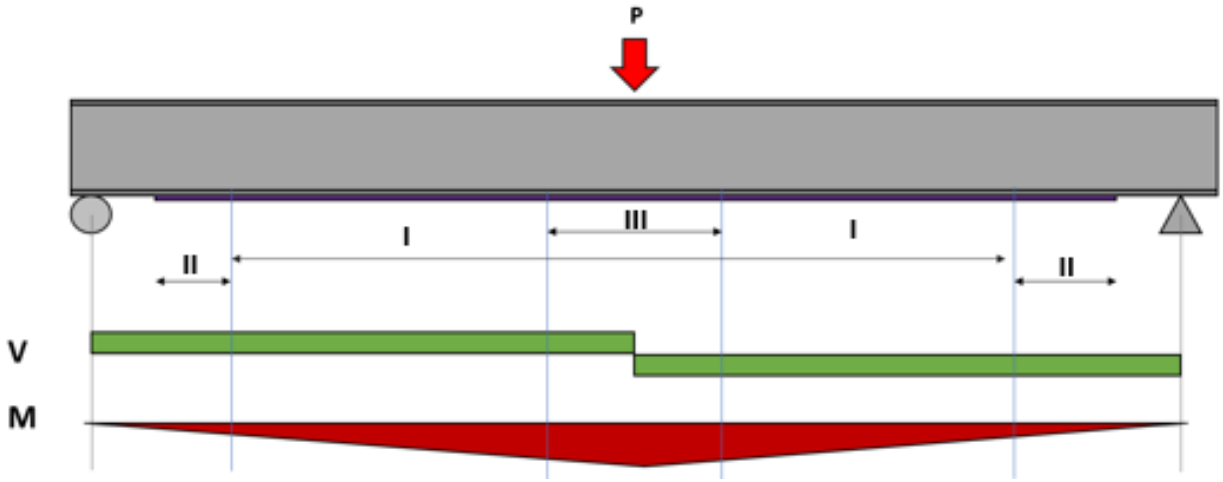

Figure 28. Shear and Moment Diagrams and General Location of Different CFRP Failure Types (Failure mode zones: I. = debonding, intermediate region; II. = debonding, near CFRP terminus, III. = CFRP rupture)

4.4.4.1 CFRP End Termination

The largest concern related to premature failures of CFRP retrofits is the complex stress state, due to interfacial and normal stresses, that occurs at the CFRP's termination when the retrofitted system is loaded. To keep interfacial and normal stresses, which are a function of bending stresses, as low as possible, the CFRP was terminated as close as practical to the supports, where the bending stresses are lower. A CFRP termination distance of 18 in from the inside face of the support was selected to provide adequate access for retrofit installation, monitoring during testing, and yet still be subjected to low flexural stress. At their termination points, the CFRP flexural strains were expected to be approximately 21% of the maximum strains at the midspan of the beam. This level of stress, combined with the implementation of spew fillet termination details (Deng and Lee 2007b) was thought to be adequate to prevent debonding at the end regions (failure mode II).

4.4.4.2 Local Flange Buckling

To prevent a local flange buckling failure of the CFRP-strengthened beam, a steel cover plate was welded to the top flange of each beam. The cover plate was grade A36 steel, measuring 10 in wide by 0.75in thick and 10 ft long. Thus, the plate extended 5 ft in each direction from the centerline of the beam.

4.4.4.3 Flexural Design

The design of each CFRP retrofit was completed utilizing a force equilibrium approach. For this reason and for simplicity, the steel was assumed to have elastic perfectly plastic properties and the CFRP was assumed to behave elastically until rupture. Using the section properties, material properties, and specifying a maximum strain at the CFRP's extreme fiber, one can determine the moment associated with the limiting level of strain for a given CFRP configuration type. The

maximum extreme fiber controlling strain is the least value of limit states I, II, and III. in Figure 28**.**

All calculations presented in this paper are based on failure mode III, the rupture of the CFRP. CFRP rupture was the target failure mode because the objective was to examine conventional prediction models and target the largest strength increase for these types of retrofits. The predicted ultimate strengths, given in Table 12, represent the strengths of each individually measured beam with their deteriorated cross-sections, not that of a nominal section.

Table 12. Analytical Retrofit Strength Predictions

Specimen		Predicted Failure Strength (Limit - CFRP Rupture) (kip-ft)	Potential % Strength Increase Over Control	Strain at Predicted Failure Load (%)
Control		408.0*	----	----
Nippon	1-BBF	470.2	15.25	0.33
	2-BBF	504.6	23.68	0.33
	1-TBF	455.7	11.69	0.33
Sika	1-BBF	622.4	52.55	2.1
	2-BBF	780	91.18	2.1
	1-TBF	725.7	77.87	2.1

*Denotes plastic moment of the section

4.4.5 Test Matrix

Table 13 shows all specimens and includes the amount of CFRP material applied to each retrofit and its equivalent area in steel. The equivalent area is expressed in terms of both stiffness (modular ratio) and strength (yield strength ratio) parameters found in Table 11.

Table 13. Testing Matrix and Steel Strength/Stiffness Equivalency Table

Specimen	Sika			Nippon		
	Cross Sectional Area (in^2)	Equivalent Steel Area (Strength) [in^2]	Equivalent Steel Area (Stiffness) [in^2]	Cross Sectional Area (in^2)	Equivalent Steel Area (Strength) [in^2]	Equivalent Steel Area (Stiffness) [in^2]
Control	NA	NA	NA	NA	NA	NA
1-BBF	0.19	2.48	0.17	0.12	0.95	0.42
2-BBF	0.37	4.93	0.34	0.25	1.89	0.82
1-TBF	0.33	4.32	0.31	0.11	0.87	0.39

4.4.6 Test Setup

Each beam specimen had a span length of 17.5 ft and was loaded in four-point bending at the quarter points, 5.45 ft from the specimen centerline. The test dimensions can be seen in Figure 29. The load was applied with a 400 kip Enerpac hydraulic cylinder controlled via a human operator. Initially, the load was applied in 10 kip increments until the point of first yield. Subsequently, loading was applied in 0.1 in increments.

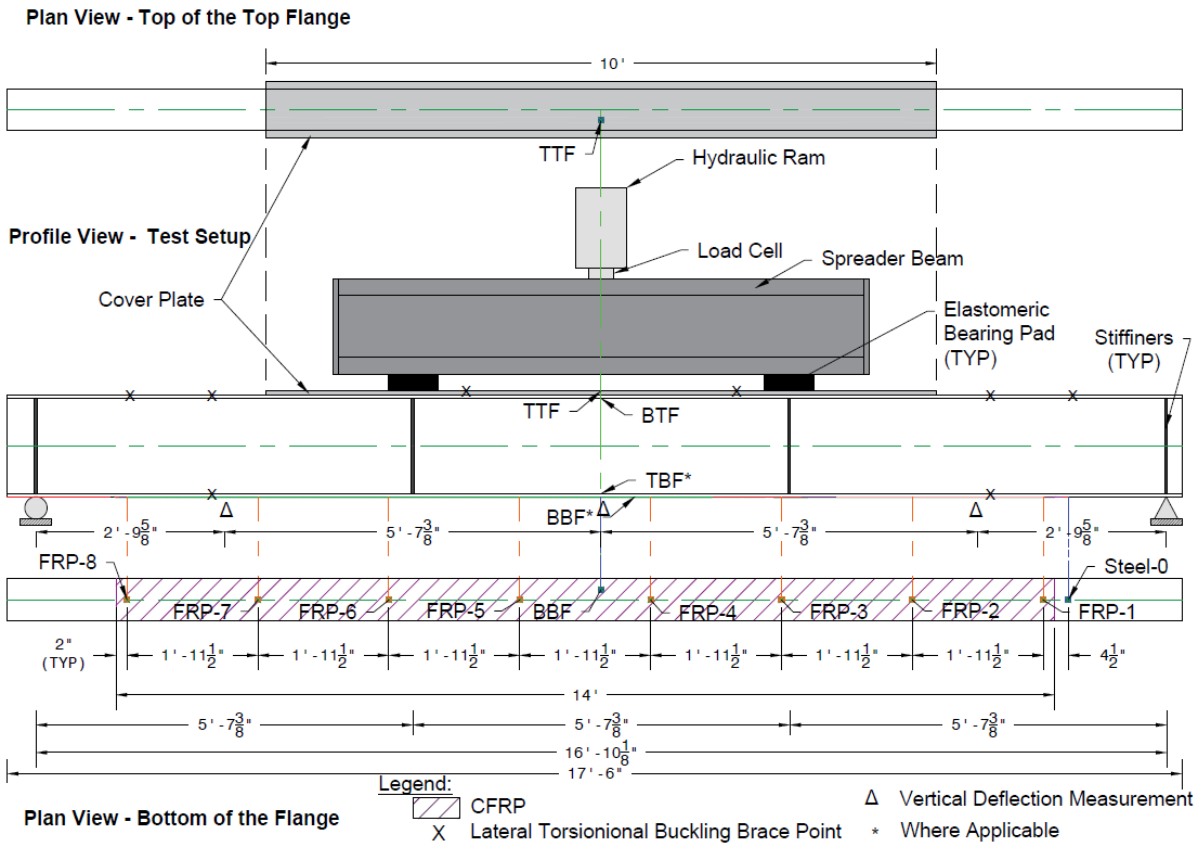

Figure 29. Plan and Profile View of Tested Beams (TYP)

4.4.6.1 Instrumentation

A Campbell Scientific CR5000 datalogger, sampled at 10 Hz, was used to collect data from:

- A load cell with a range of 400 kips and located at the midspan of the beam.

- Three vertical displacement sensors, at mid-span and one-sixth the span length from the ends of the beam.
- Eight CFRP strain gauges, two placed 2 in from CFRP termination, and then six additional gauges spaced equally (23.5 in) along the length of the CFRP.
- Three steel strain gauges. one each placed on the:
    - top of the top flange's cover plate (TTF)
    - bottom of the top flange (BTF)
    - top of the bottom flange (TBF) (where applicable)
    - bottom of the bottom flange (BBF) (where applicable).

4.5 Results and Discussion

4.5.1 Control Beam

The control beam was loaded well past its bottom flange's yield strain and into the plastic portion of the beam's capacity. The testing was terminated at 6.62 in of midspan vertical deflection, beyond any vertical deflection that the CFRP retrofits were capable of achieving. The load-displacement plot for this control beam is shown in Figure 30.

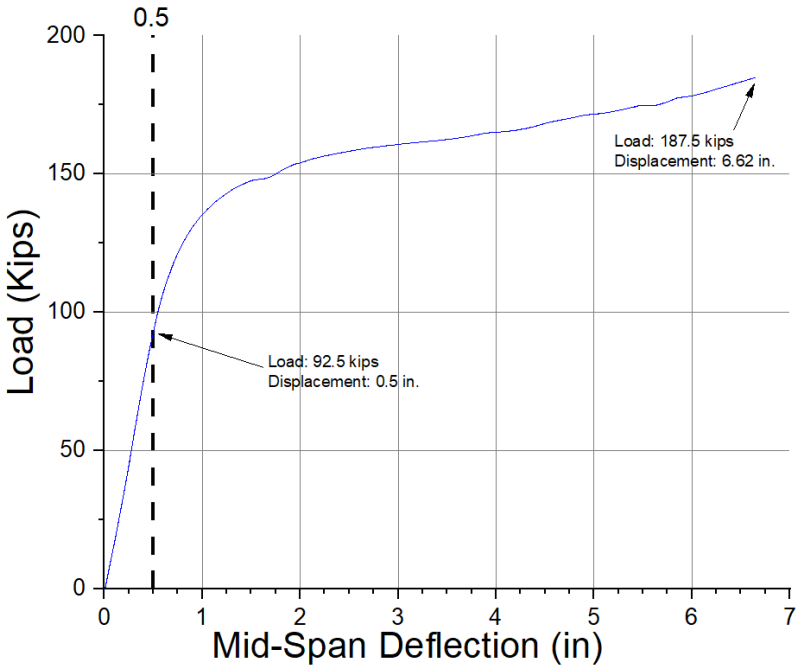

Figure 30. Load Deflection Plot for Control Beam

4.5.2 Carbodur Type S 1012 (Sika) Retrofits

4.5.2.1 Sika General Behavior

The Sika 1-BBF and Sika 1-TBF retrofitted beams were both tested until the failure of the CFRP reinforcing system. The Sika 1-BBF reinforcing system failed due to the CFRP's rupture in the constant moment region. The Sika 1-TBF reinforcing system failed due to intermediate debonding, where failure propagated towards the CFRP's end regions. The Sika 2-BBF retrofitted beam test was terminated before the failure of the reinforcing system due to local buckling at the top flange-to-cover-plate interface. Load-displacement graphs for all the Sika retrofitted beams compared to the control beam are shown in Figure 31**.** The small "sawtooth" peaks and valleys in this figure were a result of the incremental loading. The large drops in load for Sika 1-BBF and Sika 1-TBF, denoted by "X"s, indicate the points at which the CFRP retrofitting systems failed. The Sika 1_TBF retrofit has 2 "X"s because there were two unconnected strengthening systems, i.e., CFRP on the top of the bottom flange on each side of

the web. Figure 31 also shows that the Sika 2-BBF specimen was unloaded shortly after yielding of the flanges, which was completed to readjust the spreader beam.

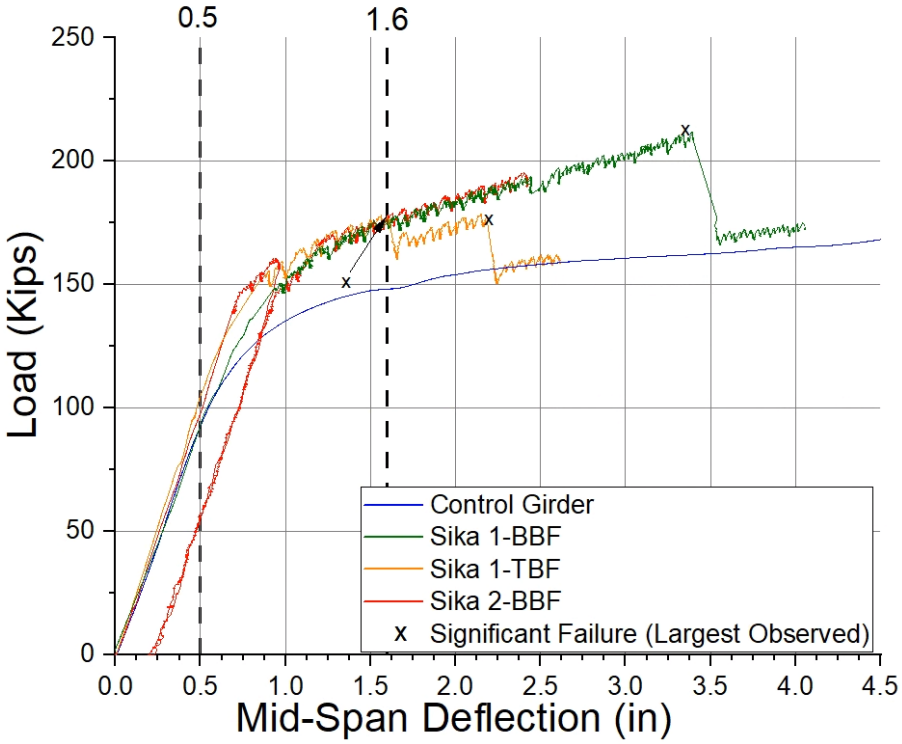

Figure 31. Load Deflection Plot of Sika Retrofits

4.5.2.2 Comparison of the CarboDur Type S 1012 (Sika) Retrofits

To compare the different retrofit configurations, an analysis of the retrofitted beams was conducted at a midspan deflection of 0.5 in, which was the transition point between elastic and inelastic behavior of the control beam, and 1.6 in, which was the lowest midspan failure deflection of the Sika retrofits.

Table 14 shows the applied loads and percent increase in capacity for each of the specimens at the specified midspan deflections of 0.5 in and 1.6 in. Compared to the control beam, the percent increase in loading at 0.5 in of displacement of these retrofitted beams ranged from 0.9%

to 14.0%. The percent increase in loading at 1.6 in of displacement of these retrofitted beams compared to the control beam ranged from 19.5% to 20.1%. The variation in these results are due to the section loss distribution, which varied for each specimen due to naturally forming corrosion, and each retrofit included a different amount of the CFRP cross-sectional area.

Table 14. Percent Increase for Loading at Different Midspan Displacements – Sika Retrofits

Specimen	Load at 0.5 in Displacement (Kip)	% Increase Over Control	Load at 1.6 in Displacement (Kip)	% Increase Over Control
Control	92.5	NA	148.2	NA
1-BBF	93.3	0.9	177.1	19.5
2-BBF	98.0	5.9	178.0	20.1
1-TBF	105.4	14.0	177.5	19.7

4.5.3 Renew Wrap Strand Sheet CF900/HM (Nippon) Retrofits

4.5.3.1 Nippon General Behavior

All Nippon specimens were tested until the failure of the CFRP reinforcing system were all due to CFRP Rupture. The load-displacement relationship for all the Nippon specimens compared to the control beam are shown in Figure 32**.** The large drops in load, denoted by "X"s, were due to significant failures in the CFRP. While there were localized failures, as denoted by purple diamonds in the figure for the Nippon 1-BBF specimen, those failures had little effect on the structure's load-deformation behavior prior to the denoted failures. Similar localized failures were observed for each Nippon specimen.

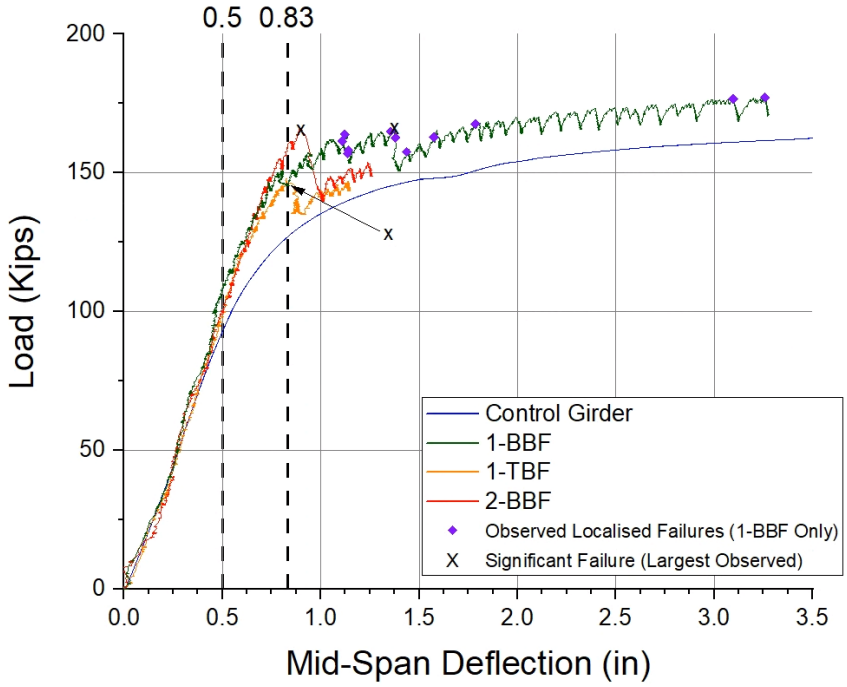

Figure 32. Load Deflection Plot of Nippon Retrofits

4.5.3.2 Comparison of the Renew Wrap Strand Sheet CF900/HM Retrofits

In comparing the different retrofit configurations, an analysis of the retrofitted beams was conducted at a midspan deflection of 0.5 in (elastic behavior) and 0.83 in (inelastic steel behavior prior to the failure of the CFRP retrofits). Table 15 shows the applied loads and percent increase in load for each of the specimens tested at those two deflections. The location of inelastic comparison, 0.83 in, was selected for the Nippon retrofits because it was the largest deformation in the inelastic region of loading at which no significant failures of the Nippon CFRP retrofits had occurred. Compared to the control beam, the percent increase in load on the retrofitted beams at 0.5 in of displacement ranged from 6.6% to 14.3%. The percent increase at 0.83 in of displacement ranged from 15.6% to 22.7%.

Table 15. Percent Increase for Loading at Different Midspan Displacements – Nippon Retrofits

Specimen	Load at 0.5 in Displacement (Kip)	% Increase Over Control	Load at 0.83 in Displacement (Kip)	% Increase Over Control
Control	92.5	NA	127.0	NA
1-BBF	105.7	14.3	147.0	15.6
2-BBF	101.6	8.6	156.0	22.7
1-TBF	99.2	6.6	147.0	15.8

4.5.4 Comparison & Analysis of Retrofits

Overall, every retrofit increased the strength and stiffness of the deteriorated steel beams. However, there are some major differences between the CarboDur Type S 1012 and the CF900/HM. The load deflection relationships for Nippon and Sika 1-BBF retrofits are shown in Figure 33, which displays three distinct differences in behavior between the two retrofit types: midspan displacement at CFRP failure, ultimate strength, and the elastic strength/stiffness ratio.

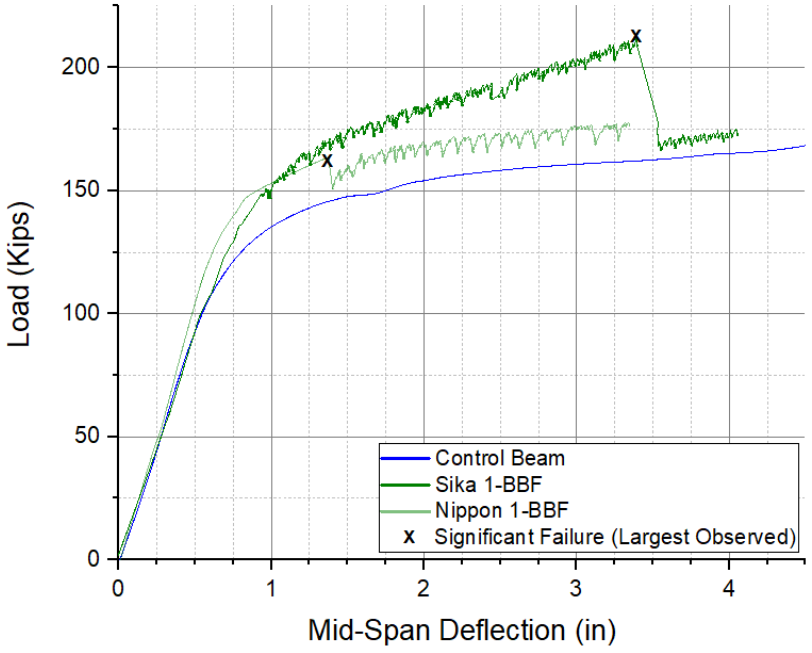

Figure 33. Load Deflection Plot of 1-BBF Retrofits

4.5.4.1 Elastic Strength

It was expected that larger amounts of applied CFRP would increase both strength and stiffness. However, the corrosion on the specimens was widespread and varied throughout. Using the average section loss resulted in an over prediction of the members' flexural capacity, as shown in Table 16. The difference between measured values and predicted values ranged from 10.4% to 19.4%. The retrofitted specimens demonstrated an increase in strength from 0.2 to 13.6% and 6.6 to 14.3% for the Sika and Nippon retrofits, respectively. The varied section loss made a comparison between specimens and the control specimen difficult. However, this discrepancy is most notable in the elastic region; in the inelastic region, the predicted values align more closely with the test results.

Table 16 Predicted and Experimental Beam Strengths

		Predicted			Experimental	
	Specimen	Ix (in^4)	Load at 0.5 in Displacement (kip)	% Increase over Control	Load at 0.5 in Displacement (kip)	% Increase over Control
	Control	118.4	114.8	NA	93.3	NA
Sika	1-BBF	120.9	117.3	2.2	94.6	0.2
	2-BBF	123.1	119.3	3.9	98.9	5.9
	1-TBF	123.3	119.8	4.4	106.0	13.6
Nippon	1-BBF	123.2	119.3	3.9	106.7	14.3
	2-BBF	123.7	120.1	4.6	102.5	8.6
	1-TBF	122.1	118.3	3.1	100.1	6.6

4.5.4.2 Inelastic Strength

The CFRP retrofits' ultimate strength provided a good point of comparison because the post-yield behavior was less influenced by localized corrosion. The strength increase of all specimens at their ultimate inelastic load are shown in Table 17. The inelastic strength increase, relative to the control specimen, ranged from 19.7 to 30.7% and 12.5 to 26.8% for the Sika and Nippon retrofits, respectively. The greater increase in strength in the inelastic portion of the retrofitted girders' behavior was due to the inelastic modulus of the steel, where the post-yield behavior of the steel was greatly affected by the elastic modulus of the CFRP.

Table 17. Inelastic Strength Increase of Retrofits at their Ultimate

Specimen		Failure Load (kip)	Failure Displacement (in)	Load on Control Beam at Same Displacement (kip)	% Increase Over the Control	Failure Mode
Nippon	1-BBF	163.5	1.36	145.4	12.5	CFRP Rupture
	2-BBF	165.2	0.90	130.3	26.8	CFRP Rupture
	1-TBF	147.1	0.83	127.2	15.6	CFRP Rupture
Sika	1-BBF	211.6	3.35	161.9	30.7	CFRP Rupture
	2-BBF	196.4	2.39	157.6	24.6	NA*
	1-TBF	177.5	1.60	148.2	19.7	Intermediate Debonding

*No failure occurred, testing was terminated

Each failure occurred at a different load, which corresponded to different extreme fiber strains and displacements. If the increase in strength of the Sika retrofits were considered at their ultimate, they would demonstrate a rather large increase in strength compared to the Nippon specimens with the same retrofits. For example, the Sika 1-BBF retrofits had 48.1 kips, or

29.4%, more ultimate capacity than the Nippon 1-BBF retrofit. This difference in load was due to the difference in the amount of CFRP material applied to each specimen and the ultimate strength of the CFRP materials. There was also a 1.97-in difference in displacement at failure between the Sika and Nippon 1-BBF retrofits, which was a 146% difference. This behavior was not surprising, considering the Sika 1-BBF specimen had 2.6 times more equivalent steel applied than that of the Nippon 1-BBF retrofit, as shown in Table 13.

While the ultimate capacity is critical, making an accurate comparison of each of these retrofits at analogous points in their behaviors is as equally important. In doing so, a comparison was made for each CFRP type at the lowest load that caused the failure. The results of this comparison can be seen in Table 18.

Table 18. Inelastic Strength Increase of Retrofits at Comparison Points

Specimen		Beam Load (kip)	Comparison Displacement (in)	Load on Control Beam at Same Displacement (kip)	% Increase Over the Control
Nippon	1-BBF	147.0	0.83	127.0	15.6
	2-BBF	156.0	0.83	127.0	22.7
	1-TBF	147.0	0.83	127.0	15.8
Sika	1-BBF	177.1	1.60	148.2	19.46
	2-BBF	177.6	1.6	148.2	19.8
	1-TBF	177.5	1.60	148.2	19.73

Table 18 best represents the expected behavior of these retrofit types, indicating that larger quantities of applied CFRP equates to a greater strength increase. However, based on the results shown in Table 18, Figure 31, and Figure 32, additional plies of CFRP did not double the load increase. In fact, all of the Sika retrofits have similar strength increases (around 20%) at a

deflection of 1.6 in. This behavior is not a discrete occurrence, but over the entire post-yield behavior of the Sika retrofits, as highlighted in Figure 31, where all three of these Sika retrofit specimens have a similar post-yield load-deflection behavior and strength. This performance of multiple layers of CFRP is attributed to poor load transfer between CFRP layers, the difference in steel cross-section of the corroded sections tested, and the unexpected failure mode (out of plane bending/LTB) of the Sika 2-BBF limiting strength increase.

The post-yield behavior and strength increase was different for the Nippon retrofits. Overall, the Nippon retrofits had a more predictable ncrease in strength for the greater amounts of CFRP that were applied. While the Sika retrofits exhibited diminishing returns as more CFRP was applied to the retrofitted beams, increasing the amount of the Nippon strengthening system showed a greater increase in strength by a factor of around 1.5. Also, shear lag was not as affective for the Nippon retrofitting system, unlike the Sika retrofits.

4.5.4.3 Elastic Stiffness

The elastic stiffness of each specimen was compared at a load of 100 kips. The increase in elastic stiffness relative to the control specimen can be seen in Table 19. The elastic stiffness increase was similar to the elastic strength increase (shown in Table 14 and Table 15). The widely varying surface profiles of the beam specimens had a similar influence on the elastic stiffness. Therefore, the comparison between each specimen and the control specimen is not a perfect comparison.

Table 19. Elastic Stiffnesses of All the Retrofits

Specimens	Control	Sika			Nippon		
		1-BBF	2-BBF	1-TBF	1-BBF	2-BBF	1-TBF
Stiffness (kip/in)	183.2	185.9	195.3	210.5	212.3	198.0	198.8
% Increase over Control (Elastic)	NA	1.5	6.6	14.9	15.9	8.1	8.5

4.5.4.4 Inelastic Stiffness

The inelastic stiffness (post-yield behavior of steel, prior to yield of the CFRP) of each specimen was calculated using two points in the tangential post-yield load-deflection behavior of these retrofits. The initial stiffness point was selected beyond the post-yield behavior and in the steady tangential portion of the load-deflection plot. The second stiffness point was selected just prior to the CFRPs rupture. These tangential slopes occurred at different loads and displacements for each specimen. The Nippon 2-BBF and 1-TBF never achieved this steady tangential behavior, so they are excluded from the comparison. The inelastic stiffness increase relative to the control specimen is shown in Table 20, demonstrating that these retrofits can increase the post-yield stiffness by 4.7 to 6.2 times. These results show that significant strength and stiffness gains can be achieved in steel structures' post-yield behavior using CFRP retrofits.

Table 20. In-Elastic Stiffnesses of All the Retrofits

Specimens	Control	Sika			Nippon		
		1-BBF	2-BBF	1-TBF	1-BBF	2-BBF	1-TBF
Stiffness (kip/in)	3.6	25.4	22.3	26.2	21.1	NA	NA
% Increase over Control (InElastic)	NA	596.5	510.0	618.6	478.5	NA	NA

4.5.4.5 Ductility

The Nippon retrofits in these tests ruptured shortly after yielding of the steel beam, while the Sika retrofits exhibited substantially more deformation before CFRP failure. This behavior was expected because of the difference in each material's rupture strain; the Nippon material had a rupture strain of 0.32%, while Sika's was 2.11%. The midspan deflections associated with the Nippon 1-BBF and the Sika 1-BBF at failure were 1.36 in and 3.46 in, respectively. Therefore, the Sika 1-BBF retrofit allowed for 2.46 times the amount of vertical deflection before the failure of the CFRP, compared to the Nippon 1-BBF.

4.5.4.6 Failure Behavior

CFRP rupture was the expected failure mode for all of the tested retrofits; however, this did not occur for the Sika 1-TBF, which failed due to intermediate debond. The failure started in the high-stress regions, beneath the point loads in Figure 29, and propagated towards the end region, ultimately resulting in end region debonding. This progressive debond can be seen in Figure 34, where initially, debonding started near strain gauge FRP_6 at timestamp 1:19. Loading continued, and more debonding near FRP_6 occured around times of 1:26 and 1:29, where nearby gauges FRP_5 and FRP_7 evidenced the redistribution of loading. Loading and debond

propagation continued until the failure of this retrofit, where there is a non-linear increase in strain gauge FRP-8 (end region), just before failure.

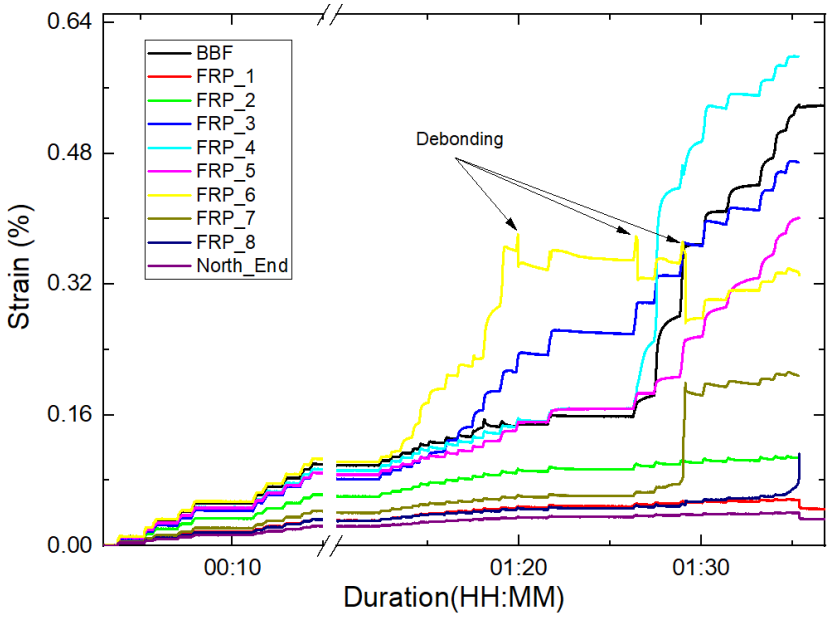

Figure 34. Sika 1-TBF Strain vs Test Duration Plot

Figure 34 also shows that gauges FRP_3 and FRP_6 have disproportionately larger strains than the other strain gauges located in the constant moment region. The high strains in FRP_3 and FRP_6 were attributed to their proximity to the stiffeners used to distribute the point loading of the spreader beam. The high-stress concentrations near the stiffeners caused an adhesive failure in the retrofit, which led to intermediate debonding and the Sika 1-TBF retrofit's eventual failure. The occurrence of high strains near the stiffeners did occur for the other five retrofits, however, not as drastically as the Sika 1-TBF retrofit. These findings lead these authors to conclude that intermediate debond is only an issue when intermediate stiffeners are used with the Sika CFRP material used on the top side of the bottom flange.

Excluding the Sika 1-TBF failure modes, the failure behavior of the two CFRP systems were very different. Figure 31 shows that after the failure (rupture) of the Sika retrofits, the specimens follow the load-deflection behavior of the control beam. The reason is that, when the Sika retrofits failed, the CFRP completely debonded, leaving only the remaining steel member to resist the flexural loads. This failure of the CFRP was likely due to the large amount of elastic strain energy that was built up in the system and instantaneously released upon CFRP failure.

The Nippon retrofits, tended to fail only in localized areas, had only a small portion of the CFRP retrofit rupture or debond, as evidenced through the localized failures in Figure 32. In general, these localized ruptures incurred some amount of debonding but generally did not propagate beyond 4 in. from the point of rupture; the CFRP located outside the failure region remained bonded to the steel. This behavior can be observed in the strain gauge data for the Nippon 1-BBF retrofit in Figure 35. As the loading applied to the beam increased, larger observed strains were recorded. Gauge FRP_1 was located at one end of the CFRP retrofit and FRP_8 at the other end, as shown in Figure 29. The midspan of the beam was located between gauges FRP_4 and FRP_5. At 54 minutes, the large drop in strain at gauge FRP_5 indicated a localized failure of the CFRP retrofit at that location. As loading continued, other localized failures were observed near gauges FRP_6 and FRP_4. After the failure near gage FRP_4, the strain values in gauge TBF (located at midspan on the top of the bottom flange) started to increase dramatically, and the remaining gauges experienced only small increases in strain. Thus, the CFRP retrofit's exterior regions were still intact, while the retrofit near midspan had mostly failed.

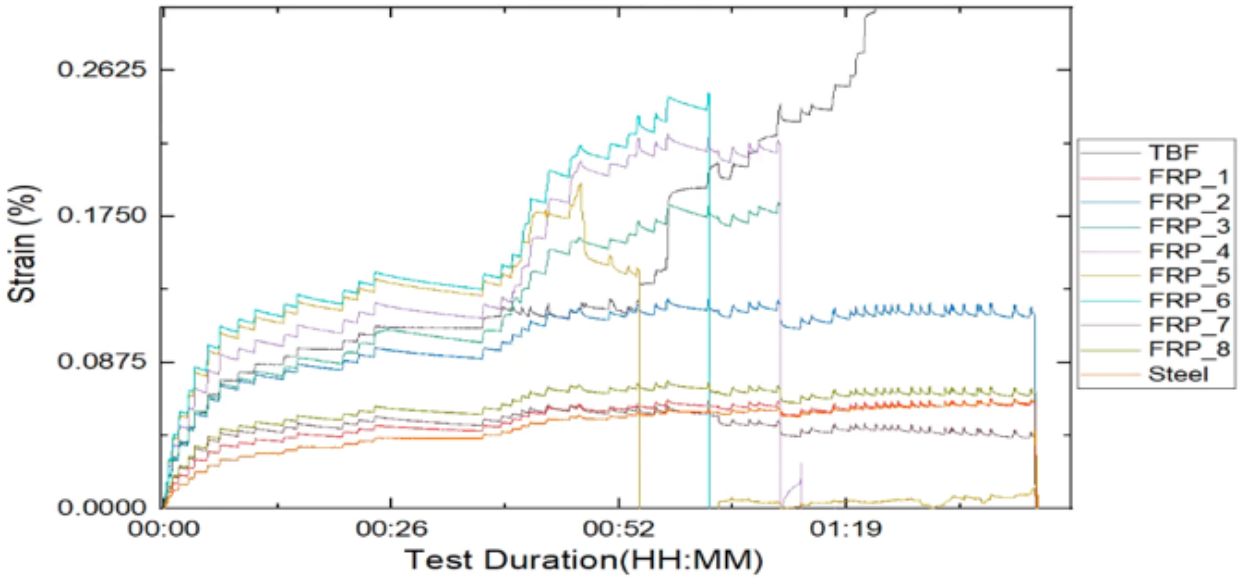

Figure 35. Nippon 1-BBF Strain Gauge Data Versus Test Duration

While this localized failure was quantified through strain gauge data, it was also observed visually and audibly during the testing. 11 audible CFRP rupture failures were heard during testing the Nippon 1-BBF specimen. After each of these failures, the researchers examined the location of failure. A typical localized Nippon CFRP rupture can be seen in Figure 36 I. &II. These observations demonstrate that many localized failures can occur before the complete failure of the Nippon CFRP retrofit.

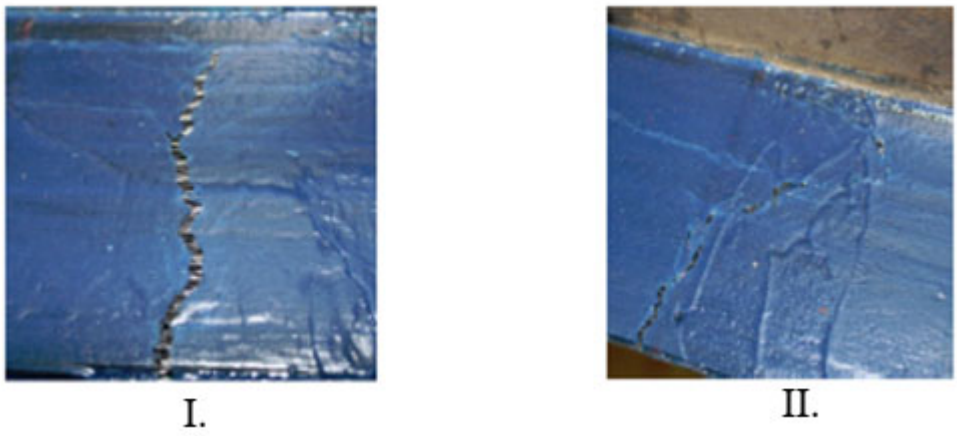

Figure 36. Examples of Nippon CFRP Rupture (I. & II.)

4.5.5 Comparison of the Prediction Model

Table 21 compares the ratio of the experimentally obtained maximum moment to the calculated moment, based on the CFRP rupture limit state. The CFRP rupture strain was based on force equilibrium, strain compatibility, and material test results. The benefits of calculating strength based on a known strain value gives the designer confidence that the design is within the limits of the CFRP material properties and also lets the designer specify whether the strength increase occurs in the inelastic or elastic region. With this design approach, the experimental versus theoretical ratios ranged from 0.69 to 0.96 for the Sika retrofits and 0.91 to 0.99 for the Nippon retrofits. The BBF retrofit predictions were also more accurate than those for the TBF retrofits. Overall, this approach provided a reasonable estimation of the ultimate capacity. It should also be noted that the Sika 1-TBF unexpectedly failed due to debonding and a comparison of its theoretical moment is not justified here.

Table 21. Comparison of the Test Data to the Prediction Model

Specimen		Assuming CFRP Rupture			Based on Strain at Experimental Failure			
		Failure Moment (Kip-ft) [1]	Theoretical Moment (Kip-ft) [2]	Experimental vs. Theoretical [1] vs. [2]	Failure Moment (Kip-ft) [3]	Strain at Failure (%) [4]	Calculated Moment, Limited by Failure Strain (Kip-ft) [5]	Experimental vs. Calculated [3] vs. [5]
Control					402.1	0.3	408.0	**0.99**
Nippon	1-BBF	466.2	470.2	**0.99**	466.2	0.215	420.8	**1.11**
Nippon	2-BBF	465.9	504.6	**0.92**	465.9	0.296	486.72	**0.96**
Nippon	1-TBF	414.8	455.7	**0.91**	414.8	0.32	461.7	**0.9**
Sika	1-BBF	594.8	622.4	**0.96**	594.8	1.53*	573.5	**1.04**
Sika	2-BBF**	**	780	**NA**	548.5	0.6	531.3	**1.03**
Sika	1-TBF	498.8	725.7	**0.69**	498.8	0.49	500.1	**1.0**

*These points were extrapolated from other strain gauges, **This retrofit did not fail

The theoretical capacity at the predicted CFRP rupture strain (column [2] in Table 22) gives useful information about potential design strength, but if the predicted strain limit is never reached, the calculation gives no insight as to how closely the analytical model can make predictions. Nevertheless, examining how closely the analytical model predicted the observed behavior during testing is important. Therefore, the analytical models were completed for each retrofit, with the highest recorded strain at the onset of significant failure in each specimen. In the Sika 1-BBF retrofit, the strain gauges had surpassed their gauge limit; therefore, the strain was determined from linear interpolation from the steel strain gauges located at midspan of the beam. The ratio of experimental strength to calculated strength is shown in Table 21. The calculated strength was determined using experimental strain gauge data, which allowed for a direct strength comparison of experimental data to that of the analytical model. With this design

approach and known strain values, the experimental versus calculated ratios ranged from (1.0 to 1.04) for the Sika retrofits and (0.9 to 1.11) for that of the Nippon retrofits. These predicted results were reasonable, considering that the steel had such a varied cross-section, and the composite systems were made up of several components with varied material properties.

In addition to a comparison of the maximum capacity, Figure 37 shows a sample plot of test data compared to seven predicted values for both the control beam and the Sika-1BBF specimen. The test data is from a steel strain gauge on the bottom of the bottom flange at midspan. The Sika 1-BBF's CFRP strain gauge data came from the most strained gauge (FRP_4) during testing. The strain gauges had a 1% strain limit, which is why there was no test data beyond that strain. However, the data was extrapolated to the CFRP retrofit's failure point, using three steel strain gauges at midspan remaining on the Sika 1-BBF specimen, and is denoted by a star in Figure 37. The prediction models trend closely with the data and provide a visual comparison tool for designers to use when considering a retrofit of this type.

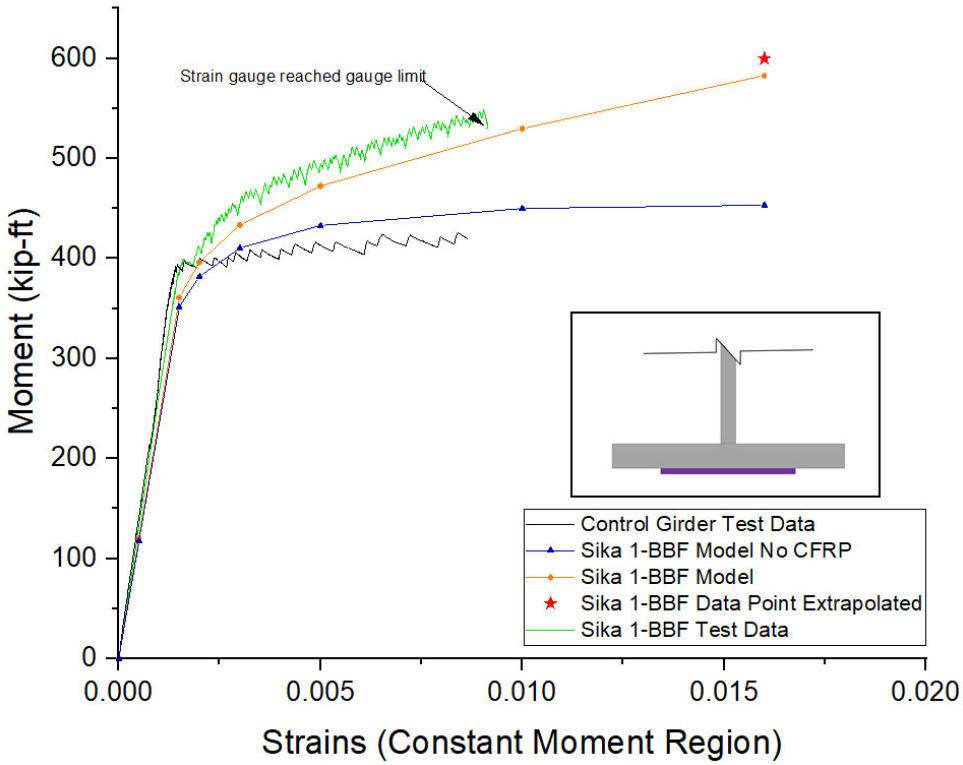

Figure 37. Moment vs. Strain Plot from Test Data and Analytical Prediction Model

4.5.6 Shear Lag

The examination of shear lag's effects on these different retrofitting systems is important when examining the behavior of the experimental versus calculated strengths of these CFRP retrofits. Values less than 1 indicated that the prediction model was over-predicting the beam's strength or there was something occurring on the beam which caused it to under preform, such as material differences, high levels of deterioration or shear lag. Strain profiles for the deformations shown in Table 18 (1.6 in and 0.82 in) were completed for the Sika and Nippon materials using the 1- and 2-BBF set ups. Figures 38 and 39 for the respective CFRP materials show the strain profiles, based on the midspan strain gauges (black circles connected via a black line). Accompanying the steel strain gauge data is a green trend line (linear regression) for the steel strain gauge data.

Besides steel strain gauge data, there is CFRP strain gauge data (4 gauges located inside or near the constant moment region), which are shown as black stars. Lastly, there is the analytical prediction for each of the retrofits based on the applied moment from the testing data (shown as a red line).

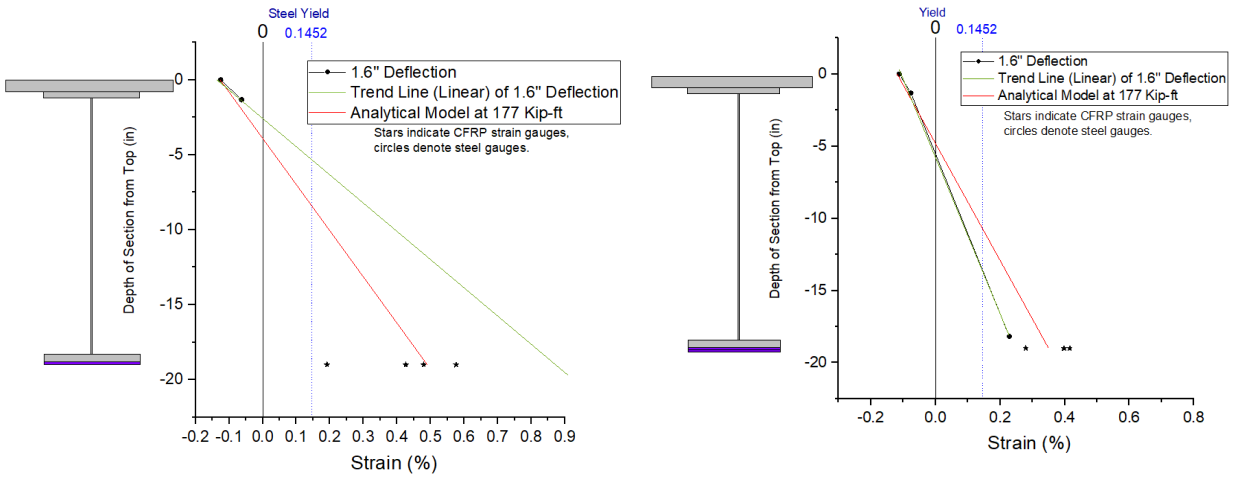

I. Sika 1-BBF Strain Profile

II. Sika 2-BBF Strain Profile

Figure 38.Sika Strain Profiles for 1 & 2 BBF Retrofits (Data vs Analytical)

When examining the behavior of the Sika 1- BBF in Figure 38 I, it appears that the CFRP has an average strain value around that of the analytical prediction; however, that value is much lower than that of the data's trend line. This behavior of CFRP strains being lesser than the data's trend line is likely because there are only 2 steel strain gauge points used to make this trend line (the gauge on the TBF was not reading at this point). Figure 38 II shows Sika 2- BBF strain profile which shows the CFRP's strain ahead of both the data and analytical prediction strains. This result was also observed for the Sika 1-TBF retrofit. While one could argue that there might have been some shear lag occurring for the Sika 1-BBF specimen based on the data, the other Sika

specimens tested did not show this same behavior, and in fact, had more strain than that of the gauged steel strain profile. This overall behavior indicates that no shear lag occurred at the location of these strain gauges.

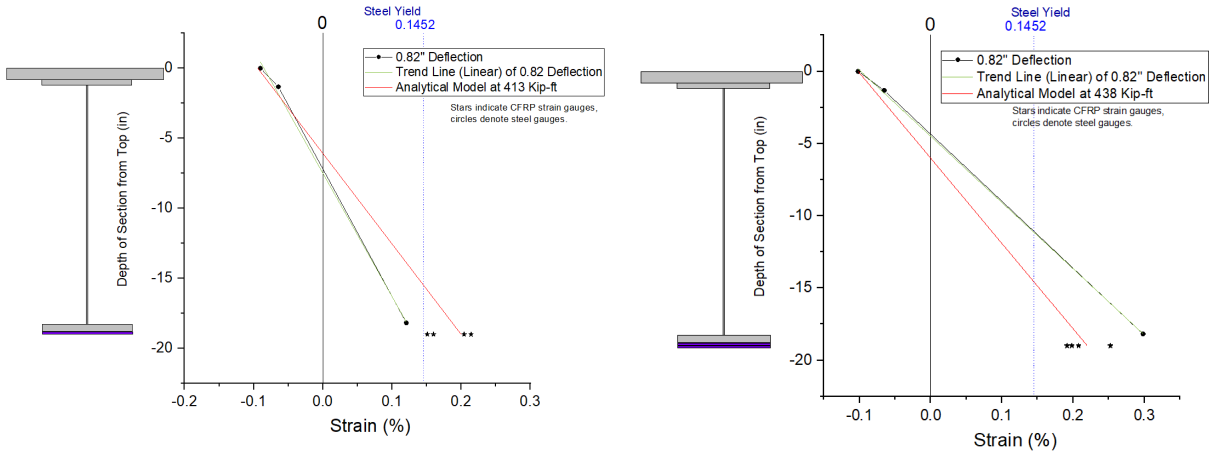

I. Nippon 1-BBF Strain Profile II. Nippon 2-BBF Strain Profile

Figure 39.Nippon Strain Profiles for 1 & 2 BBF Retrofits (Data vs Analytical)

Examining the behavior of the Nippon 1- BBF in Figure 39 I, the CFRP had an average strain value above the data's trend line and a little below the theoretical. Figure 39 II shows Nippons 2- BBF strain profile which shows the CFRP's average strain lagging behind both the steel data and analytical prediction strains, thus indicating that there was some shear lag occurring on this specimen. The behavior of CFRP strain leading the profile trendlines was observed for the Nippon 1-TBF.

Table 23 provides the percent error from the CFRP strain gauge average against the data and the analytical predictions. A negative percent error indicates that the CFRP's strain values lagged

behind the strain profile. This data indicates that there was likely little to no shear lag for the Sika retrofitted specimens. However, for two plies of the Nippon retrofitting system, it appears that shear lag contributed to lower strength and a shear reduction factor of 35% is proposed (rounded up average from the percent error data). This reduction should be applied to the elastic modulus during the design process.

Table 23. % Error from the CFRP Strain Gauge Average vs. Trend Lines for Different Retrofitting Systems

Retrofitting System	Retrofit	CFRP Strain Gauge Average in Constant Moment Region (Strain in %)	Percent Error from Data Trend Line	Percent Error from Analytical Trend Line
Sika	1-BBF	0.418	-51.9	-14.3
	2-BFF	0.373	55.3	6.5
	1-TBF	0.447	-9.7	32.3
Nippon	1-BBF	0.183	39.4	-8.7
	2-BFF	0.213	-34.0	-3.4
	1-TBF	0.249	91.2	28.8

4.6 Conclusions

Even with a variable surface profile resulting from corrosion section loss, each of the CFRP retrofits examined were a viable strengthening option. The ease of installation, strength-to-weight ratio, and increase in strength and stiffness make these CFRP retrofits a good candidate when considering the strengthening of existing structures in a deteriorated condition. The following conclusions and recommendations can be made as a result of this research:

4.6.1 Surface Variability

- CFRP flexural strengthening on steel beams with rust grades C & D can be conservatively and accurately calculated assuming CFRP rupture.

- Pitting corrosion and section loss up to 0.125 in has little effect on the CFRP retrofits' ability to achieve strengths within reasonable proximity to their calculated design strengths. However, further testing is required to determine how roughness, amplitude, and the density of the roughness affect bond strength.

4.6.2 Design

- Conventional strain compatibility calculations, used in conjunction with elastic-perfectly plastic assumptions, known material properties and section geometries, and assuming CFRP rupture, are able to closely predict the actual moment capacity , although these calculations are slightly unconservative.
- The analytical model used in this research can conservatively and relatively accurately predict the failure load, provided that the actual failure strainof the CFRP material is known.
- Installing CFRP on the top of the bottom flange results in the lowest performance compared to using one or two plies of the material on the bottom flange. The TBF configuration is more difficult to predict than the other retrofits; in the case of the Sika material, the TBF configuration failed prematurely.
- When designing flexural CFRP retrofits, the CFRP rupture design strength may be used to approximate the capacity; however, the results may be unconservative (up to 11%). Therefore, it would be appropriate to employ a strength reduction factor to ensure the maximum design strains are well below CFRP rupture. Additionally, when designing a CFRP retrofit, all appropriate failure modes should be evaluated, including:

- Strength capacity
- Maximum stress/strain associated with debond near CFRP termination
- Maximum strain associated with intermediate debond at maximum moment location

- The CFRP retrofits exhibit their greatest benefits in strength and stiffness increases after yielding of the structure.

4.6.3 Performance/Configurations

- The presence of multiple plies of CFRP has only a moderate effect on total strength.
  - For the Sika retrofits, two plies of CFRP on the bottom of the bottom flange does not significantly increase the beam's strength and stiffness in proportion to the amount of additional material applied; however, this is attributed to this beam's deteriorated condition and failure mode, not the effects of shear lag. Further testing is recommended to examine the effects of shear lag near the material's rupture.
  - For the Nippon retrofits, two plies of CFRP on the bottom of the bottom flange does moderately increase the beam's strength and stiffness. However, doubling the number of plies does not necessarily mean doubling the material performance. This lesser performance is attributed to shear lag for multiple plies of the Nippon CFRP. It is recommended that a shear lag reduction factor of 35% be applied to the elastic modulus during the design process.

- The top of bottom flange retrofit is more susceptible to intermediate debond if intermediate stiffeners are present on the retrofitted girder. Intermediate debond is associated with lower overall loading and occurred only for the Sika 1-BBF specimen. Where the Sika TBF retofits are less desirable compaired to the Sika BBF retofits.
- system, while the Nippon retrofits experience localized failure that allowed for portions of the retrofit to remain intact. This localized failure is also successive and can be observed via visual inspection, which is ideal because it indicates failure before the system's complete loss.
- The ductility of each of the CFRP repairs is dramatically lower than the baseline steel material. Therefore, well-defined limits must be set when designing CFRP retrofits.

4.7 Acknowledgments

The authors would like to acknowledge the Virginia Department of Transportation for the donation of the test specimens and the application of the CFRP configurations.

References

Al-Saidy, A. H. (2001). “Structural Behavior of Composite Steel Beams Strengthened/Repaired with Carbon Fiber Reinforced Polymer Plates.”

Chajes, M. J., Chacon, A. P., Swinehart, M. W., Richardson, D. R., and Wenczel, G. C. (2005). “Applications of Advanced Composites to Steel Bridges: A Case Study on the Ashland Bridge.” 19716(March).

Deng, J., and Lee, M. M. K. (2007a). “Fatigue Performance of Metallic Beam Strengthened with a Bonded CFRP Plate.” Composite Structures, 78(2), 222–231.

Deng, J., and Lee, M. M. K. (2007b). “Behaviour Under Static Loading of Metallic Beams Reinforced with a Bonded CFRP Plate.” Composite Structures, 78(2), 232–242.

Fernando, D., Teng, J. G., Yu, T., and Zhao, X. L. (2013). “Preparation and Characterization of Steel Surfaces for Adhesive Bonding.” Journal of Composites for Construction.

FHWA. (2012). Bridge Inspector’s Reference Manual- FHWA NHI 12-049. Federal Highway Administration.

Galal, K., Tirca, L., and Seif ElDin, H. M. (2009). “Flexural Performance of Steel Girders Retrofitted Using CFRP Material.” Composite for Construction, 16(June), 1–16.

Haghpanah, B., Chiu, S., and Vaziri, A. (2014). “Adhesively Bonded Lap Joints with Extreme Interface Geometry.” International Journal of Adhesion and Adhesives, Elsevier, 48, 130–138.

Hidekuma, Y., Kobayashi, A., Tateishi, A., Nagai, M., and Miyashita, T. (2011). “Repairing Method for the Steel Members by CFRP Strand Sheets.” Advances in FRP Composites in Civil Engineering - Proceedings of the 5th International Conference on FRP Composites in Civil Engineering, CICE 2010, 881–885.

ISO. (2007). ISO 8501-1 The Rust Grade Book.

Kim, W. S., Yun, I. H., Lee, J. J., and Jung, H. T. (2010). “Evaluation of Mechanical Interlock Effect on Adhesion Strength of Polymermetal Interfaces Using Micro-patterned Surface Topography.” International Journal of Adhesion and Adhesives, Elsevier, 30(6), 408–417.

Kim, Y. J., and Brunell, G. (2011). “Interaction Between CFRP-repair and Initial Damage of Wide-flange Steel Beams Subjected to Three-point Bending.” Composite Structures, Elsevier Ltd, 93(8), 1986–1996.

Kleffel, T., and Drummer, D. (2017). “Investigating the Suitability of Roughness Parameters to Assess the Bond Strength of Polymer-Metal Hybrid Structures with Mechanical Adhesion.” Composites Part B: Engineering, Elsevier Ltd, 117, 20–25.

Lenwari, A., Thepchatri, T., and Albrecht, P. (2005). “Flexural Response of Steel Beams Strengthened with Partial-Length CFRP Plates.” Journal of Composites for Construction.

Liu, X., Silva, P. F., and Nanni, A. (2001). “Rehabilitation of Steel Bridge Members with FRP Composite Materials.” CCC 2001 Composites in Construction, (100 mm), 613–617.

Mertz, D. R., and Gillespie, J. W. J. (1996). NCHRP-IDEA Final Report: Rehabilitation of Steel Bridge Girders Through the Application of Advanced Composite Materials. Washington, DC.

Mertz, D. R., Gillespie Jr, J. W., Chajes, M. J., and Sabol, S. (2002). “Rehabilitation of Steel Bridge Girders Using Advanced Composite Materials.” NCHRP-IDEA Program Project Final Report Project 51, 36.

Miller, T. C., Chajes, M. J., Mertz, D. R., and Hastings, J. N. (2001). “Strengthening of a Steel Bridge Girder Using CFRP Plates.” Journal of Bridge Engineering, 6(6), 514–522.

Milliken Infrastructure. (2017). “Renew Wrap Strand Sheet Adhesive (BF-E7S).”

Milliken Infrastructure. (2018). Renewwrap Installation Manual. Spartanburg, SC.

Moy, S. S. J. (2002). “Steel Beams Strengthened with Carbon Fibre Reinforced Polymer Composites.” Advanced polymer composites for structural applications in construction, (March), 195–202.

Moy, S. S. J., Barnes, F., Moriarty, J., Dier, A. F., Kenchington, A., and Iverson, B. (2000). “Structural Upgrade and Life Extension of Cast Iron Struts Using Carbon Fibre Reinforced Composites.” FRC 2000–Composites for the Millennium, (March), 3–10.

Nagai, M., Hidekuma, Y., Miyashita, T., Okuyama, Y., Kudo, A., and Kobayashi, A. (2012). “Bonding Characteristics and Flexural Stiffening Effect of CFRP Strand Sheets Bonded to Steel Beams.” Procedia Engineering, 40, 137–142.

Narmashiri, K., Jumaat, M. Z., and Sulong, N. H. R. (2012). “Strengthening of Steel I-Beams Using CFRP Strips: An Investigation on CFRP Bond Length.” Advances in Structural Engineering, 15(12), 2191–2204.

Peiris, N. A. (2011). “Steel Beams Strengthened with Ultra High Modulus CFRP Laminates.” University of Kentucky.

Phares, B. M., Wipf, T. J., Klaiber, F. W., Abu-Hawash, A., and Lee, Y.-S. (2003). “Strengthening of steel girder bridges using FRP.” Proc., 2003 Mid-Continent Transportation Research Symp, (August 2003), 1–12.

Rizkalla, S., Dawood, M., and Schnerch, D. (2008). “Development of a carbon fiber reinforced polymer system for strengthening steel structures.” Composites Part A: Applied Science and Manufacturing, 39(2), 388–397.

Salama, T., and Abd-El-Meguid, A. (2010). Strengthening Steel Bridge Girders Using CFRP. University Transportation Center for Alabama, Birmingham, AL.

Schnerch, D., Dawood, M., Rizkalla, S., and Sumner, E. (2007). "Proposed Design Guidelines for Strengthening of Steel Bridges with FRP Materials." Construction and Building Materials, 21(5), 1001–1010.

Schnerch, D., and Rizkalla, S. (2008). "Flexural Strengthening of Steel Bridges with High Modulus CFRP Strips." 13(2), 192–201.

Shields, C. K., Hajjar, J. F., and Nozaka, K. (2004). Repair of Fatigued Steel Bridge Girders with Carbon Fiber Strips.

Sika. (2014). Sika CarboDur System. Pfäffikon ZH, Switzerland.

Da Silva, L. F. M., Ferreira, N. M. A. J., Richter-Trummer, V., and Marques, E. A. S. (2010). "Effect of Grooves on the Strength of Adhesively Bonded Joints." International Journal of Adhesion and Adhesives, Elsevier, 30(8), 735–743.

Wipf, T. J., Phares, B. M., Klaiber, F. W., Lee, Y. S., and Al-Saidy, A. H. (2005). Strengthening Steel Girder Bridges with Carbon Fiber – Reinforced Polymer Plates. Transportation Research.

Yao, Q., and Qu, J. (2002). "Interfacial Versus Cohesive Failure on Polymer-Metal Interfaces in Electronic Packaging-Effects of Interface Roughness." Journal of Electronic Packaging, Transactions of the ASME, 124(2), 127–134.

Yu, Y., Chiew, S. P., and Lee, C. K. (2011). "Bond failure of steel beams strengthened with FRP laminates - Part 2: Verification." Composites Part B: Engineering, 42(5), 1122–1134.

CHAPTER 5: Large Scale Laboratory Testing and Field Testing of Flexural CFRP Retrofits on Corroded Steel Girders

Chapter 5 consists of the manuscript " Load Test to Evaluate a Flexural Repair of a Deteriorated Bridge with Carbon Fiber Reinforced Polymer Strand Sheets". This paper is to be submitted to Elsevier's Engineering Structures Journal.

Load Test to Evaluate a Flexural Repair of a Deteriorated Bridge with Carbon Fiber Reinforced Polymer Strand Sheets

Samuel T. Sherry[1*], Matthew Hebdon[1], Ph.D., P.E.

[1]Thomas M. Murray Structural Engineering Laboratory, Charles E. Via, Jr. Department of Civil Engineering and Environmental Science, Virginia Tech, 255 Inventive Lane, Blacksburg, VA 24060

[*]Corresponding Author. sher3004@vt.edu

5.1 Abstract

With transportation infrastructure deteriorating and being subject to ever-increasing demands, one easily implementable technique to flexurally strengthen steel bridge beams is the use of carbon fiber-reinforced polymers (CFRPs). Advantages of CFRPs include their high strength-to-weight ratio and ease of installation. This study investigated the application of multiple plies of high modulus CFRP strand sheets to increase the flexural capacity of steel beams that had experienced corrosion section loss. The CFRP retrofits were evaluated through large-scale laboratory testing and in situ testing on a simply supported steel beam bridge. The laboratory testing confirmed that the CFRP retrofit could return a deficient beam to its original elastic moment capacity - a 37.9% increase over its deteriorated capacity. The in-situ testing showed that this retrofit effectively reduced localized stresses, by a minimum of 50%, and deformations, by a minimum of 23.6%.

The retrofit also greatly influenced live load distribution from localized behavior to more even distribution across the bridge's width. Lastly, the corrosion damage on these beams did not significantly reduce the strength, stiffness, or bondability of the CFRP retrofit on the tested beam.

5.2 Introduction

Bridges may be reduced to sub-par performance as members deteriorate and traffic demands increase with time. Some of these deteriorated or structurally deficient bridges must be load posted due to inadequate load capacity, which may be controlled by a small number of problematic bridge beams (FHWA 2012). Some DOT are interested in using carbon fiber-reinforced polymer (CFRP) laminates as a non-conventional means of rehabilitating individual bridge members to their original capacity. The advantages of CFRP materials are their high strength-to-weight ratio, ease of installation, and mitigation of further corrosion issues. However, there is little literature relating to CFRP materials being applied to steel structures with realistic corrosion section loss or a variable surface profile due to corrosion. Additionally, the use of a high modulus strand sheet has not been thoroughly examined and has never been applied to an existing steel bridge structure in the United States. Finally, there is little data on how a CFRP retrofit will impact the live load distribution of a structure when only severely deteriorated members are rehabilitated. This research project investigated the strength and stiffness provided through a CFRP retrofit of individual bridge beams, both in large-scale laboratory testing and on an in situ bridge. Lastly, this research characterized the amounts and types of corrosion these CFRP retrofits were applied to. This detailed characterization of corrosion will provide guidance on appropriate applications for high modulus (HM) CFRP strand sheets.

5.2.1 Laboratory Retrofits

In 1996, Mertz and Gillespie completed some of the earliest work on structural steel beams retrofitted with CFRP materials to determine if CFRP retrofits were a viable solution, how well they matched conventional strength predictions, and what types of detailing performed the best. Since then, there has been much research relating to specific topics, including prediction models, bond length, CFRP types, fatigue life, and durability. The topics of most relevance to this research can be parsed into the laboratory testing of undeteriorated and deteriorated beam retrofits.

Due to the difficulty of finding corroded steel members of the same size and relative amounts of corrosion damage, researchers have opted to create "simulated" corrosion damage on steel beams (Al-Saidy et al. 2004; Kim and Brunell 2011; Liu et al. 2001). In each of these studies, the simulated corrosion is not conventional because it does not have a variable roughness along the length of a beam, but has a section of steel removed from an area to represent localized section loss. The steel beams were obtained directly from a steel mill or manufacturer. These research projects focused more on retrofit behavior than the effects of a corroded surface profile on strength. The most promising research was able to return steel beams to flexural strengths 24% above their strength with section loss (Al-Saidy et al. 2004).

The researchers Chajes et al. (2005), Mertz et al. (2002), and Mertz & Gillespie (1996), all of whom tested corroded steel members in the laboratory, provided limited data on the extent of the corrosion damage of their specimens. Mertz and Gillespie (1996) applied and tested CFRP retrofits on I 24x80 steel bridge beams with an estimated amount of corrosion damage ranging from 30 to 40%. The CFRP retrofits applied to the beams were able to return the beams to their original strengths and subsequently failed due to lateral-torsional buckling. Mertz et al. (2002)

tested two more corroded I 24x80 steel bridge beams (removed from the same bridge as the 1996 Mertz and Gillespie study), and examined the fatigue life of the CFRP retrofits. This corrosion damage had no detrimental effects on the CFRP's strength or stiffness even after 10 million stress cycles, which simulated 4.6 years of average daily truck traffic. Chajes et al. (2005) were able to reduce strains using CFRP on a structurally deficient steel through-beam bridge; however, the extent of the corrosion damage was not documented.

Both the simulated corrosion-damaged beams and the actual corrosion-damaged beams showed increased strengths due to the CFRP retrofits. However, the impact that varying levels of section loss have on a CFRP retrofit has not been investigated, nor has the impact of variable surface profiles as experienced in a severely corroded surface.

5.2.2 In situ Retrofits

There have been many effective research studies conducted on the flexural strengthening/retrofitting of in situ bridges comprised of steel beams with CFRP (Chajes et al. 2005; Mertz et al. 2002; Miller et al. 2001; Moy 2002; Moy et al. 2000; Peiris 2011; Phares et al. 2003; Wipf et al. 2005). The majority of these studies were proof of concept and were on bridges with little to no structural corrosion deterioration requiring the use of a CFRP retrofit. They serve as data points that CFRP retrofits can reduce stresses, strains, and deflections on a steel bridge structure. One such example is a CFRP retrofit implemented by Miller et al. (2001) on a steel beam-concrete deck composite in Delaware. The CFRP retrofits reduced strains by 10% and increased stiffness by 11% during the live load testing. While CFRP retrofits have been shown to increase strength and stiffness, the in situ applications have been limited to structures not requiring retrofitting.

5.2.3 Flexural CFRP Strand Sheet Retrofits

The CFRP material used in this research, Renew Wrap Strand Sheet CF900/HM, is a material that has been subject to minimal large-scale laboratory testing (Tabrizi et al. 2015) and no known field testing or implementation on structures in the United States. Outside of the United States, Kobayashi et al. (2015) have completed CFRP strand sheet retrofits in the field, while Hidekuma et al. (2011) and Nagai et al. (2012) have completed work on CFRP strand sheet retrofits on large-scale laboratory tests. Hidekuma et al. (2011) made a direct comparison of different types of CFRPs (pre-cured strand sheets, plate material, and uncured sheet material) subject to tensile and flexural loading. The strand sheet materials were able to obtain retrofit strengths above that of the steel yield; however, the CFRP plate retrofits had debonding failures at 30 to 60% of the steel's yield strength. Nagai et al. (2012) looked at steel beams retrofitted with 10 plies of CFRP strand sheets to investigate how CFRP splices affect bond behavior and what dictates material debond for CFRP strand sheets. This work proposed that debond of this CFRP-to-steel would occur when the stress of the steel near the CFRP termination exceded 280 MPa (40.6 ksi). Finally, Tabrizi et al. (2015) examined how low modulus (LM) and intermediate modulus (IM) CFRP strand sheets influenced the flexural behavior on steel beams. As expected, the IM CFRP had an 8% increase in the elastic strengthening and an 18% increase in stiffness compared to the LM CFRP retrofitted beams. However, shear lag was observed for the IM CFRP. Shear lag is a phenomenon where the strain profile of a section is not linear through the depth of the section. In the cases of CFRP, the strain measurement (at the extreme fibers) is lower than that of the expected based on the steel strain profile, and this is considered lagging strain behavior. This lagging behavior means the optimum benefits of the material are not being utilized. Coupled with the research and the manufacturer's provided guidance on implementation practices

(NEXCO-West 2015) and design, the efficacy of high modulus CFRP strand sheets as a retrofit solution for structures in the U. S. was investigated.

5.3 Research Objectives

The objectives of this research can be broken up into two sections (large-scale laboratory testing and in situ testing). The first objective of the large-scale laboratory testing recreated and tested a replica beam with the same section loss as beam 5 from the Simmons Gap Road Bridge, which controlled the bridge's load. After testing this control beam, the researchers designed and tested a high modulus CFRP strand sheet flexural retrofit on a replica beam. This retrofitted response verified on the retrofitted replica beam would be sufficient to increase the required elastic strength and stiffness of beam 5 on the Simmons Gap Road Bridge. Finally, the researchers determined whether the corrosion damage and surface roughness on the tested flexural retrofit affected the bond or strength of the CFRP retrofit.

In examing the in situ testing, the objective of this part of the research included live load testing on the Simmons Gap Road Bridge (pre and post-retrofit) to measure its response. Where the live load test data was analyzed to see how the response (member stresses, deflections, and load distribution) of the Simmons Gap Road Bridge changed as a result of the high modulus CFRP strand sheet flexural retrofit on beam 5.

5.4 Simmons Gap Road Bridge

The Simmons Gap Road Bridge over the Lynch River was constructed in 1979 and was load posted due to significant corrosion damage. The bridge consisted of two simply supported spans, each with nine W18x50 beams. The bridge has spans of 34 ft (span 1) and 16ft (span 2), a width

of 22 ft, and a skew angle of 23°. A plan view of span 1 of the Simmons Gap Road Bridge is shown in Figure 40.

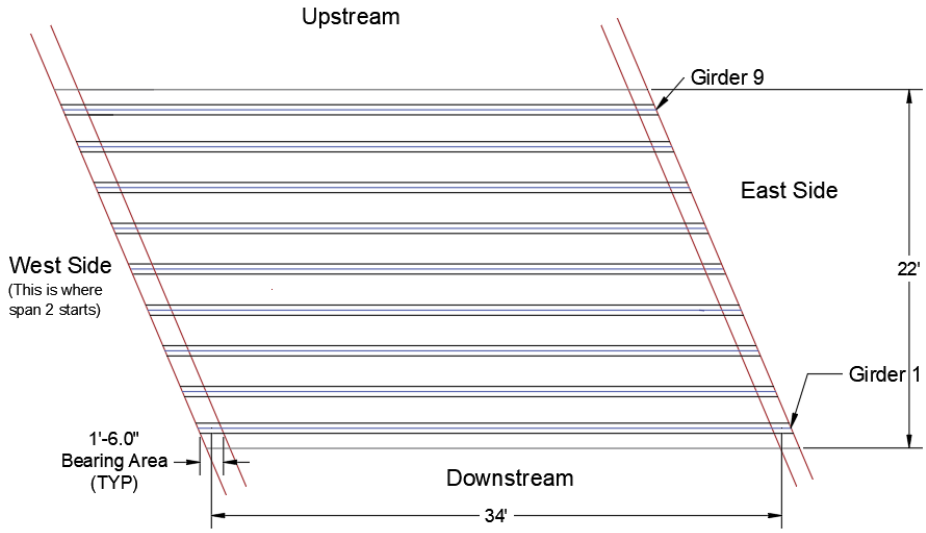

Figure 40. Profile View Span 1 of the Simmons Gap Road Bridge

The most recent load rating, performed in 2018, resulted in a bridge posting controlled by beam 5 due to flange section loss. The remaining bottom flange thickness of beam 5 controlled the flexural rating of the beam and the bridge. The bottom flange of beam 5 had as little as ¼ in (greater than 50% section loss) of material remaining throughout a significant portion of its length. Due to this load posting impact on traffic, VDOT requested assistance from Virginia Tech to develop a flexural CFRP retrofitting system capable of returning beam 5 above its original elastic strength and stiffness.

5.4.1 Inspection of Corrosion

Based on a visual analysis of the Simmons Gap Road Bridge, the most significant corrosion damage on beam 5 was located approximately 17 ft from the west side of the bridge's pier support. A detailed area, 2 ft long, was then measured for thickness with calipers at finite

locations (starting 16 ft from the west side of the pier support) to quantify this region of significant corrosion section loss. Thickness measurements of the bottom flange of beam 5 (over the 2 ft region) were taken with a Neiko 01407A Electronic Digital Caliper with a set of deep measuring attachments. These measurement readings were taken at the approximate center of each of the 1 in by 1 in mesh grids shown in Figure 41. These measurements comprised 168 readings over an area of 24 in by 7.5 in (width of the flange).

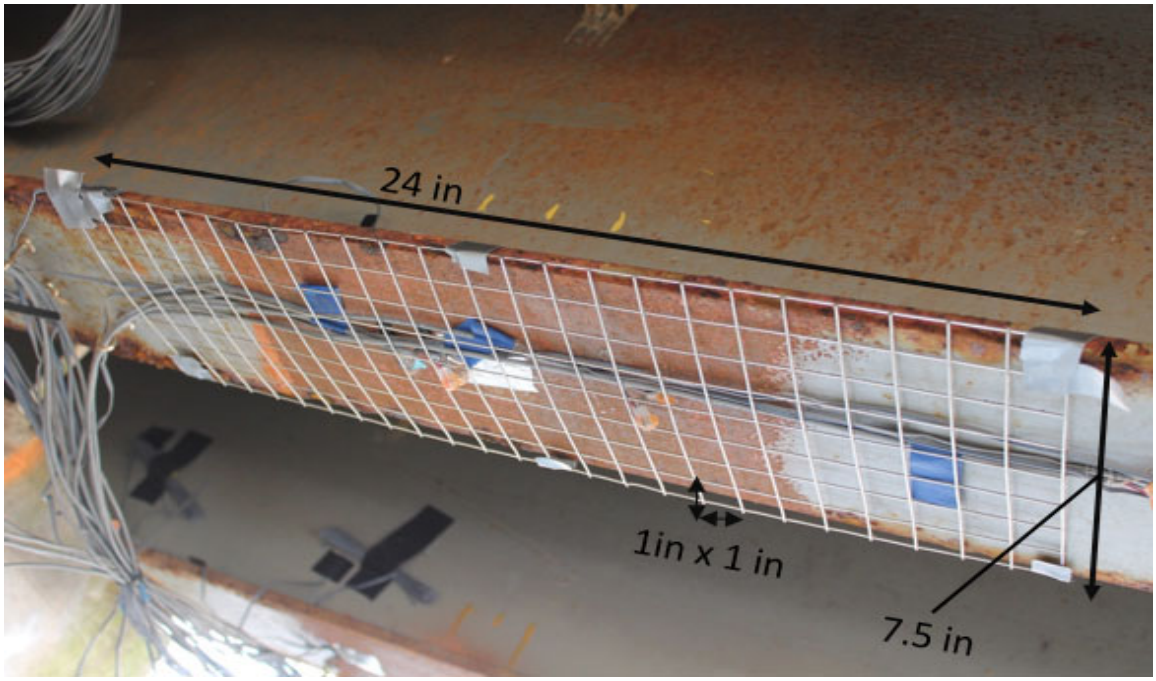

Figure 41. Mesh Grid (7 in. x 24 in.) on the Bottom of the Bottom Flange used to Take Thickness Measurement at 1 in Increments (168 total readings).

Based on the caliper readings and known locations of the corrosion damage measurements on beam 5 of the Simmons Gap Road Bridge, a heat map of bottom flange section loss was created (shown in Figure 42). The vast majority of the corrosion damage was localized on the top of the downstream side of the bottom flange. The corrosion damage of the flange was averaged across

the flange's width at defined datums. Twenty-four datums were defined for the 24 grid measurement locations along the length of the beam where measurements were taken. The minimum average flange thickness out of the 24 datums was 0.44 in (a black dotted line shows its location in Figure 42). This flange thickness of 0.44 in was then used to determine the amount of CFRP required to return this beam to its original capacity.

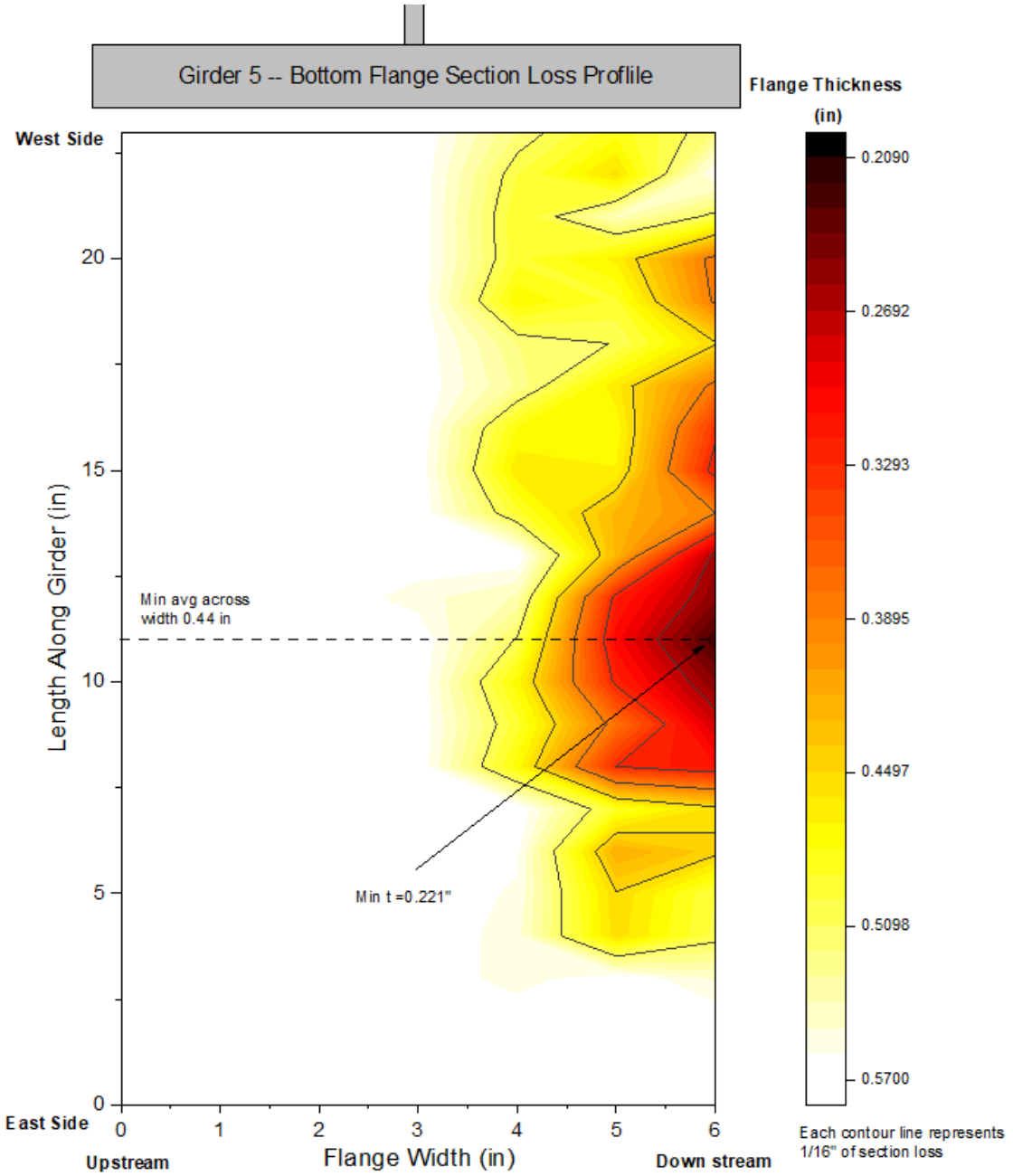

Figure 42. Heat Map of Beam 5's Bottom Flange Section Loss

5.5 Laboratory Testing – Methodology

The large-scale laboratory testing consisted of designing an elastic retrofit capable of returning beam 5 from the Simmons Gap Road Bridge to its original elastic capacity (uncorroded state). Once this design was completed, two beams (retired W18X50 beams with corrosion) were prepared and tested. The tested beams consisted of a control beam to simulate the condition of beam 5 in its current deteriorated and un-retrofitted state and a CFRP retrofitted beam to demonstrate the efficacy of deteriorated beam 5 with the proposed CFRP retrofit. These laboratory-tested beams were fabricated with conditions and section loss as close to the actual bridge beam as possible. They consisted of the same beam cross-section, both had extensive corrosion damage, the same span length, and were approximately the same age. The specimen preparations that went into these beams included recreating this region of extreme corrosion, cleaning the corrosion and debris off of these beams to achieve a good bond, and applying the CFRP retrofit. Lastly, the control and retrofitted beams were tested until failure.

5.5.1 Surface Roughness/Section Loss Characterization of the Retrofitted Beam Specimens

Before applying the CFRP retrofit on the retrofitted beam specimen, an extensive investigation of corrosion damage and surface roughness was completed. This data documented the severity and types of corrosion present on the bottom side of the bottom flange (BBF) to which a CFRP retrofit would be attached. Figure 43 I. and III. shows the corrosion damage on the pre-retrofitted beam after some spot cleaning with a needle gun, which was used to remove non-corrosion products (tar & sealer). The BBF was visually inspected using ISO 8501-1 (2007) to grade the

surface and rust condition before preparing the surfaces. These rust grades range from ‘A’ (little to no rust) to ‘D’ (millscale has rusted away and has general pitting). The majority of the observed rusting on the surfaces to be retrofitted comprised of grades ‘C’ and ‘D’.

I. Representative Corrosion on the Pre-retrofitted Beam Specimen (BBF Near the End)

II. Stochastic Pattern on the Pre-retrofitted Beam Specimen (BBF Near the End)

III. Total Corrosion Overview on the Pre-retrofitted Beam Specimen

IV. DIC Being Used on the Stochastic Patterned Pre-retrofitted Beam Specimen

Figure 43. I.-IV. Different Stages of Inspection on the Pre-retrofitted Beam Specimen

After the visual inspection, the entire 2,970 in^2 of the BBF's surfacewas inspected with a digital image correlation (DIC) system, shown in Figure 43 IV. The DIC system used in this testing consisted of a pair of 12 Megapixel CMOS sensors on an 800mm adjustable base, manufactured by GOM. The use of stereo vision and a stochastic pattern allowed for creating a 3D surface in space. This 3D surface was then analyzed to look at surface roughness parameters and section loss. This 3D surface consisted of over 9,697 inspection points. This roughly corresponded to a data point being taken on a 0.5-in by 0.-n grid over the entire flange's bottom surface area. All points were examined for their deviation from a reference plane. These measurements provide the difference for each point inspected compared to the reference plane in the direction of the flange's thickness (Z-direction). The reference plane was created by evaluating all the points' Z locations. With the Z-location data, the mean reference plane was created from a Gaussian distribution (ignoring values outside three standard deviations). Figure 44 I. shows an example surface deviation heat map and a datum along the length of the plot. Figure 44 II. shows how the reference plane was defined, where the green plane in Figure 44 II. is the datum from which surface points (gray surface plane) are measured.

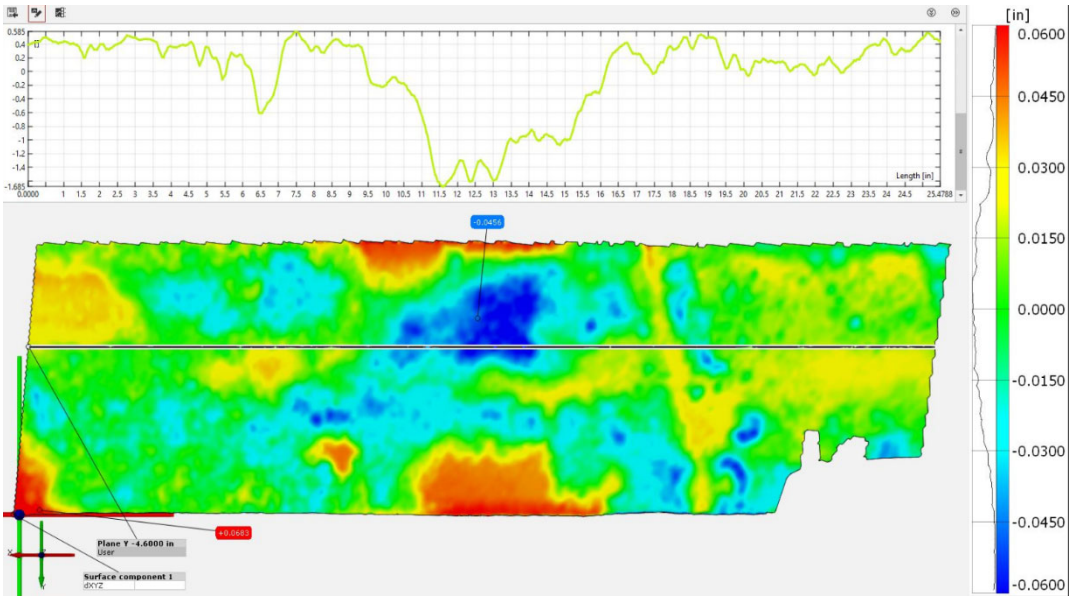

I. A Small Portion of the Surface Deviation Heat Map

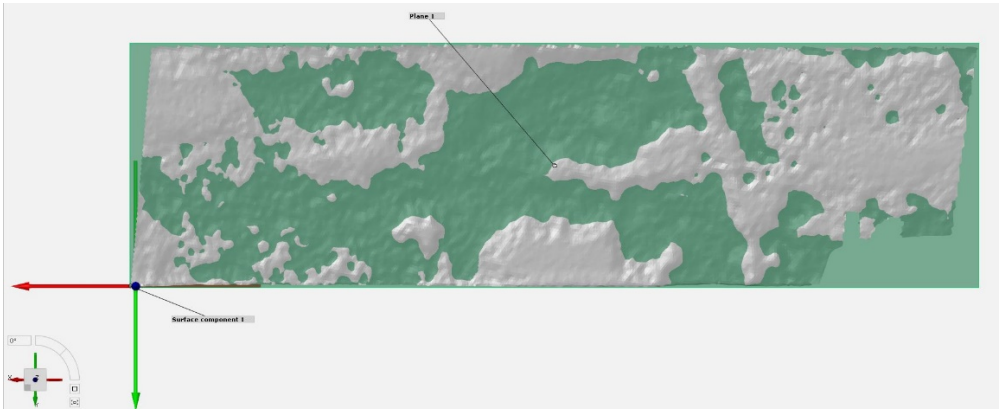

II. How the Reference Plane was Defined (Gray=3D Surface, Green= Reference Plane)

Figure 44. Example Surface Deviation Profile from the Retrofitted Beams Bottom of the Bottom Flange

All of the surface deviation data was extracted and used to create a histogram to determine the distribution of deviation from the normal. This data had a standard deviation of 0.0195 in. With this information, the histogram was translated by three standard deviations in the negative direction. This translation was completed to move the deviation surface to the outside face of the flange (original surface). Once this was completed, the thickness of the nominal flange (0.57 in)

was added to this. This data can be seen in Figure 45 and provides information on the current corrosion deterioration on the BBF. The mean data (0.507 in) corresponds to an 11% section loss, and the maximum section loss (0.303 in) corresponds to a 46.8% section loss. This surface also had a maximum valley depth below the mean line of 0.204 in and a maximum peak height above the mean line of 0.158 in. This data demonstrates the amount of section loss present on the bottom of the beam's flange, which this retrofit was subject to. This data assumes that the top side of the bottom flange is in pristine (flat/smooth) condition. However, based on a visual inspection, this smooth/flat assumption is not accurate. This assumption is an indication that the corrosion damage shown in Figure 45 is conservative; however, any discussion on surface roughness or variation is accurate.

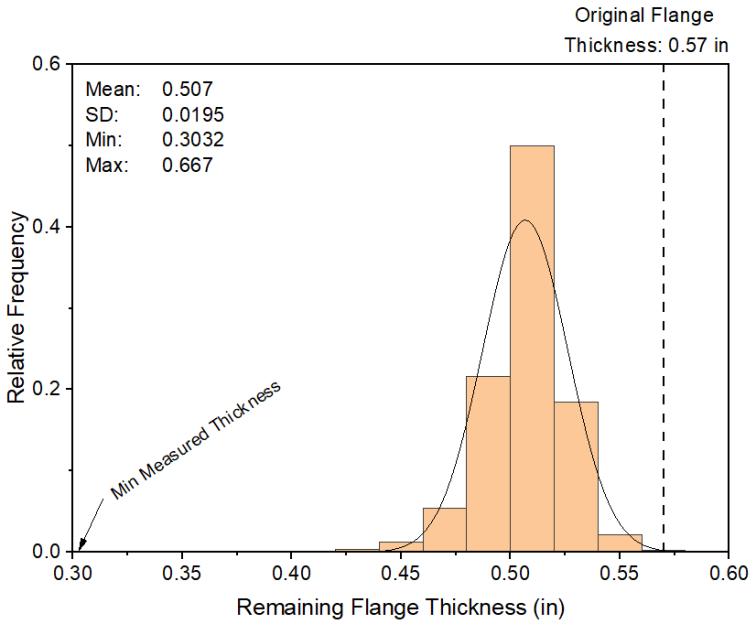

Figure 45. Histogram of Corroded Steel Surface Deviations

5.5.2 Recreation of Severe Corrosion Damage on LaboratoryBeams

An angle grinder was used to remove sections of realistic "corrosion deterioration" from the tested laboratory beams to recreate the severe corrosion damage observed on beam 5 of the

bridge. The location of the flange section removed was 16 ft from the west side of the bridge's pier support, and in the laboratory, it was 16 ft from the southern support. The section removal process was aided by 3D printing a reverse mold of the corrosion section loss data points taken from the 168 caliper readings on beam 5. The 3D reverse mold provided a topographical map to locate where material needed to be removed and served as a template to check flushness. Figure 46 shows the recreated beam 5 corrosion on the control specimen. Figure 46 is representative for both the control and retrofitted beam.

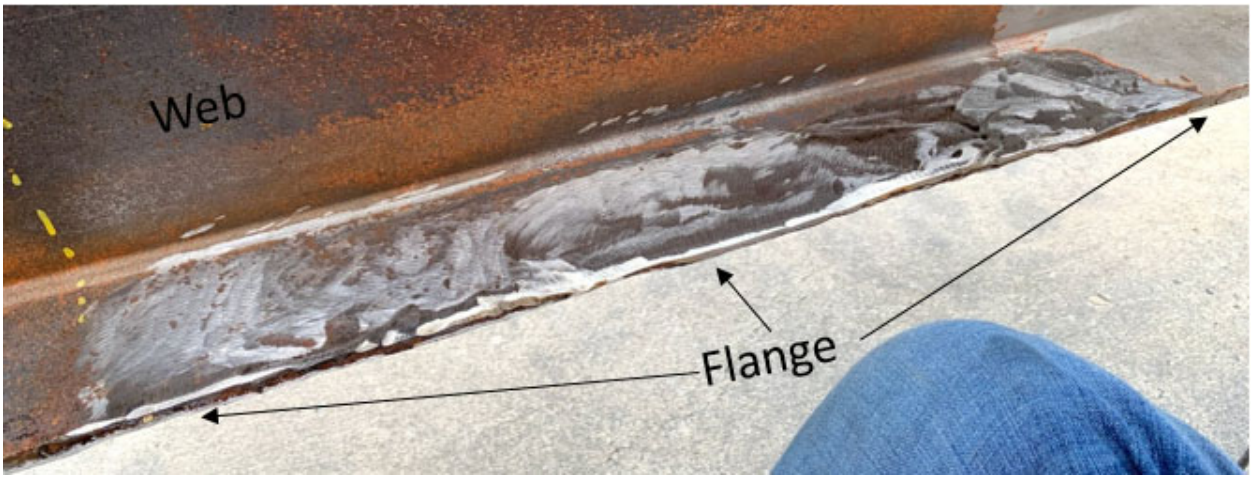

Figure 46. Recreated Beam 5 Corrosion on Laboratory Tested Beams

Readings from the control and retrofitted beams' recreated corrosion damage were compared against the field corrosion data of beam 5 of the Simmons Gap Road Bridge. The average results of this analysis are shown in Table 24. The results from this data show that the average recreated corrosion damage on the control and retrofitted beam were 11.4 and 2.2 % more corroded than of the corrosion on beam 5 of the Simmons Gap Road Bridge

Table 24. Corrosion Damage Measurements from Laboratory and Field Inspections

	Avg (in)	Min (in)	Max (in)
Beam 5 Measured Field Corrosion	0.44	0.21	0.57
Control Beam Recreated Corrosion	0.39	0.18	0.50
Retrofitted Beam Recreated Corrosion	0.43	0.17	0.54

5.5.3 Tested Material Properties

Although the manufacturer provided nominal mechanical properties for the CFRP materials, the researchers performed material testing on the CFRP, adhesive, and steel (removed from unyielded portions of the laboratory tested beams). The results from testing are shown in Table 25. These material properties were used extensively in all of the calculations for the design strength and stiffness of steel and CFRP retrofitted structures in this report. The steel material properties obtained from the laboratory-tested beam were used for the strength calculations for the Simmons Gap Road Bridge's pre and post-retrofits (laboratory and field).

Table 25.Tested CFRP & Steel Material Properties

Property or Dimension	Nippon		Laboratory Tested Beam's Steel
	CRFP*	Adhesive	
Yield Strength (ksi)	--	--	38.8
Tensile Strength (ksi)	157.8	5.8	67.7
Modulus of Elasticity (ksi)	47,575	896	28,141
Elongation at Break (%)	0.33	1.18	17.3
Thickness (in)	0.057**	--	--
Width (in)	19.7	--	--

* Material properties based on the diameter of a strand (13 strands per in of width)
**Diameter of an individual strand

5.5.4 Retrofit Design

With known material properties from Table 25, the modular ratio between the CFRP and the steel (n) was 1.64. Based on previous testing conducted at Virginia Tech, the shear lag factor

(S_L) from large-scale flexural tests were observed to be as large as 50% (Sherry et al. 2021). Therefore the shear lag factor was conservatively taken as 0.5. With these design parameters, the design process was completed. The total amount of cross-sectional CFRP applied to beam 5 of the Simmons Gap Road Bridge was 1.846 in^2, which corresponded to three plies of 7 in wide CFRP on the BBF, and three plies of 3 in wide CFRP on both sides of the top of the bottom flange (TBF). A cross-sectional view of this CFRP retrofit is shown in Figure 47.

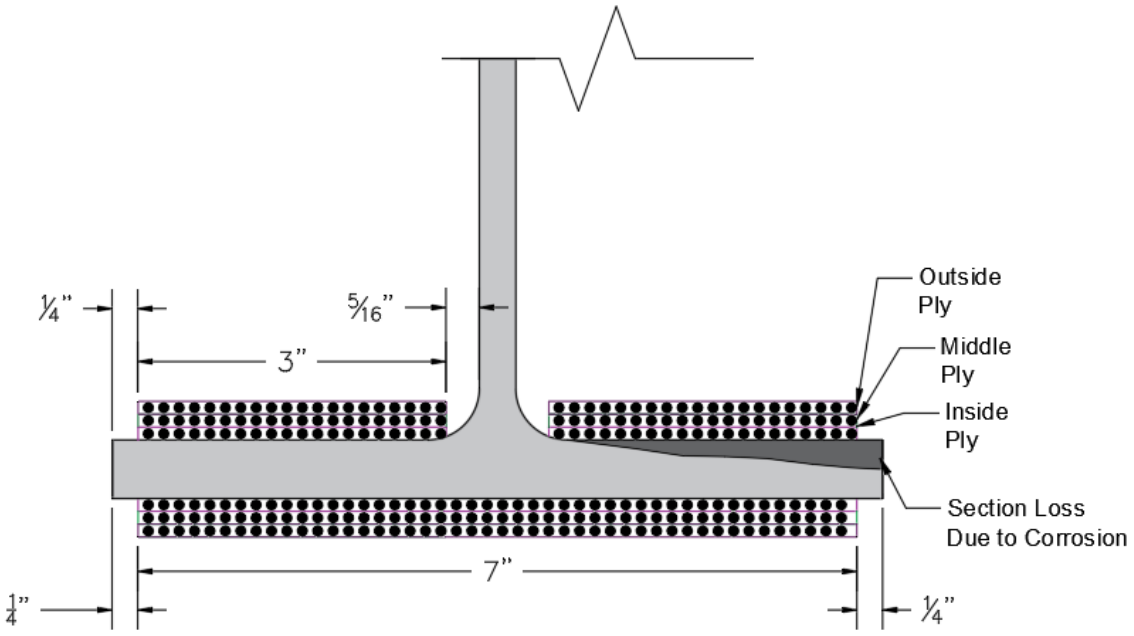

Figure 47. Beam 5 CFRP Retrofit Typical Sheet

The retrofit design used an elastic strength analysis that was carried out by examining the moment strength of the original beam 5, the current strength of beam 5 resulting from the section loss, and the proposed retrofitted strength of beam 5. This was completed by calculating the moment of inertia and then using the moment of inertia to calculate the elastic section modulus (S_x) for each of the beams of interest. A detailed explanation of how these strengths were

calculated can be found in “Load Test to Evaluate a Flexural Repair of a Deteriorated Bridge with Carbon Fiber Reinforced Polymers” (Sherry and Hebdon 2021). The strengths of beam 5 at different stages of its service life are provided in Table 26. The proposed retrofit returned beam 5 to 1.14% above its original capacity and 18.38% above its deteriorated capacity. Additionally, this retrofit forced the controlling component of the beam from the tension flange to the compression flange.

Table 26. Different Strengths of Beam 5 and Proposed Retrofit

Section	Elastic Section Modulus (Sx) [in^3]		Controlling Value (Sx) [in^3]	Yield Moment (Kip-ft)
	Bottom	Top		
Original Beam 5	87.9	87.9	87.9	284.2
Deteriorated State Beam 5	75.1	85.5	75.1	242.8
CFRP Retrofitted Beam 5	94.4	88.9	88.9	287.4

5.5.5 Beam Specimen Preparation

Per the manufacturer’s recommendations, steel structures should be cleaned to a “white metal” condition before applying the CFRP retrofits (NEXCO-West 2015). The removal of any contaminants (rust, dirt, grease, paint, mill scale, and oxidization layers) is crucial to achieving an adequate bond strength. To achieve the desired cleanliness level, the laboratory tested, and the field-tested beams were blast cleaned. These beams were blast-cleaned to Sa 2 ½ or Sa 3 according to ISO 2007. The blasting media used for cleaning was “Black Beauty”, a coal slag abrasive blasting media, grit size 36-54.

CFRP Installation 5.5.5.1

All CFRP was installed according to the manufacturer's recommendations (NEXCO-West 2015). The installation guide is available from the manufacturer; however, the general procedures of CFRP installation are described, and visual references are shown in "Load Test to Evaluate a Flexural Repair of a Deteriorated Bridge with Carbon Fiber Reinforced Polymers" (Sherry and Hebdon 2021). There are a couple of points to note in regards to the installation of the CFRP materials. CFRP adhesives should be installed within 4 hours of the completion of the blasting process. This reduces the chance of oxidation layers forming on the surface of the steel. The materials used in this research required that if the relative humidity at the site of the curing adhesives ever exceeded above 85%, the surface of the resin needed to be lightly sanded and wiped clean before the application of further adhesives.

5.5.6 Testing Setup and Instrumentation

Each laboratory tested beam specimen had a span length of 33 ft and was loaded in four-point bending. This loading subsequently had shear span lengths of 13 ft and a constant moment region length of 7 ft. Pin and roller supports were used to support the beam tests. Test dimensions and the instrumentation layout are shown in Figure 48. Also shown in Figure 48 are the brace points which were used to control lateral-torsional buckling on the test specimen. The typical braced lengths were 6 ft. however, due to the testing setup, there was a braced length of 10 ft 4.5 in at midspan of the specimen. The load was applied with a 400 kip Enerpac hydraulic cylinder (RR20013) controlled with a 10,000 psi electric Enerpac pump. A Campbell Scientific CR5000 datalogger, sampled at 10 Hz, was used to collect data from a 500 kip load cell, vertical displacement sensors, carbon fiber strain gauges, and steel strain gauges (locations shown in Figure 48).

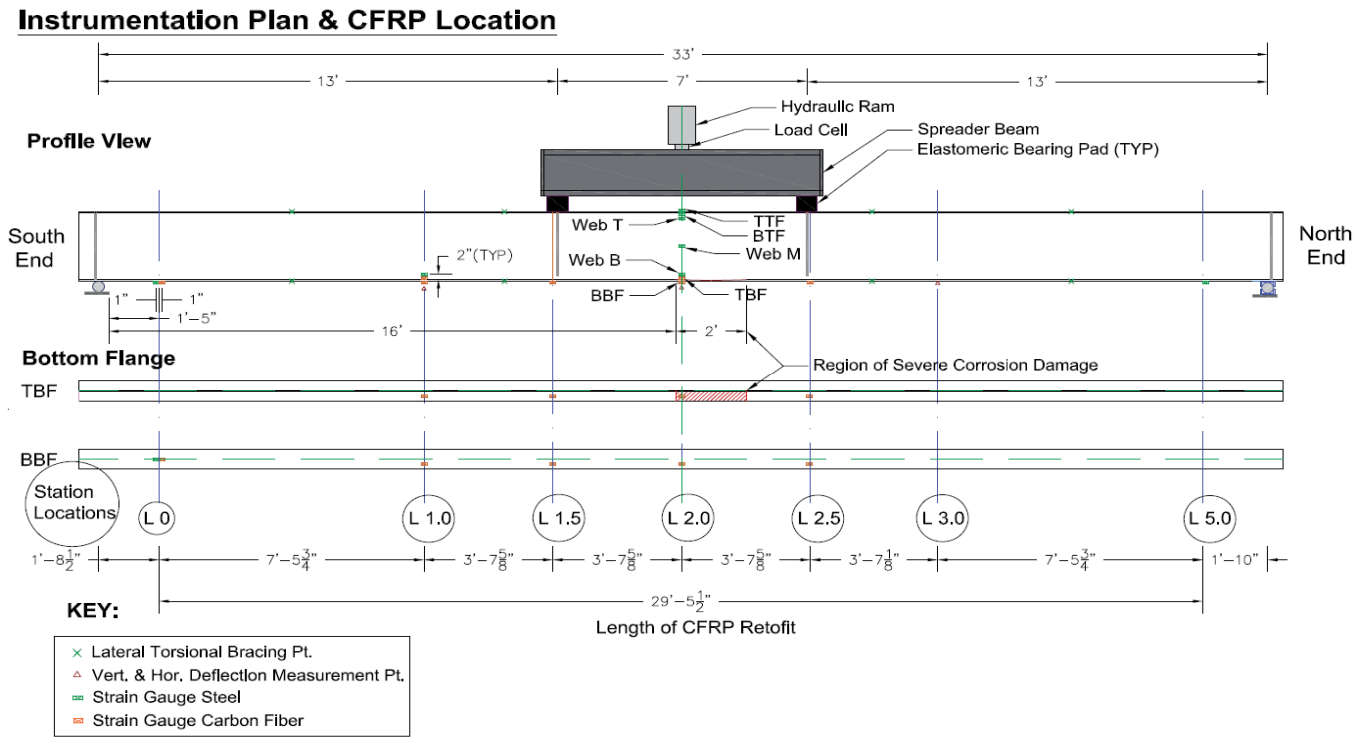

Figure 48. Test Setup & Instrumentation Plan of Laboratory Tested Beams

5.6 Laboratory Testing – Results and Discussion

The loading of all the tested beams was carried out in a step-wise fashion in 5 kip increments before reaching the yield moment. After the yield moment of the beams was reached, the beams were loaded in 0.1 in increments until the termination of testing. An isometric view of the control beam being loaded is shown in Figure 49.

Figure 49. View of the Control Beam Before Testing

5.6.1 Control

The control beam was first loaded elastically, unloaded, and then loaded again past its elastic limit until 5 in of midspan deformation. The elastic (blue line) results and inelastic (red line) loading of the control beam are shown in Figure 50. The elastic-perfectly plastic (EPP) behavior of the original beam is shown as a solid black line in Figure 50. The elastic response of the control beam is below that of the original beam's elastic behavior, which is a clear indication that the tested control beam is in a deteriorated state compared to its original condition. The yield moment of the control beam was 216 kip-ft, which was an 11% decrease from the calculated yield moment (242.8 kip-ft) based on corrosion measurement data. The yield moment of the control beam was 216 kip-ft, which was a 23.9 % decrease from the original W18x50's yield moment (284 kip-ft). The ultimate moment of the control beam was 266.5 kip-ft.

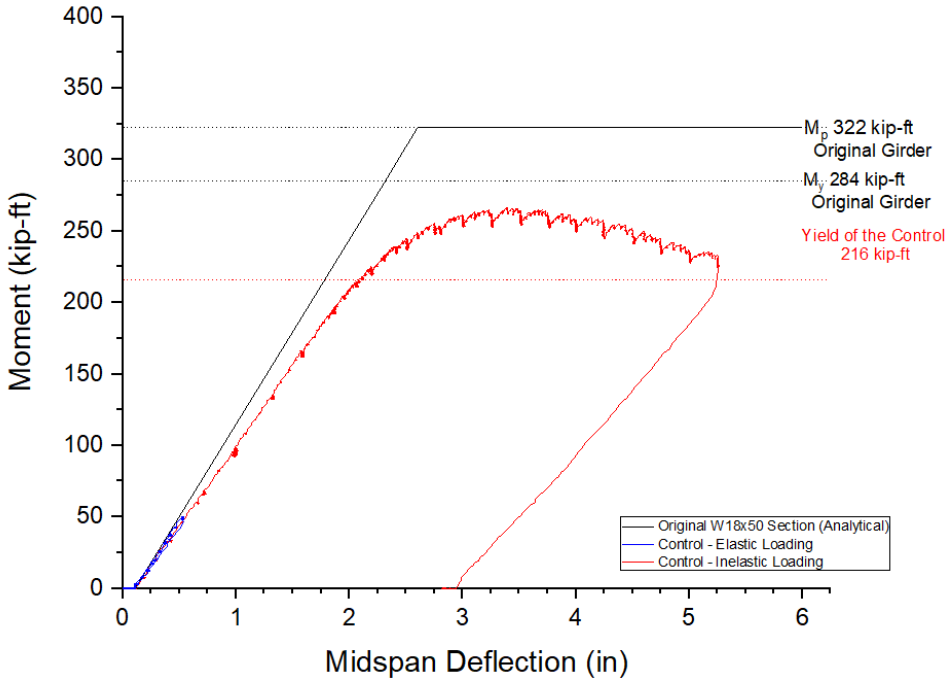

Figure 50. Moment vs. Deflection Plot of the Control Beam

The testing was terminated due to significant local flange buckling and out-of-plane deformations, where at the end of testing the top flange had displaced out of plane over 2 in. The main failure mode observed was local flange buckling, which contributed to lateral-torsional buckling between the brace points.

5.6.2 Retrofitted Beam

Initially, the retrofitted beam was loaded elastically with its simulated severe corrosion damage and no retrofit. The unretrofitted testing was completed to see how well the retrofitted beam's unretrofitted response matched the control beam’s behavior. The retrofitted testing was loaded elastically (up to 75% of its calculated yield) and then unloaded. After the elastic loadings, the unretrofitted beam was retrofitted. Following the required ten days of curing, the retrofitted beam was tested. This retrofitted beam was then loaded past its elastic behavior until 5.5 in of midspan deformation.

The pre-retrofit elastic loading (green line) and inelastic (light gray line) loading of the retrofitted beam are shown in Figure 51. Superimposed on top of the inelastic load response is the inelastic response envelope (blue line) where the inelastic response envelope best represents the actual behavior of the retrofitted beam. The elastic loading of the pre-retrofitted beam (green line) matches closely with the elastic portion of the control beam's inelastic loading. The fact the control beam and the pre-retrofitted beam have similar responses is an indication that the amount of corrosion on these beams was very similar. Due to this similar behavior, comparisons about the retrofitted beam were made against the unretrofitted control beam. The retrofitted beam's yield moment was 298.9 kip-ft, a 23.1 % increase from the calculated yield moment of the unretrofitted control (242.8 kip-ft). The yield moment of the retrofitted beam was 298.9 kip-ft, which is a 5.2 % increase from the original W18x50's yield moment (284 kip-ft). The ultimate moment of the retrofitted beam was 331 kip-ft, which was 2.8% above that of the analytical prediction for the original beam's strength (322 kip-ft).

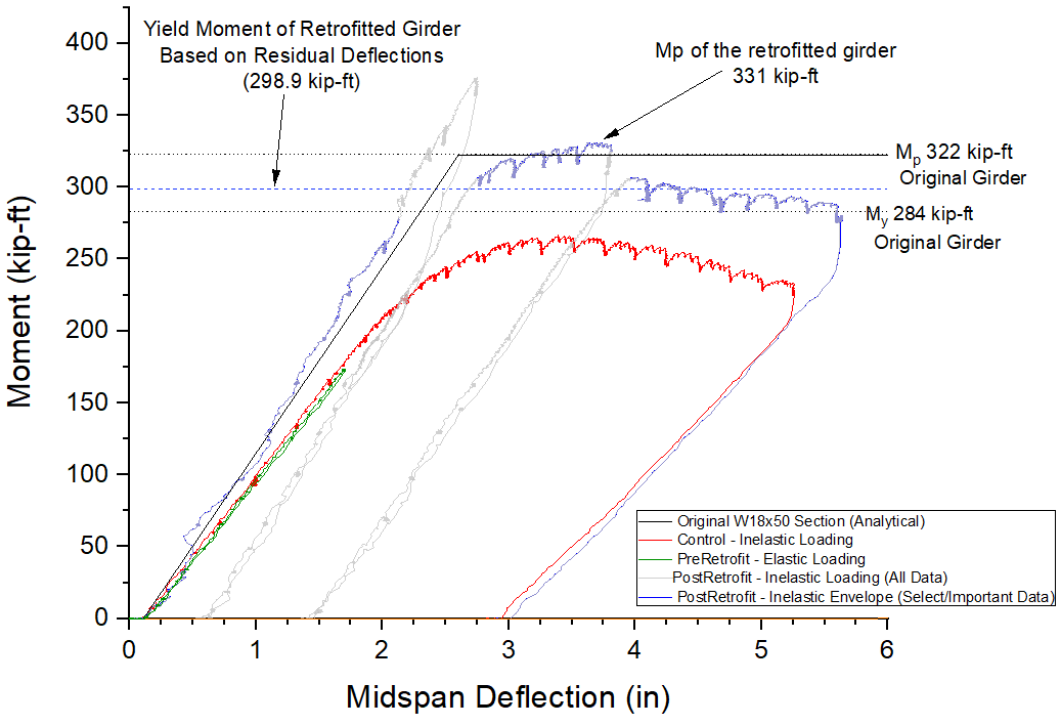

Figure 51. Moment vs. Deflection Plot of the Control Beam

During testing, safety chains were used as a failsafe to support the spreader beam in case of a failure. As the spreader beam was loaded downwards, it reached a point where it came in contact with the safety chains (at a fixed location), and was not observed by the research team. As the safety chains started to take load, the slope of the moment displacement plot changes (stiffness increases after 277 kip-ft) as shown in the grey line of Figure 51. Once this behavior was noticed, at a moment of 374 kip-ft, the beam was unloaded and the chains were adjusted to allow for more displacement. The beam was then reloaded, and the stiffness of the reloading was shown to be very similar to the retrofitted beam before the loading of the chains. Loading was continued until 3.8 in vertical deflection. At this point, the beam started to exhibit signs of lateral-torsional buckling, likely due to a slight misalignment of the spreader beam. The retrofitted beam was then unloaded to readjust the spreader beam for better load distribution. The

beam was reloaded for a final time where the out-of-plane bending still occurred. The testing was terminated due to out-of-plane deformations. At the end of testing, the top flange had displaced out of plane over 2 in. The primary failure mode observed was lateral-torsional buckling with some locations of local flange buckling. No failure of the CFRP was observed.

After reviewing the test data, the inelastic load response was highlighted to show the inelastic response envelope of the data, as shown in the blue line of Figure 51. This shows the expected behavior of a retrofitted beam had the loading of the chains not occurred and no reloading occurred. The retrofitted beam's yield moment was found (298.9 kip-ft) by subtracting the residual deformations from the second portion of inelastic loading (loading after the chains) and selecting the point where this moment deflection plot started to indicate nonlinear behavior.

5.6.3 Comparison of Results

5.6.3.1 Prediction Models

One area of interest when looking at the elastic strengths from testing was how close the prediction equations matched test data. Table 27 shows the elastic capacity of the different beams tested compared to the predicted elastic strength values shown in Table 26**.** The elastic strength ratios of the control and the retrofitted beam are compared to the analytical predictions, with resulting values of 0.89 and 1.04, respectively. Note that a ratio less than 1 indicates that the prediction models are over-predicting the strength of the given beam. It is believed that the deteriorated compression flange led to lower than anticipated testing values for the control beam. In contrast, the extreme compression flange buckling was not much of a concern for the retrofitted beam, which was within 4% of expected.

Table 27. Elastic Strengths of Different Beams Compared to the Calculate Strengths (Table 3)

	M_y from testing (Kip-ft)	M_y from Analytical Predictions (Kip-ft)	Ratio Test Values/ Analytical Predictions
Control Beam	216	242	0.89
Retrofitted Beam	298	287	1.04

This CFRP retrofit reduced the strains on the retrofitted beam compared to the control beam at the same amount of elastic loading. Figure 52 shows the control (blue line) strain profile and retrofitted (green line) beam at an applied load of 175 kip-ft over the depth of the specimens. These values were taken from strain gauges located at midspan. Based on a linear regression (best fit) for the different strain profiles, the retrofits decreased the strains on the control beam by 25.6%. This reduction in strain was for the global profile; however, if just the strain gauge near the region of corrosion damage is examined, this value further decreased a reduction in strain of 30%.

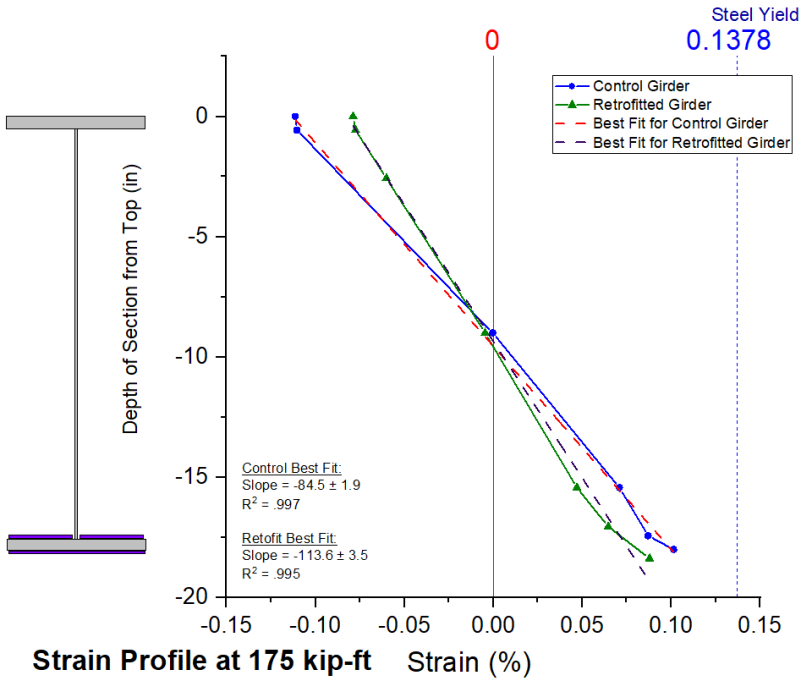

Figure 52. Beams Strain Profile Pre and Post Retofit

5.6.3.2 Elastic Strength Increase

Based on the results from Figure 51, the retrofitted beam was able to increase the elastic and inelastic strength by 12% and 9 % over that of the original beam's strength, respectively. This retrofit was deemed adequate to return the Simmons Gap Road Bridge to its original strength, assuming similar amounts of corrosion on both the tested laboratory beams and beam 5 from the Simmons Gap Road Bridge.

5.7 Field Testing – Methodology

The same retrofit design, beam specimen preparations, and CFRP installation used in the 5.6 Laboratory Testing – Results and Discussion were used for the field retrofit of beam 5 of the Simmons Gap Road Bridge.

5.7.1 Loading and Load Protocol

A VA Type 3 (single unit) truck, shown in Figure 53 was used to complete the pre and post-retrofit live load testing of the Simmons Gap Road Bridge. There was a 1.9% decrease in the weight of the pre and post-retrofit VA Type 3 trucks used to load this bridge (47.9 kips vs. 47 kips). This small weight difference and the difference in the distribution of load were considered a negligible difference in the response behavior of the pre and post-retrofitted bridge.

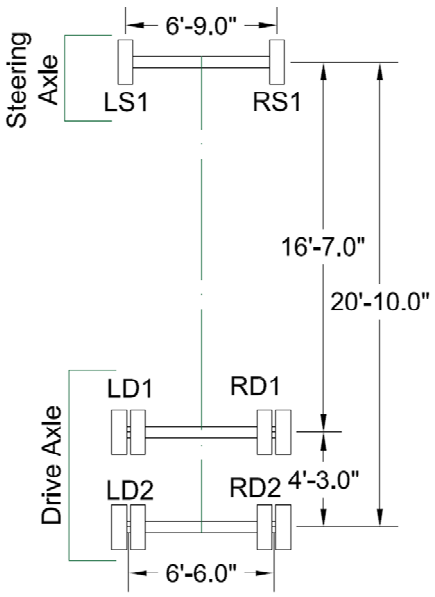

Figure 53. Axle Spacing of the VA Type 3 Trucks Used to Load the Simmons Gap Road Bridge

The Simmons Gap Road Bridge's live load test protocol consisted of loading individual bridge beams with the wheel line of the VA type 3 over a beam of interest. The loading of each beam was completed for the following cases: static (applying loads at midspan – L1.0, and shear loading – L2.0) and 5 MPH rolling pass over the bridge. For the static loading, the truck's location was based on the centroid of the rear axle wheels. This centroid was applying a desired "point load" over a region of interest. Each loading was completed three times to ensure reproducibility.

5.7.2 Test Setup and Instrumentation

Each beam in the bridge had a span length of 33 ft 9 in and was supported directly on concrete abutments (no bearings). Only beams 9 through 4 were instrumented for the live load testing because it was believed that the bridge behavior would be symmetric about beam 5. Beam 4 was instrumented in case this symmetric behavior assumption was incorrect. A Campbell Scientific

CR9000 datalogger, sampled at 10 Hz, was used to collect data from vertical displacement sensors at midspan of each beam, carbon fiber strain gauges, and steel strain gauges.

5.8 Field Testing – Results and discussion

It was determined that a comparison of the retrofits' effects would be carried out for the 5 MPH pass. While the static and 5 MPH data were very close in their results, it was determined that loading at some speed provided more realistic results than stationary test results.

Figure 54 shows representative plots of deformation vs. time and stress vs. time for the post-retrofitted loading of beam 5 of the Simmons Gap Road Bridge. Figure 54 demonstrates the loading that this bridge was subject to and how these plots were used to collect data. Similar plots were created for each load pass, loading type, and for each loaded beam.

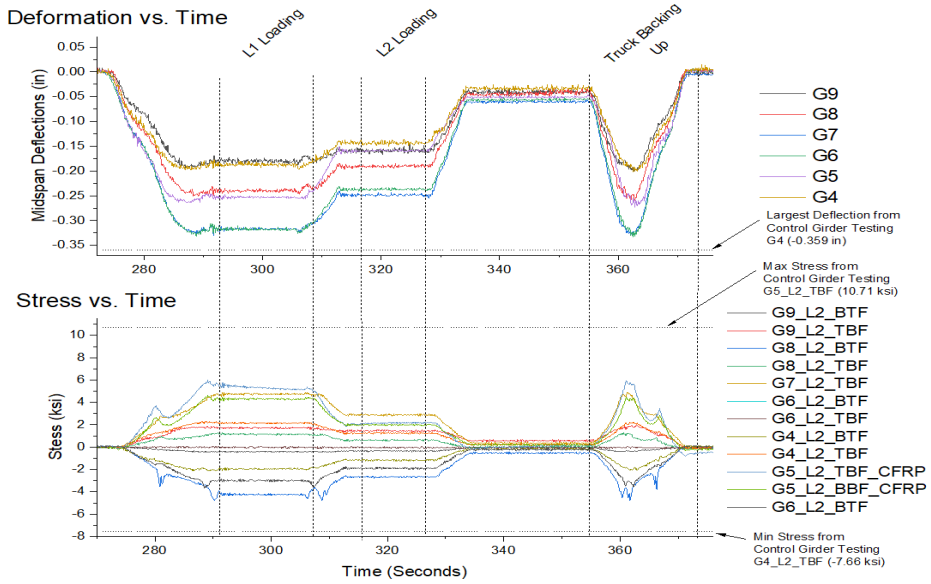

Figure 54. Post-retrofit Loading of Beam 5 -- Deformation vs. Time Plot (Upper) and Strain vs. Time Plot (Lower)

Figure 54 also highlights the differences in the envelope of deflections and stresses for the pre-retrofitted beam (shown by dotted black lines) compared to the post-retrofit behavior. There was

a 7.5% decrease in the envelope data for deflections and a 37.6% and 43.9% decrease in envelope data for compression flange and tension flange strains, respectively.

The deflection data from the 5 MPH loading on beams 5 were plotted to show the pre-and post-retrofit deflection profiles, as shown in Figure 55. This figure also shows where the location of the truck wheels when making these load passes (red arrows = beam 5 loading). The data points in Figure 55 are connected with straight lines to show the distribution for each case.

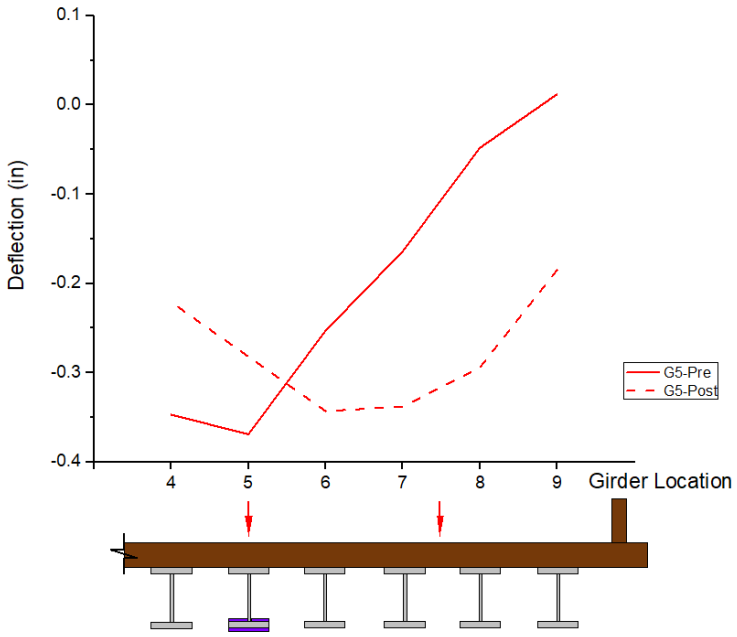

Figure 55. Comparison of Deflections for Pre and Post-Retrofit Behaviour for Beam 5's Loadings

When examining the beam 5 deflection, it is clear that the corrosion damage on beam 5 greatly influences the pre-retrofit behavior. The majority of the deflections occur in beam 5 and the beams adjacent to beam 5. The severe corrosion damage causes the adjacent beams (4 and 6) to make up for the lack of stiffness and strength in beam 5. Therefore, beams 7-9 do not see a uniform load because most of the loading is concentrated near the weak beam (5). The post-

retrofit behavior for beam 5 loading has reversed this behavior where the distribution of load appears more uniform over the bridge cross-section.

The reduction in deflections after the retrofit also translated to a reduction in stresses near beam 5 and a more uniform distribution of stresses across the bridge's width. Table 28 provides the percent change of deflections and stresses from the pre-retrofit to post-retrofit testing of the Simmons Gap Road Bridge. A positive percent change indicates an increase in stress or deformation, and a negative percent change indicates a reduction in stress or deformation. The results in Table 28, beam 5 loading shows that the stresses and deformations in beams 4 and 5 were greatly lower (by at least 23.6% for deformations and at least 50% for stresses). The remaining instrumented beams for the beam 5 loading at 5 MPH saw increases in deformations and stresses as expected since the load was more evenly distributed to adjacent beams.

Table 28. Percent Change of Deflections and Stress from the Pre-retrofit to Post-retrofit Testing of the Simmons Gap Road Bridge

		Percent Change from Pre-retrofit to Post-retrofit Midspan (L2) Deflections	Percent Change from Pre-retrofit to Post-retrofit Midspan (L2) BTF Stress	Percent Change from Pre-retrofit to Post-retrofit Midspan (L2) TBF Stress
Beam 5 Loading (5 MPH)	Beam 9	1641.7	579.2	465.1
	Beam 8	512.5	432.8	113.3
	Beam 7	106.1	--	106.5
	Beam 6	35.6	6.1	53.7
	Beam 5	-23.6	--	-52.2
	Beam 4	-36.3	-69.7	-54.7

5.9 Summary & Conclusions

The primary findings resulting from this study were:

5.9.1 Large-Scale Testing

- The re-creation and testing of a replica beam 5 from the Simmons Gap Road Bridge with a CFRP retrofit were successful in returning this beam back above its original strength. This research showed that a CFRP retrofit had a yield moment (M_y) of 5.2% above the original beam. The CFRP retrofit had a plastic moment (M_p) of 2.8% above the original beam.

- This research showed that a CFRP retrofit reduced global strains by 25.6% compared to the control beam.

- The failure mode of this CFRP retrofit was not CFRP rupture but rather lateral-torsional buckling and local flange buckling.

5.9.2 Field Testing

- The installation of the Nippon CFRP strand sheet in the field was a success. The installed retrofit was sufficient in returning beam 5 back to its original elastic strength capacity based on the laboratory test data.

- This retrofit effectively reduced localized stresses (a minimum of 50%) and deformations (a minimum of 23.6%) on the Simmons Gap Road Bridge.

- This retrofit also greatly affected the live load distribution on the Simmons Gap Road Bridge (for the case of beam 5 loading). This research showed that for a specific loading (beam 5), three of the instrumented beams were taking a significant portion of the load coming across the bridge. After the retrofitting, this load was more uniformly distributed across the width of the bridge.

5.9.3 Surface Variability/Corrosion

- The recreated corrosion damage on the control beams and corrosion damage on the Simmons Gap Road Bridge (up to 50 percent section loss of the bottom flange) did not significantly influence the strength, stiffness, or bondability of the CFRP retrofit on the tested beam.

- The mean corrosion section loss of 11%, the maximum valley depth below the mean line (0.204 in), and a maximum peak height above the mean line (0.158 in.) on the retrofitted laboratory tested beam also did not significantly influence the strength, stiffness, or bondability of the CFRP retrofit.

- CFRP retrofits completed on steel with rust grades C & D (laboratory testing), which were blast-cleaned to Sa 2 ½ or Sa 3, were able to achieve inelastic strengths 2.8% above the original analytical predictions. The failure mode of this testing was LTB and compression flange buckling, not CFRP failure.

5.10 Acknowledgments

The authors would like to acknowledge the Virginia Department of Transportation's Culpeper District and the Virginia Transportation Research Council for their assistance in testing the Simmons Gap Road Bridge.

References

Al-Saidy, A. H., Klaiber, F. W., and Wipf, T. J. (2004). "Repair of Steel Composite Beams with Carbon Fiber-Reinforced Polymer Plates." Journal of Composites for Construction, 8(2), 163–172.

Chajes, M. J., Chacon, A. P., Swinehart, M. W., Richardson, D. R., and Wenczel, G. C. (2005). "Applications of Advanced Composites to Steel Bridges: A Case Study on the Ashland Bridge." 19716(March).

FHWA. (2012). Bridge Inspector's Reference Manual- FHWA NHI 12-049. Federal Highway Administration.

Hidekuma, Y., Kobayashi, A., Tateishi, A., Nagai, M., and Miyashita, T. (2011). "Repairing Method for the Steel Members by CFRP Strand Sheets." Advances in FRP Composites in Civil Engineering - Proceedings of the 5th International Conference on FRP Composites in Civil Engineering, CICE 2010, 881–885.

ISO. (2007). ISO 8501-1 The Rust Grade Book.

Kim, Y. J., and Brunell, G. (2011). "Interaction Between CFRP-repair and Initial Damage of Wide-flange Steel Beams Subjected to Three-point Bending." Composite Structures, Elsevier Ltd, 93(8), 1986–1996.

Kobayashi, A., Hidekuma, Y., and Tateishi, A. (2015). “Strengthening of steel and concrete structures using CFRP in Japan.” 978–984.

Liu, X., Silva, P. F., and Nanni, A. (2001). “Rehabilitation of Steel Bridge Members with FRP Composite Materials.” CCC 2001 Composites in Construction, (100 mm), 613–617.

Mertz, D. R., and Gillespie, J. W. J. (1996). NCHRP-IDEA Final Report: Rehabilitation of Steel Bridge Beams Through the Application of Advanced Composite Materials. Washington, DC.

Mertz, D. R., Gillespie Jr, J. W., Chajes, M. J., and Sabol, S. (2002). “Rehabilitation of Steel Bridge Beams Using Advanced Composite Materials.” NCHRP-IDEA Program Project Final Report Project 51, 36.

Miller, T. C., Chajes, M. J., Mertz, D. R., and Hastings, J. N. (2001). “Strengthening of a Steel Bridge Beam Using CFRP Plates.” Journal of Bridge Engineering, 6(6), 514–522.

Moy, S. S. J. (2002). “Steel Beams Strengthened with Carbon Fibre Reinforced Polymer Composites.” Advanced polymer composites for structural applications in construction, (March), 195–202.

Moy, S. S. J., Barnes, F., Moriarty, J., Dier, A. F., Kenchington, A., and Iverson, B. (2000). “Structural Upgrade and Life Extension of Cast Iron Struts Using Carbon Fibre Reinforced Composites.” FRC 2000–Composites for the Millennium, (March), 3–10.

Nagai, M., Hidekuma, Y., Miyashita, T., Okuyama, Y., Kudo, A., and Kobayashi, A. (2012). “Bonding Characteristics and Flexural Stiffening Effect of CFRP Strand Sheets Bonded to Steel Beams.” Procedia Engineering, 40, 137–142.

NEXCO-West. (2015). “Design and Installation Manual for Upgrading of Steel Structures with the use of Carbon Fiber Sheets.” (2), 62.

Peiris, N. A. (2011). “Steel Beams Strengthened with Ultra High Modulus CFRP Laminates.” University of Kentucky.

Phares, B. M., Wipf, T. J., Klaiber, F. W., Abu-Hawash, A., and Lee, Y.-S. (2003). “Strengthening of steel beam bridges using FRP.” Proc., 2003 Mid-Continent Transportation Research Symp, (August 2003), 1–12.

Sherry, S. T., and Hebdon, M. (2021). Load Test to Evaluate a Flexural Repair of a Deteriorated Bridge with Carbon Fiber Reinforced Polymers. Virginia Department of Transportation – Technical Assistance Project Final Report, Charlottesville.

Sherry, S. T., Hebdon, M., and Kassner, B. (2021). “Flexural Strengthening Retrofits of Corroded Steel Members Using CFRP—Large Scale Results and Implementation and Best Practices.” ASCE Journal of Bridge Engineering.

Tabrizi, S., Kazem, H., Rizkalla, S., and Kobayashi, A. (2015). “New Small-diameter CFRP Material for Flexural Strengthening of Steel Bridge Beams.” Construction and Building Materials, Elsevier Ltd, 95, 748–756.

Wipf, T. J., Phares, B. M., Klaiber, F. W., Lee, Y. S., and Al-Saidy, A. H. (2005). Strengthening Steel Beam Bridges with Carbon Fiber – Reinforced Polymer Plates. Transportation Research.

CHAPTER 6: Conclusions, Recommendations, and Future Work

Chapter 6 consists of conclusions and recommendations from the results of experimental testing described in Chapters 3, 4, and 5. The conclusions and recommendations (section 6.1 and 6.2,

respectively) have been provided in sequential order and split up accordingly based on the portion of the research they were completed in. Section 6.3 provides a list of potential future work pertaining to the advancement of CFRP retrofits being used on steel structures. Section 6.4 provides this author's contributions to the field of structural engineering as a result of the conducted research.

6.1 Conclusions

6.1.1 Small Scale Laboratory Testing – Bond Strength Investigation

6.1.1.1 Prediction Equations and Bond Performance

Conventional CFRP types (Sika) and prediction models(with the exclusion of Fernando (2010)) can be used to calculate estimates of ultimate strength predictions and estimated effective bond length predictions. The L.J. Hart-Smith (1973) prediction model performed more favorably in estimating ultimate strengths and effective bond lengths compared to the Xia and Teng (2005) model. However, if the most accurate results are desired, it is recommended that G_f and δ_f are found experimentally and used with the Xia and Teng (2005) model to calculate the effective bond length and ultimate strength of the joint.

The accuracy of the strength predictions for the Nippon specimens can not be commented on due to the CFRP rupture limit state. This research highlights the need to check the additional limit state of CFRP rupture when calculating the ultimate capacity of a joint. The effective bond length prediction models provide overly conservative values (around double) for non-conventional CFRP types (Nippon) unless the Yuan et al. (2004) prediction model is used.

6.1.1.2 Simulated Corrosion

The simulated corrosion in this study seemed to have little effect on enhancing the ultimate bond strength or ductility of the Sikadur30 adhesive. What little effect the corrosion did seem to have was the 12.5% increase in the displacements of the Nippon DSJs prior to failure. The 2.2% mass loss had minimal effects on the bond strength of these DSJs. When adequately cleaned, the superficial corrosion pitting is not likely to cause problems in developing adequate bond strengths associated with CFRP retrofits' effective bond lengths.

6.1.2 Large Scale Laboratory Testing and Field Testing of Flexural CFRP Retrofits on Corroded Steel Girders

6.1.2.1 Surface Variability

CFRP retrofits completed on steel with rust grades C & D, which were blast-cleaned to Sa 2 ½ or Sa 3 were able to achieve expected vs calculated capacity design within 10% (excluding the Sika 1-TBF). Pitting corrosion and section loss up to 0.125 in had little effect on the CFRP retrofits' ability to achieve strengths within reasonable proximity to their calculated design strengths.

6.1.2.2 Design

Conventional strain compatibility calculations, used in conjunction with elastic-perfectly plastic assumptions, known material properties (assuming CFRP rupture is reached), and section geometries, were able to predict the moment capacity within 8% (overpredicts) of actual strengths (excluding the Sika-TBF). Where further analysis of the prediction equations showed, calculations were within 11% of predicted. When designing flexural CFRP retrofits, the CFRP rupture design strength may be used to approximate the capacity of the retrofit. Additionally, when designing a CFRP retrofit, all appropriate failure modes should be evaluated. It is recommended that an analysis of the retrofit be carried out for: the strength capacity, maximum

stress/strain associated with debonding near CFRP termination, and maximum strain associated with intermediate debond at the maximum moment location.

6.1.2.3 Performance/Configurations

The presence of multiple plies of CFRP had a moderate effect on total strength. For the Sika retrofits, two plies of CFRP on the bottom of the bottom flange did not significantly increase the beam's strength and stiffness in proportion to the amount of additional material applied; however, this is attributed to this beam's condition (deteriorated) not the effects of shear lag. While the material was doubled from Nippon 1-BBF to 2-BBF, the strength increase was only 1.46 that of the Nippon 1-BBF retrofit at 0.83 in of deflection. This lesser performance is attributed to shear lag for multiple plies of the Nippon CFRP. It is recommended that a minimum shear lag reduction factor of 25% be applied to the elastic modulus during the design process.

Placing CFRP strengthening systems on top of the bottom flange is as effective as the bottom-of-bottom flange configurations and may be easier to install. However, the 1-TBF retrofit is more susceptible to intermediate debond if intermediate stiffeners are present on the retrofitted girder. Intermediate debond is associated with lower overall loading and occurred only for the Sika 1-BBF specimen.

The Sika retrofits tend to experience global or total failure of the reinforcing system. In contrast, the Nippon retrofits experience localized failure that allowed for portions of the retrofit to remain intact. This localized failure is also successive and can be observed via visual inspection, which is ideal because it indicates failure before the system's complete loss.

6.1.3 Load Test to Evaluate a Flexural Repair of a Deteriorated Bridge with Carbon Fiber Reinforced Polymer Strand Sheets

6.1.3.1 Large-Scale Testing

The re-creation and testing of a replica beam 5 from the Simmons Gap Road Bridge in the laboratory with a CFRP retrofit was successful in returning this deteriorated beam back above its original strength. The CFRP retrofit beam had a plastic moment (M_p) of 2.8% above the original beam. The CFRP retrofit was able to reduced global strains by 25.6% compared to the control beam. Lastly, the failure mode of this CFRP retrofit was not CFRP rupture but rather lateral-torsional buckling and local flange buckling, which is an indication of this retrofit's ability to return the structure above its original strength while not failing the retrofit.

6.1.3.2 Field Testing

The installation of the Nippon CFRP strand sheet in the field was a success. The installed retrofit was sufficient in returning beam 5 back above its original elastic strength capacity based on the laboratory test data. This field retrofit effectively reduced localized stresses (a minimum of 50%) and deformations (a minimum of 23.6%) on the Simmons Gap Road Bridge. The retrofit also greatly affected the live load distribution on the Simmons Gap Road Bridge (for the case of beam 5 loading). This research showed that for a specific loading (beam 5), three of the instrumented beams were taking a significant portion of the load coming across the bridge. After the retrofitting, this load was more uniformly distributed across the width of the bridge.

6.1.3.3 Surface Variability/Corrosion

The recreated corrosion damage on the control beams and corrosion damage on the Simmons Gap Road Bridge (up to 50 percent section loss of the bottom flange) did not

significantly influence the strength, stiffness, or bondability of the CFRP retrofit on the tested beams. CFRP retrofits completed on steel with rust grades C & D (laboratory testing), which were blast-cleaned to Sa 2 ½ or Sa 3, were able to achieve inelastic strengths 2.8% above the original analytical predictions.

6.2 Recommendations

Based on the conclusions from the small scale laboratory testing, large scale laboratory testing, and field testing of CFRP retrofits used on corroded steels, the following recommendations are made:

6.2.1 General:

1. The mean corrosion section loss of 11%, with maximum valley depth below the mean line (0.204 in), and a maximum peak height above the mean line (0.158 in.) on the tested steel did not significantly influence the strength, stiffness, or bondability of the CFRP retrofit when the corroded steel was blast-cleaned to grades Sa 2 ½ or Sa 3. It is recommended that this level of cleanliness Sa 2 ½ or Sa 3 be utilized for all CFRP retrofits for steel.

6.2.2 Small Scale Laboratory Testing – Bond Strength Investigation

2. Prediction models(with the exclusion of Fernando (2010)) can be used to calculate estimates of ultimate strength predictions and estimated effective bond length predictions for DSJs (there degree of accuracy varies). However, if the most accurate results are desired, it is recommended that G_f and δ_f are found experimentally and used with the Xia and Teng (2005) model to calculate the effective bond length and ultimate strength of

DSJs. Further more when calculating these strengths the additional limit state of CFRP rupture needs to be checked.

3. The effective bond length prediction models for the Nippon CFRP provided overly conservative values,with the exception Yuan et al. (2004). Furthermore, the use of an L_c value greater than 50% of the CFRP strand sheet's perimeter is recommended to calculate the effective bond length for more accurate results.

6.2.3 Large Scale Laboratory Testing and Field Testing of Flexural CFRP Retrofits on Corroded Steel Girders

4. It is recommended that conventional strain compatibility calculations, used in conjunction with elastic-perfectly plastic assumptions, known material properties (assuming CFRP rupture is reached), and section geometries, are used to predict the moment capacity of CFRP retrofits.
5. The presence of multiple plies of CFRP had a moderate effect on Nippon 2-BBF's total strength. It is recommended that a shear lag reduction factor of 25% be applied to the Nippon 2-BBF (elastic modulus) during the design process.
6. It is recommended that 1-TBF CFRP strengthening systems not be used beams where intermediate stiffeners are present on the girder. This detail causes stress concentrations associated with early failure (intermediate debond).

6.2.4 Load Test to Evaluate a Flexural Repair of a Deteriorated Bridge with Carbon Fiber Reinforced Polymer Strand Sheets

7. It is recommended that CFRP retrofits should be applied to the full length of the deteriorated beams, extending as close to the supports of the beam as possible (The maximum length of the retrofit needs to be checked against (NEXCO-West 2015)).
8. It is recommended that these retrofits be implemented when an increase in strength or stiffness is required on deteriorated steel structures. These retrofits have been shown to be an effective means of altering the distribution factor of bridge beams lacking in stiffness.

6.3 Future Work

The following items are suggested for future work of CFRP retrofits used on corroded steels:

6.3.1 Small Scale Laboratory Testing – Bond Strength Investigation

1. The accuracy of the strength predictions for the Nippon specimens can not be commented on due to the CFRP rupture limit state. Further testing on non-conventional CFRP types (Nippon) is needed to analyze the accuracy of these prediction models. Where this testing will look at either different moduli CFRPs or adhesives of different strengths.
2. Varying ranges of mass losses more significant than what was tested here need to be examined to further study the effects corrosion has on bond strength.
3. Further testing is required to determine how roughness, amplitude, and the density of the roughness affect bond strength.

6.3.2 Large Scale Laboratory Testing and Field Testing of Flexural CFRP Retrofits on Corroded Steel Girders

4. Further research is needed to determine what kind of clearance is needed between a CFRP retrofit and a stiffener to mitigate intermediate debond.
5. Further research is needed to determine the effects that subsequent layers of CFRP (more than 2) will have on shear lag, where it is unknown how multiple layers of CFRP will affect the strength of flexural CFRP retrofit.
6. Further research is needed to study the effective lengths of flexural CFRP retrofits on actual test beams, which involves a detailed inspection of intermediate debond and end debond.

6.3.3 Large Scale Laboratory Testing and Field Testing of Flexural CFRP Retrofits on Corroded Steel Girders

7. Further research is needed to study the effects on CFRP retofit's capabilities being applied to minimal amounts of steel.
8. Further research is needed to study the effects on the long-term durability/degradation of CFRP retrofits installed in situ on in-service bridge structures.
9. Further research is needed on how the retrofitting of multiple beams on the same bridge will affect live load distribution, especially on girders with little to no corrosion deterioration next to severely corroded beams.

6.4 Ph.D. Contributions

The original contributions of this research are as follows:

1. Investigating the efficacy of strength and effective length prediction models on conventional and non-conventional CFRP types.
    a. Where specific equations are suggested for the different CFRPs used in this research.
    b. Prior to this research (to this author's knowledge), there was no investigation on the use of prediction models for strength and effective length of strand sheet CFRPs. This author suggests the use of the Yuan et al. (2004) equation with the further recommendation of an L_c value greater than 50% of the CFRP strand sheet's perimeter when calculating the effective bond length on strand sheet CFRPs.
2. Investigating the application of CFRP materials on a steel surface with a variable profile.
    a. Prior to this research, the application of CFRP on large scale flexural retrofits with corrosion deterioration was only completed on a minimal number of laboratory tests which did not quantify the corrosion damage or consider corrosion as a variable that affected overall strength.
    b. Prior to this research, the application of CFRP on small scale steel coupons with "representative" simulated corrosion had never been completed. This research serves as a guide and a data point for further tests of its kind, which can be used for different CFRP strengthening systems to observe how corrosion damage will affect bond strength.
    c. This research implemented the novel use of a DIC system to highlight different corrosion deterioration and surface variability. These details included where CFRP retrofits can be applied for average section loss, maximum corrosion

damage, and surface variations from a normal plane. Where this kind of analysis can hopefully inform future investigations on CFRP retrofits being applied to steel with a variable profile.

d. Following the corrosion research findings, large scale flexural CFRP retrofits were installed on a structurally deficient bridge, which were currently in service and in need of repair to meet state and federal load rating minimums. Only a few flexural CFRP retrofits in the United States have been completed on steel bridges, of which, to this authors knowledge, none of them were structurally deficient due to corrosion-related issues

3. Investigating the use of a newly developed high modulus CFRP strand sheet.
    a. Prior to this research, the application of HM CFRP strand sheets on small scale steel coupons had never been thoroughly documented. It was unknown how this material would behave and if conventional prediction models (effective length and ultimate strength) would work.
    b. Following the small and large scale research findings on HM CFRP strands sheets, a HM CFRP strand sheet CFRP flexural retrofit was completed on a structurally deficient steel bridge. The use of HM CFRP strand sheets as a flexural retrofit on steel bridge beams is the first of its kind in the United States. This research was carried out to validate laboratory test data (on a single retrofitted girder) compared to a single retrofitted girder in a bridge structure. This research also serves as one of a small number of studies that provides information on how a CFRP retrofit affected load redistribution on a bridge structure.
4. Expanding the knowledge of flexural CFRP/steel retrofits.

a. This research provides information on CFRP best practices to provide industry with a guideline on when and where CFRP retrofits are applicable to use on corroded and uncorroded steel structures.

b. This research identified how different CFRP material types (NM plates & HM strand sheets) affect the overall strength and stiffness of CFRP retrofits (via large and small scale testing).

c. This research identified how different CFRP configurations (BBF, TBF, and multiple plies) affect the overall strength and stiffness of CFRP retrofits.

d. This research shows multiple plies of CFRP can be influenced by the effects of shear lag.

e. This research provided an overview of how well elastic analysis and inelastic analysis are capable of predicting the ultimate strength of different CFRP retrofits.

References

AASHTO. (2012). *Guide Specifications for Design of Bonded FRP Systems for Repair and Strengthening of Concrete Bridge Elements*.

AASHTO. (2018a). *Guide Specifications for the Design of Concrete Bridge Beams Prestressed with Carbon Fiber-Reinforced Polymer (CFRP) Systems*.

AASHTO. (2018b). *The Manual for Bridge Evaluation*. American Association of State Highway and Transportation Officals.

ACI. (2002). *Guide to Concrete Repair*.

ACI. (2017). *440.2R-17: Guide for the Design and Construction of Externally Bonded FRP*

Systems for Strengthening Concrete Structures. *440.2R-17: Guide for the Design and Construction of Externally Bonded FRP Systems for Strengthening Concrete Structures*.

Adams, R. D., and Peppiatt, N. A. (1974). "Stress Analysis Of Adhesive-Bonded Lap Joints." *JOURNAL OF STRAIN ANALYSIS*, 9(3), 185–196.

AISC. (2016). *Specification for Structural Steel Buildings AISC/ANSI 360-16*. Chicago.

Al-Mosawe, A., Al-Mahaidi, R., and Zhao, X. L. (2015). "Effect of CFRP properties, on the bond characteristics between steel and CFRP laminate under quasi-static loading." *Construction and Building Materials*, Elsevier Ltd, 98, 489–501.

Al-Saidy, A. H. (2001). "Structural Behavior of Composite Steel Beams Strengthened/Repaired with Carbon Fiber Reinforced Polymer Plates."

Al-Saidy, A. H., Klaiber, F. W., and Wipf, T. J. (2004). "Repair of Steel Composite Beams with Carbon Fiber-Reinforced Polymer Plates." *Journal of Composites for Construction*, 8(2), 163–172.

Anderson, T. L. (2017). *Fracture Mechanics Fundamentals and Applications*. CRC Press.

Au, C., and Büyüköztürk, O. (2006). "Debonding of FRP plated concrete: A tri-layer fracture treatment." *Engineering Fracture Mechanics*, 73(3), 348–365.

Batuwitage, C., Fawzia, S., Thambiratnam, D., and Al-Mahaidi, R. (2017). "Evaluation of bond properties of degraded CFRP-strengthened double strap joints." *Composite Structures*, Elsevier Ltd, 173, 144–155.

Belingardi, G., Goglio, L., and Tarditi, A. (2002). "Investigating the effect of spew and chamfer size on the stresses in metal/plastics adhesive joints." *International Journal of Adhesion and*

Adhesives, 22(4), 273–282.

Bilotta, A., Faella, C., Martinelli, E., and Nigro, E. (2013). "Design by testing procedure for intermediate debonding in EBR FRP strengthened RC beams." *Engineering Structures*, Elsevier Ltd, 46, 147–154.

Bocciarelli, M. (2009). "Response of Statically Determined Steel Beams Reinforced by CFRP Plates in the Elastic-Plastic Regime." *Engineering Structures*, Elsevier Ltd, 31(4), 956–967.

Buyukozturk, O., Gunes, O., and Karaca, E. (2004). "Progress on understanding debonding problems in reinforced concrete and steel members strengthened using FRP composites." *Construction and Building Materials*, 18(1), 9–19.

Carpinteri, A., Cornetti, P., and Pugno, N. (2009). "Edge debonding in FRP strengthened beams: Stress versus energy failure criteria." *Engineering Structures*, Elsevier Ltd, 31(10), 2436–2447.

Chajes, M. J., Chacon, A. P., Swinehart, M. W., Richardson, D. R., and Wenczel, G. C. (2005). "Applications of Advanced Composites to Steel Bridges: A Case Study on the Ashland Bridge." 19716(March).

Chen, J. F., and Teng, J. G. (2001). "ANCHORAGE STRENGTH MODELS FOR FRP AND STEEL PLATES BONDED TO CONCRETE." *Journal of Structural Engineering*, 127(c), 784–791.

Chotickai, P. (2018). "Effect of pre-installed corrosion on steel plate-CFRP bond characteristics." *International Journal of Adhesion and Adhesives*, Elsevier Ltd, 84(May), 431–437.

Colombi, P., and Poggi, C. (2006). “An experimental, analytical and numerical study of the static behavior of steel beams reinforced by pultruded CFRP strips.” *Composites Part B: Engineering*, 37(1), 64–73.

Cruz, J. S., and Barros, J. (2004). “Modeling of bond between near-surface mounted CFRP laminate strips and concrete.” *Computers and Structures*, 82(17–19), 1513–1521.

Dawood, M., and Rizkalla, S. (2010). “Environmental durability of a CFRP system for strengthening steel structures.” *Construction and Building Materials*, Elsevier Ltd, 24(9), 1682–1689.

Dawood, M., Rizkalla, S., and Sumner, E. (2007). “Fatigue and Overloading Behavior of Steel–Concrete Composite Flexural Members Strengthened with High Modulus CFRP Materials.” *Journal of Composites for Construction*, 11(6), 659–669.

Deng, J., and Lee, M. M. K. (2007a). “Behaviour Under Static Loading of Metallic Beams Reinforced with a Bonded CFRP Plate.” *Composite Structures*, 78(2), 232–242.

Deng, J., and Lee, M. M. K. (2007b). “Fatigue Performance of Metallic Beam Strengthened with a Bonded CFRP Plate.” *Composite Structures*, 78(2), 222–231.

Deng, J., Lee, M. M. K., and Moy, S. S. J. (2004). “Stress Analysis of Steel Beams Reinforced with a Bonded CFRP Plate.” *Composite Structures*, 65(2), 205–215.

Fawzia, S. (2007). “Bond Characteristics Between Steel and Carbon Fiber Reinforced Polymer (CFRP) Composites.” Monash University, Melbourne, Australia.

Fawzia, S., Al-Mahaidi, R., Zhao, X. L., and Rizkalla, S. (2006). “Strengthening of circular hollow steel tubular sections using high modulus CFRP sheets.” *Construction and Building*

Materials, 21(4), 839–845.

Fawzia, S., Zhao, X., and Al-mahaidi, R. (2010a). "Bond – slip models for double strap joints strengthened by CFRP." 92, 2137–2145.

Fawzia, S., Zhao, X. L., and Al-Mahaidi, R. (2010b). "Bond-slip models for double strap joints strengthened by CFRP." *Composite Structures*, Elsevier Ltd, 92(9), 2137–2145.

Fawzia, S., Zhao, X. L., Al-Mahaidi, R., and Rizkalla, S. (2005). "Bond characteristics between cfrp and steel plates in double strap joints." *Advanced Steel Construction*, 1(2), 17–27.

Fernando, D., Teng, J. G., Yu, T., and Zhao, X. L. (2013). "Preparation and Characterization of Steel Surfaces for Adhesive Bonding." *Journal of Composites for Construction*.

Fernando, N. D. (2010). "Bond behaviour and debonding failures in CFRP-strengthened steel members." *PhD Thesis, Civil and Structural Department*, PhD Thesis, 343.

FHWA. (2012). *Bridge Inspector's Reference Manual- FHWA NHI 12-049*. Federal Highway Administration.

Fisher, J. W., Barthelemy, B. M., Mertz, D. R., and Edinger, J. A. (1980). *Fatigue Behavior of Full-Scale Welded Bridge Attachments*. *National Cooperative Highway Research Program Report*.

Fisher, J. W., Sullivan, M. D., Hausammann, H., and Pense, A. W. (1979). *Detection and Repair of Fatigue Damage in Welded Highway Bridges*. *National Cooperative Highway Research Program Report 206*.

Frostig, Y., and Rabinovich, O. (2000). "CLOSED-FORM HIGH-ORDER ANALYSIS OF RC BEAMS STRENGTHENED WITH FRP STRIPS." *Journal of Composites for*

Construction, 4, 65–74.

Fu, B., Chen, G. M., and Teng, J. G. (2017). "Mitigation of intermediate crack debonding in FRP-plated RC beams using FRP U-jackets." *Composite Structures*, 176, 883–897.

Galal, K., Tirca, L., and Seif ElDin, H. M. (2009). "Flexural Performance of Steel Girders Retrofitted Using CFRP Material." *Composite for Construction*, 16(June), 1–16.

Goland, M. A., and Reissner, E. (1944). "The stress in a cemented joint." *Journal of Appled Mechanics*, A17–A27.

Haghani, R., Al-Emrani, M., and Kliger, R. (2010). "Stress distribution in adhesive joints with tapered laminates g - Effect of tapering length and material properties." *Journal of Composite Materials*, 44(3), 287–302.

Haghpanah, B., Chiu, S., and Vaziri, A. (2014). "Adhesively Bonded Lap Joints with Extreme Interface Geometry." *International Journal of Adhesion and Adhesives*, Elsevier, 48, 130–138.

Hamoush, S. A., and Ahmad, S. H. (1990). "Debonding of Steel Plate-strengthened Concrete Beams." *Journal of Structral Engineering*, 116(2), 356–371.

Hart-Smith, L. J. (1973). *Adhesive-Bonded Double-Lap Joints*. Hampton, VA.

Hearing, B. (2000). "Delamination in Reinforced Concrete Retrofitted with Fiber Reinforced Plastics."

Heshmati, M., Haghani, R., and Al-Emrani, M. (2017). "Durability of CFRP/steel joints under cyclic wet-dry and freeze-thaw conditions." *Composites Part B: Engineering*, Elsevier Ltd, 126, 211–226.

Hidekuma, Y., Kobayashi, A., Tateishi, A., Nagai, M., and Miyashita, T. (2011). "Repairing Method for the Steel Members by CFRP Strand Sheets." *Advances in FRP Composites in Civil Engineering - Proceedings of the 5th International Conference on FRP Composites in Civil Engineering, CICE 2010*, 881–885.

Hmidan, A., Kim, Y. J., and Yazdani, S. (2011). "CFRP Repair of Steel Beams with Various Initial Crack Configurations." *Journal of Composites for Construction*, 15(6), 952–962.

Högberg, J. L. (2006). "Mixed mode cohesive law." *International Journal of Fracture*, 141(3–4), 549–559.

Hyer, M. W. (2009). *Stress Analysis of Fibre-Reinforced Composite Materials*. *DEStech Publications, Inc*.

ISO. (2007). *ISO 8501-1 The Rust Grade Book*.

Jiao, H., and Zhao, X. L. (2004). "CFRP strengthened butt-welded very high strength (VHS) circular steel tubes." *Thin-Walled Structures*, Elsevier Ltd, 42(7), 963–978.

Kazem, H., Guaderrama, L., Selim, H., Rizkalla, S., and Kobayashi, A. (2016). "Strengthening of steel plates subjected to uniaxial compression using small-diameter CFRP strands." *Construction and Building Materials*, Elsevier Ltd, 111, 223–236.

Kim, S. J., Smith, S. T., and Young, B. (2011). "Effect of Surface Preparation on the Strength of FRP-to-Mild Steel and FRP-to-Stainless Steel Joints." *Advances in FRP Composites in Civil Engineering - Proceedings of the 5th International Conference on FRP Composites in Civil Engineering, CICE 2010*, 869–872.

Kim, W. S., Yun, I. H., Lee, J. J., and Jung, H. T. (2010). "Evaluation of Mechanical Interlock

Effect on Adhesion Strength of Polymermetal Interfaces Using Micro-patterned Surface Topography." *International Journal of Adhesion and Adhesives*, Elsevier, 30(6), 408–417.

Kim, Y. J. (2017). "Performance of Steel Girders Repaired with Advanced Composite Sheets in a Corrosive Environment." *Mountain-Plains Consortium*.

Kim, Y. J., and Brunell, G. (2011a). "Interaction Between CFRP-repair and Initial Damage of Wide-flange Steel Beams Subjected to Three-point Bending." *Composite Structures*, Elsevier Ltd, 93(8), 1986–1996.

Kim, Y. J., and Brunell, G. (2011b). "Interaction between CFRP-repair and initial damage of wide-flange steel beams subjected to three-point bending." *Composite Structures*, Elsevier Ltd, 93(8), 1986–1996.

Kim, Y. J., and Kent, A. H. (2012). "Predictive response of notched steel beams repaired with CFRP strips including bond-slip behavior." *International Journal of Structrual Stability and Dynamics*.

Kinloch, A. J. (1987). *Adhesion and Adhesives*. SPRINGER-SCIENCE+BUSINESS MEDIA, B.V.

Kleffel, T., and Drummer, D. (2017). "Investigating the Suitability of Roughness Parameters to Assess the Bond Strength of Polymer-Metal Hybrid Structures with Mechanical Adhesion." *Composites Part B: Engineering*, Elsevier Ltd, 117, 20–25.

Kobayashi, A., Hidekuma, Y., and Tateishi, A. (2015). "Strengthening of steel and concrete structures using CFRP in Japan." 978–984.

Lau, K. T., Dutta, P. K., Zhou, L. M., and Hui, D. (2001a). "Mechanics of bonds in an FRP

bonded concrete beam." *Composites Part B:Engineering*, 32(6), 491–502.

Lau, K. T., Shi, S. Q., and Zhou, L. M. (2001b). "Estimation of stress intensity factor (KI) for an FRP bonded concrete beam using the superposition method." *Magazine of Concrete Research*, 53(1), 31–41.

Lenwari, A., Thepchatri, T., and Albrecht, P. (2005). "Flexural Response of Steel Beams Strengthened with Partial-Length CFRP Plates." *Journal of Composites for Construction*.

Li, A., Xu, S., Wang, H., Zhang, H., and Wang, Y. (2019). "Bond behaviour between CFRP plates and corroded steel plates." *Composite Structures*, Elsevier, 220(March), 221–235.

Liu, H., Al-Mahaidi, R., and Zhao, X. L. (2009). "Experimental study of fatigue crack growth behaviour in adhesively reinforced steel structures." *Composite Structures*, Elsevier Ltd, 90(1), 12–20.

Liu, X., Silva, P. F., and Nanni, A. (2001). "Rehabilitation of Steel Bridge Members with FRP Composite Materials." *CCC 2001 Composites in Construction*, (100 mm), 613–617.

De Lorenzis, L., Fernando, D., and Teng, J. G. (2013). "Coupled mixed-mode cohesive zone modeling of interfacial debonding in simply supported plated beams." *International Journal of Solids and Structures*, Elsevier Ltd, 50(14–15), 2477–2494.

De Lorenzis, L., Paggi, M., Carpinteri, A., and Zavarise, G. (2010). "Linear elastic fracture mechanics approach to plate end debonding in rectilinear and curved plated beams." *Advances in Structural Engineering*, 13(5), 875–889.

De Lorenzis, L., and Zavarise, G. (2008). "Modeling of mixed-mode debonding in the peel test applied to superficial reinforcements." *International Journal of Solids and Structures*,

45(20), 5419–5436.

De Lorenzis, L., and Zavarise, G. (2009). “Cohesive zone modeling of interfacial stresses in plated beams.” *International Journal of Solids and Structures*, Elsevier Ltd, 46(24), 4181–4191.

Lu, X. Z., Teng, J. G., Ye, L. P., and Jiang, J. J. (2007). “Intermediate Crack Debonding in FRP-Strengthened RC Beams: FE Analysis and Strength Model.” *Journal of Composites for Construction*, 11(2), 161–174.

Malek, A. M., Saadatmanesh, H., and Ehsani, M. R. (1998). “Prediction of Failure Load of R/C Beams Strengthened with FRP Plate Due to Stress Concentration at the Plate End.” *ACI Structural Journal*, V95.

Mertz, D. R., and Gillespie, J. W. J. (1996). *NCHRP-IDEA Final Report: Rehabilitation of Steel Bridge Girders Through the Application of Advanced Composite Materials*. Washington, DC.

Mertz, D. R., Gillespie Jr, J. W., Chajes, M. J., and Sabol, S. (2002). “Rehabilitation of Steel Bridge Girders Using Advanced Composite Materials.” *NCHRP-IDEA Program Project Final Report Project 51*, 36.

Mertz, D. R., and Kulicki, J. (2006). “Evolution of Vehicular Live Load Models During the Interstate Design Era and Beyond.” *Transportation Research Circular E-C104*.

Miller, T. C., Chajes, M. J., Mertz, D. R., and Hastings, J. N. (2001). “Strengthening of a Steel Bridge Girder Using CFRP Plates.” *Journal of Bridge Engineering*, 6(6), 514–522.

Milliken Infrastructure. (2017). “Renew Wrap Strand Sheet Adhesive (BF-E7S).”

Milliken Infrastructure. (2018). *Renewwrap Installation Manual*. Spartanburg, SC.

Moy, S. S. J. (2002). "Steel Beams Strengthened with Carbon Fibre Reinforced Polymer Composites." *Advanced polymer composites for structural applications in construction*, (March), 195–202.

Moy, S. S. J., Barnes, F., Moriarty, J., Dier, A. F., Kenchington, A., and Iverson, B. (2000). "Structural Upgrade and Life Extension of Cast Iron Struts Using Carbon Fibre Reinforced Composites." *FRC 2000–Composites for the Millennium*, (March), 3–10.

Nagai, M., Hidekuma, Y., Miyashita, T., Okuyama, Y., Kudo, A., and Kobayashi, A. (2012). "Bonding Characteristics and Flexural Stiffening Effect of CFRP Strand Sheets Bonded to Steel Beams." *Procedia Engineering*, 40, 137–142.

Narmashiri, K., Jumaat, M. Z., and Sulong, N. H. R. (2012). "Strengthening of Steel I-Beams Using CFRP Strips: An Investigation on CFRP Bond Length." *Advances in Structural Engineering*, 15(12), 2191–2204.

National Academies of Sciences, Engineering, and M. (2010). *Design Guidelines for Durability of Bonded CFRP Repair/Strengthening of Concrete Beams*. *Design Guidelines for Durability of Bonded CFRP Repair/Strengthening of Concrete Beams*, The National Academies Press, Washington, DC.

National Academies of Sciences, Engineering, and M. (2019). *Design of Concrete Bridge Beams Prestressed with CFRP Systems*. *Design of Concrete Bridge Beams Prestressed with CFRP Systems*, The National Academies Press, Washington, DC.

NEXCO-West. (2015). "Design and Installation Manual for Upgrading of Steel Structures with

the use of Carbon Fiber Sheets." (2), 62.

Nguyen, T. C., Bai, Y., Al-Mahaidi, R., and Zhao, X. L. (2012a). "Time-dependent behaviour of steel/CFRP double strap joints subjected to combined thermal and mechanical loading." *Composite Structures*, Elsevier Ltd, 94(5), 1826–1833.

Nguyen, T. C., Bai, Y., Zhao, X. L., and Al-Mahaidi, R. (2012b). "Durability of steel/CFRP double strap joints exposed to sea water, cyclic temperature and humidity." *Composite Structures*, Elsevier Ltd, 94(5), 1834–1845.

Nozaka, K., Shields, C. K., and Hajjar, J. F. (2005a). "Design of a Test Specimen to Assess the Effective Bond Length of Carbon Fiber-Reinforced Polymer Strips Bonded to Fatigued Steel Bridge Girders." *Journal of Composites for Construction*.

Nozaka, K., Shields, C. K., and Hajjar, J. F. (2005b). "Effective Bond Length of Carbon-Fiber-Reinforced Polymer Strips Bonded to Fatigued Steel Bridge I-Girders." *Journal of Bridge Engineering*.

Ojalvo, I. U., and Eidinoff, H. L. (1978). "Bond thickness effects upon stresses in single-lap adhesive joints." *AIAA Journal*, 16(3), 204–211.

Pang, Y., Wu, G., Wang, H., and Liu, Y. (2019). "Interfacial bond-slip degradation relationship between CFRP plate and steel plate under freeze-thaw cycles." *Construction and Building Materials*, Elsevier Ltd, 214, 242–253.

Peiris, A., and Harik, I. (2018). "FRP-steel bond study of IM and UHM CFRP strips." *Construction and Building Materials*, 185, 628–637.

Peiris, N. A. (2011). "Steel Beams Strengthened with Ultra High Modulus CFRP Laminates."

University of Kentucky.

Pham, H. B., and Al-Mahaidi, R. (2005). “Modelling of CFRP-concrete shear-lap tests.” *Construction and Building Materials*, 21(4), 727–735.

Phares, B. M., Wipf, T. J., Klaiber, F. W., Abu-Hawash, A., and Lee, Y.-S. (2003). “Strengthening of steel girder bridges using FRP.” *Proc., 2003 Mid-Continent Transportation Research Symp*, (August 2003), 1–12.

Photiou, N. K., Hollaway, L. C., and Chryssanthopoulos, M. K. (2006). “Strengthening of an artificially degraded steel beam utilising a carbon / glass composite system.” 20, 11–21.

Quantrill, R. J., Hollaway, L. C., and Thorne, A. M. (1996). “Predictions of the maximum plate end stresses of FRP strengthened beams: Part II.” *Magazine of Concrete Research*, 48(4), 343–351.

Rabinovich, O., and Frostig, Y. (2000). “Closed-form High-Order Analysis of RC Beams Strengthened with FRP Strips.” *Journal of Composites for Construction*, 65–74.

Rabinovitch, O. (2004). “Fracture-mechanics failure criteria for RC beams strengthened with FRP strips--a simplified approach.” *Composite Structures*, 64(3–4), 479–492.

Rabinovitch, O. (2008). “Debonding analysis of fiber-reinforced-polymer strengthened beams: Cohesive zone modeling versus a linear elastic fracture mechanics approach.” *Engineering Fracture Mechanics*, 75(10), 2842–2859.

Rizkalla, S., and Dawood, M. (2006). “High modulus carbon fiber materials for retrofit of steel structures and bridges.” (July), 11–14.

Rizkalla, S., Dawood, M., and Schnerch, D. (2008). “Development of a carbon fiber reinforced

polymer system for strengthening steel structures." *Composites Part A: Applied Science and Manufacturing*, 39(2), 388–397.

Roberts, T. M. (1989). "Approximate analysis of shear and normal stress concentrations in the adhesive layer of plated RC beams." *Struct Eng.*

Salama, T., and Abd-El-Meguid, A. (2010). *Strengthening Steel Bridge Girders Using CFRP*. University Transportation Center for Alabama, Birmingham, AL.

Sallam, H. E. M., Ahmad, S. S. E., Badawy, A. A. M., and Mamdouh, W. (2006). "Evaluation of steel I-beams strengthened by various plating methods." *Advances in Structural Engineering*, 9(4), 535–544.

Sayman, O. (2012). "Elasto-plastic stress analysis in an adhesively bonded single-lap joint." *Composites Part B: Engineering*, Elsevier Ltd, 43(2), 204–209.

Schnerch, D. (2005). "Strengthening of Steel Structures with High Modulus Carbon Fiber Reinforced Polymer (CFRP) Materials." *Thesis*, 265.

Schnerch, D., Dawood, M., Rizkalla, S., and Sumner, E. (2007). "Proposed Design Guidelines for Strengthening of Steel Bridges with FRP Materials." *Construction and Building Materials*, 21(5), 1001–1010.

Schnerch, D., and Rizkalla, S. (2008a). "Flexural Strengthening of Steel Bridges with High Modulus CFRP Strips." *Journal of Bridge Engineering*, 13(2), 192–201.

Schnerch, D., and Rizkalla, S. (2008b). "Flexural Strengthening of Steel Bridges with High Modulus CFRP Strips." 13(2), 192–201.

Shen, H.-S., Teng, J. G., and Yang, J. (2001). "INTERFACIAL STRESSES IN BEAMS AND

SLABS BONDED WITH THIN PLATE." *JOURNAL OF ENGINEERING MECHANICS*, 127, 399–406.

Shields, C. K., Hajjar, J. F., and Nozaka, K. (2004). *Repair of Fatigued Steel Bridge Girders with Carbon Fiber Strips*.

Sika. (2014a). *Sikadur 30 Product Data Sheet*.

Sika. (2014b). *Sika CarboDur System*. Pfäffikon ZH, Switzerland.

Da Silva, L. F. M., Ferreira, N. M. A. J., Richter-Trummer, V., and Marques, E. A. S. (2010). "Effect of Grooves on the Strength of Adhesively Bonded Joints." *International Journal of Adhesion and Adhesives*, Elsevier, 30(8), 735–743.

Smith, S. T., and Teng, J. G. (2001). "Interfacial Stresses in Plated Beams." *Composite Structures*, 57(1–4), 125–134.

Stratford, T., and Cadei, J. (2006). "Elastic analysis of adhesion stresses for the design of a strengthening plate bonded to a beam." *Construction and Building Materials*, 20(1–2), 34–45.

Tabrizi, S., Kazem, H., Rizkalla, S., and Kobayashi, A. (2015). "New Small-diameter CFRP Material for Flexural Strengthening of Steel Bridge Girders." *Construction and Building Materials*, Elsevier Ltd, 95, 748–756.

Taljsten, B. (1997). "Strengthening of Beams by Plate Bonding." *Journal of Materials in Civil Engineering*, 206–212.

Tavakkolizadeh, M., and Saadatmanesh, H. (2003a). "Fatigue Strength of Steel Girders Strengthened with Carbon Fiber Reinforced Polymer Patch." *Journal of Structural*

Engineering, 129(2), 186–196.

Tavakkolizadeh, M., and Saadatmanesh, M. (2003b). "Strengthening of Steel–Concrete Composite Girders Using Carbon Fibre Reinforced Polymer Sheets." *Journal of Structral Engineering*, 129(1), 30–40.

Teng, J. G., Fernando, D., Yu, T., and Zhao, X. L. (2011). "Treatment of Steel Surfaces for Effective Adhesive Bonding." *Advances in FRP Composites in Civil Engineering - Proceedings of the 5th International Conference on FRP Composites in Civil Engineering, CICE 2010*, 865–868.

Teng, J. G., Smith, S. T., Yao, J., and Chen, J. F. (2003). "Intermediate crack-induced debonding in RC beams and slabs." *Construction and Building Materials*, 17(6–7), 447–462.

Teng, J. G., Zhang, J. W., and Smith, S. T. (2002). "Interfacial stresses in reinforced concrete beams bonded with a soffit plate: A finite element study." *Construction and Building Materials*, 16(1), 1–14.

Tsai, M. Y., Oplinger, D. W., and Morton, J. (1998). "Improved theoretical solutions for adhesive lap joints." *International Journal of Solids and Structures*, Elsevier Science Ltd, 35(12), 1163–1185.

Varastehpour, H., and Hamelin, P. (1997). "Strengthening of concrete beams using fiber-reinforced plastics." *Materials and Structures/Materiaux et Constructions*, 30(3), 160–166.

Volkersen, O. (1938). "Recherches sur la Thiorie des Assemblages Colles." *Construction mktalliaue*, 3–13.

Wang, H.-T., Wu, G., Dai, Y.-T., and He, X.-Y. (2016). "Experimental Study on Bond Behavior

between CFRP Plates and Steel Substrates Using Digital Image Correlation." *Journal of Composites for Construction*, 20(6), 04016054.

Wang, Y., Xu, S., Wang, H., and Li, A. (2017). "Predicting the residual strength and deformability of corroded steel plate based on the corrosion morphology." *Construction and Building Materials*, Elsevier Ltd, 152, 777–793.

Wipf, T. J., Phares, B. M., Klaiber, F. W., Lee, Y. S., and Al-Saidy, A. H. (2005). *Strengthening Steel Girder Bridges with Carbon Fiber – Reinforced Polymer Plates*. *Transportation Research*.

Wu, C., Zhao, X., Duan, W. H., and Al-Mahaidi, R. (2012a). "Bond characteristics between ultra high modulus CFRP laminates and steel." *Thin-Walled Structures*, Elsevier, 51(January), 147–157.

Wu, C., Zhao, X. L., Al-Mahaidi, R., and Duan, W. H. (2010). "Experimental study on bond behaviour between UHM CFRP laminate and steel." *Advances in FRP Composites in Civil Engineering - Proceedings of the 5th International Conference on FRP Composites in Civil Engineering, CICE 2010*, 890–893.

Wu, G., Wang, H. T., Wu, Z. S., Liu, H. Y., and Ren, Y. (2012b). "Experimental Study on the Fatigue Behavior of Steel Beams Strengthened with Different Fiber-reinforced Composite Plates." *Journal of Composites for Construction*, 16(2), 127–137.

Xia, S. H., and Teng, J. G. (2005). "Behaviour of FRP-To-Steel Bonded Joints." *Proceedings of the International Symposium on Bond Behaviour of FRP in Structures*.

Xu, S., Li, H., Wang, Y., Wang, Y., and Wang, Y. (2020). "Influence of corrosion on the bond

behavior in CFRP-steel single lap joints." *Construction and Building Materials*, Elsevier Ltd, 236, 117607.

Yang, Q. S., Peng, X. R., and Kwan, A. K. H. (2006). "Strain energy release rate for interfacial cracks in hybrid beams." *Mechanics Research Communications*, 33(6), 796–803.

Yao, Q., and Qu, J. (2002). "Interfacial Versus Cohesive Failure on Polymer-Metal Interfaces in Electronic Packaging-Effects of Interface Roughness." *Journal of Electronic Packaging, Transactions of the ASME*, 124(2), 127–134.

Yu, T., Fernando, D., Teng, J. G., and Zhao, X. L. (2012). "Experimental study on CFRP-to-steel bonded interfaces." *Composites Part B: Engineering*, 43(5), 2279–2289.

Yu, Y., Chiew, S. P., and Lee, C. K. (2011). "Bond failure of steel beams strengthened with FRP laminates - Part 2: Verification." *Composites Part B: Engineering*, 42(5), 1122–1134.

Yuan, H., Teng, J. G., Seracino, R., Wu, Z. S., and Yao, J. (2004). "Full-range behavior of FRP-to-concrete bonded joints." *Engineering Structures*, 26(5), 553–565.

Yuan, H., Wu, Z., and Yoshizawa, H. (2001). "Theoretical solutions on interfacial stress transfer of externally bonded steel/composite laminates." *Structural Engineering/Earthquake Engineering*, 18(1).

Zhang, L., and Teng, J. G. (2010). "Finite element prediction of interfacial stresses in structural members bonded with a thin plate." *Engineering Structures*, Elsevier Ltd, 32(2), 459–471.

Zhao, X.-L. (2013). *FRP-Strengthened Metallic Structures*.

Zhao, X. L., and Zhang, L. (2007). "State-of-the-art review on FRP strengthened steel structures." *Engineering Structures*, 29(8), 1808–1823.